Doctor of Philosophy

Roles of eIF2alpha phosphorylation in anti-oxidative stress response and autophagy

The Graduate school of the University of Ulsan

Department of Biological science

Mi-Jeong Kim

Roles of eIF2alpha phosphorylation in anti-oxidative stress response and autophagy

Supervisor: Professor **Sung Hoon Back**, Ph.D

A Dissertation

Submitted to
The Graduate School of the University of Ulsan
In partial Fulfillment of the Requirements
for the degree of

Doctor of Philosophy

By

Mi-Jeong Kim

Department of Biological Science
Ulsan, Korea
August 2021

Roles of eIF2alpha phosphorylation in anti-oxidative stress response and autophagy

This certifies that the dissertation
of Mi-Jeong Kim is approved by

Committee Chair Dr. JEONG WOO PARK

Committee Member Dr. BYUNG JU LEE

Committee Member Dr. SU WOL CHUNG

Committee Member Dr. BYOUNG HEON KANG

Committee Member Dr. SUNG HOON BACK

Department of Biological Science

Ulsan, Korea.

August 2021

CONTENTS

Roles of eIF2alpha phosphorylation in anti-oxidative stress response and autophagy

Chapter 1. Reduced EGFR Level in eIF2α Phosphorylation–deficient Hepatocytes is Responsible for Susceptibility to Oxidative Stress

Abstract ---------- 2

Introduction ----------3

Materials and Methods ----------6

Results and Discussion ----------11

Figures ----------17

Reference ----------29

Chapter 2. eIF2α phosphorylation is a critical event for autophagosome maturation upon ER stress

Abstract ----------35

Introduction ----------37

Materials and Methods ----------42

Results ----------49

Figures ----------66

Discussion ----------98

Reference ----------104

국문요약 ----------113

Appendix. **Butyrate Prevents TGF-β1-Induced Alveolar Myofibroblast Differentiation and Modulates Energy Metabolism**

Metabolites 2021 Apr 22;11(5):258.

CHAPTER 1

Reduced EGFR Level in eIF2α Phosphorylation–deficient Hepatocytes is Responsible for Susceptibility to Oxidative Stress

Abstract

Reactive oxygen species (ROS) play a significant role in intracellular signaling and regulation, particularly when they are maintained at physiologic levels. However, excess of ROS can cause cell damage and induce cell death. I recently reported that eIF2α phosphorylation protects hepatocytes from oxidative stress and liver fibrosis induced by fructose metabolism. Here, I found that hepatocyte-specific eIF2α phosphorylation-deficient mice have significantly reduced expression of the EGF receptor (EGFR) and altered EGFR-mediated signaling pathways. EGFR-mediated signaling pathways are important for cell proliferation, differentiation, and survival in many tissues and cell types. Therefore, I studied whether the reduced amount of EGFR is responsible for the eIF2α phosphorylation-deficient hepatocytes' vulnerability to oxidative stress. Reactive oxygen species (ROS) such as hydrogen peroxide and superoxides induce both EGF receptor tyrosine phosphorylation and eIF2α phosphorylation. eIF2α phosphorylation-deficient primary hepatocytes, or EGFR knockdown cells, have decreased ROS scavenging ability compared to normal cells. Therefore, these cells are particularly susceptible to oxidative stress. However, overexpression of EGFR in these eIF2α phosphorylation-deficient primary hepatocytes increased ROS scavenging ability and alleviated ROS-mediated cell death. Therefore, I hypothesize that the reduced EGFR level in eIF2α phosphorylation–deficient hepatocytes is one of critical factors responsible for their susceptibility to oxidative stress.

Introduction

The epidermal growth factor receptor (EGFR), or ErbB1 receptor (ErbB1), is one of four members of the ErbB family of tyrosine kinase receptors. ErbB1 is expressed in various tissues and mediates cell proliferation, differentiation, migration and survival through various signaling pathways [1]. When a ligand such as epidermal growth factor (EGF) [2] binds to the EGFR receptor, it forms homo- and hetero-dimers with all four family members [1, 2]. Ligand-activated EGFR proteins are auto-phosphorylated and cross-phosphorylated at multiple tyrosine residues (such as Y1068), which are located in the C-terminal non-catalytic sequence [3]. The autophosphorylated tyrosine residues are believed to serve as docking sites for a variety of signaling molecules (such as Src homology 2) that contain phosphotyrosine-binding domains [3, 4]. Subsequently, the activated EGFR triggers the following four main downstream signaling pathways: the PI3K/Akt pathway, the phospholipase C-gamma (PLC-γ)/protein kinase C (PKC) pathway, the ras/raf/MEK/MAPK pathway [comprised of the activation of extracellular signal-regulated kinase (ERK) and JUN N-terminal kinase (JNK)], and the signal transducers and activators of transcription (STATs) pathway [5-7]. The four signaling pathways collectively control cell proliferation, differentiation, migration, and survival.

Apart from ligand-dependent EGFR tyrosine activation, accumulating evidence has shown that reactive oxygen species (ROS) are involved in another mechanism of EGFR transactivation [8-13]. Diverse modes of EGFR activation have been suggested in which ROS are directly or indirectly involved in EGFR transactivation [12, 14]. First, ROS directly modulate a specific cysteine residue (Cys797) within the EGFR kinase domain that is associated with increased tyrosine kinase activity [15]. Next, the ROS induce oxidation of reduction-oxidation targets, such as protein tyrosine (Tyr) phosphatases (PTPs), to enhance EGFR Tyr phosphorylation [16]. Finally, ROS induce cysteine oxidation within Src and ADAM17, which results in their activation and further EGFR transactivation [17].

ROS-involved EGFR transactivation can initiate multiple signaling pathways that are similar to ligand-dependent EGFR tyrosine activation. Ultimately, this signaling helps to protect cells against oxidative stress. Oxidative stress activates AKT via the EGFR/PI3K-dependent pathway in a number of cell types [18]. After activation of the EGFR/PI3K-dependent pathway, the PI3K/Akt pathway inhibits glycogen synthase kinase 3β (GSK-3β) and thereby induces nuclear translocation of nuclear factor erythroid 2-related factor 2 (Nrf2) [19, 20]. Nuclear factor erythroid 2-related factor 2 subsequently induces the expression of an array of ROS-detoxifying enzymes and stimulates the production of antioxidants, including GSH [20]. Activated AKT also phosphorylates and inactivates components of the cell death machinery including Bax, Bad and caspase 9 [21, 22]. Activated AKT also regulates the activity of FOXO3, which is a member of the Forkhead family of transcription factors that induces genes necessary for cell death [21, 23]. Therefore, AKT increases the cell's antioxidant capacity and thereby promotes cell survival under oxidative stress in transcription-independent and/or dependent manners. Next, it has been previously shown that H_2O_2-induced EGFR transactivation increases PLC-γ1-mediated pro-survival function. Genetic ablation and pharmacological inhibition of PLC-γ1 enhances a cell's susceptibility to hydrogen peroxide-induced cell death; however, it is not clear how activated PLC-γ1 mitigated the cellular oxidative damage [24-26]. Oxidative stress also triggers the phosphorylation of STAT proteins (STAT1, STAT3 and STAT5), which can induce genes that control cell growth and survival [27-29]. During oxidative stress, EGFR transactivation is transferred by Janus kinases 1 and 2 (JAK1/2) or c-Src to STAT-1/3 and STAT-5. JAK1/2 and c-Src kinases modulate STATs activation in at least the following two ways: (1) by direct phosphorylation of STATs; and (2) by phosphorylating the EGFR at Y845.

Eukaryotic translation initiation factor 2 alpha (eIF2α) is a subunit of the trimeric eIF2 complex that is involved in the initiation step of cap-dependent mRNA translation [30]. The eIF2 complex delivers the initiator methionyl-tRNA (Met-tRNAi) to the ribosome during

translation initiation of cytoplasmic mRNAs in eukaryotic cells. Mammalian cells respond to various forms of physiological or pathological stress (such as hypoxia, amino acid deprivation, glucose deprivation, viral infection, endoplasmic reticulum (ER) stress, and oxidative stress) by blocking the translational initiation process through phosphorylation of eIF2α at Serine 51. Such stresses are sensed by the four mammalian eIF2α protein kinases: PERK, GCN2, PKR, and HRI, which respond to distinct stimuli [31, 32]. However, it has been reported that oxidative stress also activates multiple eIF2α kinases (including PERK, PKR and GCN) and regulates the eIF2 complex through eIF2α phosphorylation [33, 34]. Therefore, several groups, including ours, have reported that genetic loss of the eIF2α kinases or eIF2α phosphorylation make cells susceptible to death by oxidative stress [33-37]. In addition, I recently suggested that fructose diet-induced hepatocyte death results from a diminished antioxidant capacity in hepatocyte-specific eIF2α phosphorylation deficient mice [37]. However, I did not identify the upstream signaling pathways whose activation in response to oxidative stress may play important roles in maintaining the antioxidant capacity and alleviating oxidative hepatocyte damage. Here, I report that hepatocyte-specific eIF2α phosphorylation-deficient mice have significantly reduced expression of the EGF receptor (EGFR) and altered EGFR-mediated signaling pathways. Both the EGF receptor and EGFR-mediated signaling pathways are required for a cell to appropriately defend against oxidative stress. Therefore, EGFR knockdown cells have decreased ROS scavenging ability and aggravated oxidative stress-mediated cell death. Conversely, enhanced expression of EGFR increased ROS scavenging ability and alleviated ROS-mediated cell death in eIF2α phosphorylation-deficient primary hepatocytes. Therefore, those results suggest that a decreased EGFR level partially explains the susceptibility of eIF2α-phosphorylation-deficient hepatocytes to ROS.

Materials and Methods

Animals and in vivo EGF treatment

S/A;fTg/0 (*Cont.*) and *A/A;fTg/0;Cre^{Hep}/0* (*A/A^{Hep}*) mice have been previously described [37]. The animals were housed with 12 h light and 12 h dark cycles and provided with standard rodent chow (Purina; Cargill Inc., USA) and water ad libitum. All animal care and procedures were conducted according to the protocols and guidelines approved by the University of Ulsan Animal Care and Use Committee (UOUACUC) (No. SHB-17-010).

The *Cont.* and *A/A^{Hep}* mice fasted for 12 hours prior to in vivo EGF-mediated EGFR stimulation. After anesthesia was induced, the mice received 0.9% saline or 0.9% saline containing recombinant murine EGF (PeproTech, Korea, 0.5 μg/g of body weight) via the vena cava. The liver was removed 5 minutes after this injection. The specimens were frozen and stored at -80 °C until homogenization.

Quantitative RT-PCR

Total RNAs were isolated from liver tissues by using the Trizol reagent (Life Technologies, USA). cDNA was prepared with a High Capacity cDNA RT kit (Ambion, USA) for quantitative real-time (qRT)-PCR. qRT-PCR was carried out using the SYBR green PCR master mix (Bio-Rad, USA) with the appropriate primers on a StepOnePlus™ Real Time System (Applied Biosystems, USA). The specificity of each primer pair was confirmed by using melting curve analysis. The housekeeping *β-actin* gene was amplified in parallel with the *EGFR* gene. Relative copy numbers, compared to the *β-actin* gene, were calculated using $2^{-\Delta\Delta Ct}$. The primer sequences used were as follows: 5'-AGGACTGGGCAATCTGTTGGA-3' and 5'-GAAGATCGAAGACCTGGTGCTGTAA-3' (*EGFR*); 5'-GATCTGGCACCACACACCTTCT-3' and 5'- GGGGTGTTGAAGGTCTCAAA-3' (*β-actin*).

Western blot analysis and antibodies

Liver tissues and cells were homogenized in Nonidet P40 lysis buffer (1% NP40, 50 mM Tris-Cl pH 7.5, 150 mM NaCl, 0.05% SDS, 0.5 mM Na-vanadate, 100 mM NaF, 50 mM β-glycerophosphate, 1 mM PMSF) that was supplemented with Halt Protease Inhibitor Cocktail (Thermo Fisher Scientific). The homogenates were centrifuged at 12,000 g for 15 min at 4°C, and the supernatants were collected. The liver lysates or cell lysates were used for Western

blotting, as described [37]. The following were purchased from Sigma-Aldrich: α-Tubulin (T5168), β-Actin (A5441), Flag (F1804). The following were purchased from Santa Cruz Biotechnology: eIF2α (SC-133132), STAT3 (SC-482), STAT5 (SC-835). The following were purchased from Cell Signaling Technology: Phospho-EGFR (Y1068) (#3777), AKT (#4691), Phospho-AKT (S473) (#4060), ERK (#4695), Phospho-ERK (T202/Y204) (#4407), Phospho-STAT3 (Y705) (#4113), Phospho-STAT5 (Y694) (#9314). The following were purchased from Merck Milipore: EGFR (06-847). The following were purchased from Abcam: P-eIF2α (S31) (ab32157). The secondary peroxidase-conjugated antibodies were purchased from Thermo Fisher Scientific or Jackson ImmunoResearch.

Chemicals

Dichlorodihydrofluorescein diacetate (DCF-DA) was purchased from Thermo Fisher Scientific. The following were purchased from Sigma-Aldrich: crystal violet, parformaldehyde, polybrene (Hexadimethrine bromide), hydrogen peroxide, menadione, propidium iodide (PI), Hoechst 33258, 4′,6-diamidino-2-phenylindole (DAPI), dihydroethidine hydrochloride (DHE), and N-acetyl-L-cysteine (NAC).

Preparation of primary hepatocytes

The primary mouse hepatocytes were obtained as has been described previously [37]. The isolated primary hepatocytes were inoculated on collagen-coated plates with/without round coverslips (5×10^5 cells/well in 6-well plates), and cultured in high glucose-DMEM (WelGENE) medium containing 10% FBS (WelGENE), and 1% penicillin/ streptomycin (WelGENE). The medium was replaced with FBS-free DMEM media 2 h after plating. The hepatocytes were incubated for another 12 h before the experimental treatment.

Cell lines and Cell culture

Immortalized embryonic hepatocytes were cultured in Medium 199 (WelGENE, Korea) that was supplemented with 10% fetal bovine serum (WelGENE) and 1% penicillin-streptomycin (WelGENE), as previously described [38]. AML12 muse normal hepatocytes were obtained from the American Type Culture Collection (ATCC). The cells were cultured in DMEM/F12 (WelGENE) that was supplemented with 10% fetal bovine serum (WelGENE), 100 nM dexamethason (Sigma-Aldrich), 1% insulin-transferrin-selenium-pyruvate supplement (ITSP,

WelGENE), and 1% penicillin-streptomycin (WelGENE). The Lenti-X™ 293T Cell Line (CLONTECH, USA) was cultured in DMEM (WelGENE) containing 10% fetal bovine serum (WelGENE) and 1% penicillin-streptomycin (WelGENE).

Generation of *EGFR* knockdown cell lines

The five MISSION shRNA clones of mouse EGFR (NM_007912.1; a protein of 1210 amino acids) that were inserted into the pLKO.1 vector (TRCN0000023479 to TRCN0000023483) were purchased from Sigma-Aldrich. A negative control (NC) shRNA sequence that was cloned into the pLKO.1 vector was included as a control. Each pLKO.1 shRNA construct was cotransfected with the Lenti-X™ Packaging Single Shots (VSV-G) (CLONTECH) into the Lenti-X™ 293T cells. The lentiviral particles were produced according to the manufacturer's instructions. The immortalized embryonic hepatocytes and AML12 cells were infected with recombinant lentiviruses in the presence of polybrene (8.0 μg/ml) for 2 days. Next, the hepatocytes were cultured with fresh complete media containing puromycin (1.0 μg/ml for hepatocyte and 0.75 μg/ml for AML12) for 3–4 weeks to select for *EGFR* knockdown cells. The EGFR expression level was routinely tested by using Western blot. I chose immortalized embryonic hepatocytes that stably expressed the *EGFR* shRNA targeting the sequence GCTTTCGAGAACCTAGAAATA (TRCN0000023483, referred to as shEGFR-83), or AML12 cells that stably expressed the *EGFR* shRNA targeting the sequence CCTGTCCAACTATGGGACAAA (TRCN0000023481, referred to as shEGFR-81) for further experiments.

Production of recombinant adenovirus expressing mouse EGFR-Flag

The C-terminal Flag tagged mouse epidermal growth factor receptor (mEGFR-Flag) expression vector pCMV3-mEGFR-Flag was purchased from Sino Biological. The pShuttle-CMV-mEGFR-Flag vector was then constructed by inserting the cDNA fragment encoding mEGFR-Flag from the pCMV3-mEGFR-Flag treated with *Bgl II-Fill in-Not I* into the pShuttle-CMV treated with *Hind III-Fill in-Not I*. The AdEasy vector system was used to generate the mEGFR-Flag expressing recombinant adenovirus according to the manufacturer’s instructions (Agilent Technologies, USA). In brief, the shuttle vector was then electrophoresed into BJ5183 cells that contained the adenoviral vector Adeasy to generate a recombinant adenoviral plasmid. The recombinants were amplified in HEK-293A cells and purified by CsCl (Sigma-Aldrich) gradient centrifugation. Viral preparations were collected and desalted, and

titers were determined by using the AdEasy Viral Titer Kit (Agilent Technologies) according to the manufacturer's instructions. The efficiency of adenoviral infection was assessed by immunofluorescence detection of the C-terminal Flag tag of mEGFR.

Cell viability and death analysis

Cell viability analysis by using crystal violet was performed as has been previously described with slight modifications [39]. In brief, the drug-treated cells were washed twice with cold PBS. The cells were stained with crystal violet solution (0.625 g of crystal violet dissolved in a solution containing 50 ml of 37% paraformaldehyde and 450 ml of methanol) for 4 min at room temperature. The stained cells were washed three times in tap water, and the plates were allowed to dry. Microscopic images of the stained cells were taken with a Primovert inverted microscope (Zeiss) equipped with an Axiocam ERc 5s camera. The cells were then lysed with 1% SDS solution, and dye uptake was measured at 550 nm by using a microplate reader (SpectraMax iD3, Molecular Devices, USA).

Cell death analysis using propidium iodide (PI) and Hoechst 33258 were performed as previously described [37]. The drug-treated cells on the coverslips were double-stained with PI (1 μg/ml) and Hoechst 33258 (1 μg/ml), and fixed with 3.5% (w/v) paraformaldehyde at room temperature for 15 min. The coverslips were then mounted on glass slides for observation under fluorescence microscopy (Olympus microscope). At least 500 cells were counted. A quantitation of dead cells (apoptotic and necrotic cells) was expressed as a percentage of total cells counted.

Microscopy and image analysis

Intracellular ROS levels were measured by using confocal microscopy using the fluorescent probes DHE or DCF-DA, as described previously [37]. The drug-treated primary hepatocytes and immortalized hepatocytes were plated on collagen coated 35 mm coverglass bottom dishes (SPL, Korea) and cultured overnight. The next day, the cells were treated with the indicated chemicals. After treatment, the cells were stained with DHE (15 μM) or DCF-DA (15 μM) in phenol red-free culture medium for 30 min. Fluorescence images of the living cells were obtained using an FV1200-OSR confocal laser microscope (Olympus, Tokyo, Japan).

For the immunofluorescence detection of mEGFR-Flag proteins, immortalized embryonic hepatocytes (2×10^5) were plated on 6-well plates coated with 0.01% collagen in PBS and cultured overnight. The next day, the cells were infected with adenovirus encoding mEGFR-Flag (Ad-mEGFR-Flag) at a multiplicity of infection of 100 for 12 hrs. The cells were

then fixed with 4% paraformaldehyde in PBS for 15 min, and permeabilized with 0.1% Triton X-100 in PBS for 4 min. The cells were blocked with 3% bovine serum albumin in PBS for 30 min, and incubated with the indicated primary antibody overnight at 4°C. The cells were further incubated with a Tetramethylrhodamine (TRITC)-conjugated secondary antibodies at room temperature for 1 h. The nuclei were stained with DAPI (Sigma-Aldrich). Finally, the cells were observed by confocal laser microscopy by using an FV1200-OSR microscope. The scale bars (μm) have been inserted into the microscopic images.

Statistical analysis

Experiments were repeated three times in each case. The data were analyzed using GraphPad Prism 5 (GraphPad Software, Inc, USA). Unpaired 2-tailed Student's *t*-tests were performed to determine the statistical significance of the paired samples. $P<0.05$ was considered statistically significant. Error bars represent the standard error of the mean (SEM) in every case.

Results and Discussion

The hepatocyte-specific eIF2α phosphorylation-deficient mouse model has reduced EGFR expression and altered EGF/EGFR-mediated signaling pathways

The mRNA levels of EGFR (or the ErbB1 receptor) were diminished to ~40% in the liver tissues of hepatocyte-specific eIF2α phosphorylation (P-eIF2α)-deficient mice (Fig. 1A). Similarly, the levels of the EGFR (~60%) and phosphorylated EGFR (P^{Y1068}-EGFR, ~30%) proteins were significantly reduced in P-eIF2α deficient liver tissues (Figs. 1B and 1C).

In order to examine the effect of decreased EGFR in intact livers, starved control and A/A^{Hep} mice were injected with either saline or recombinant EGF. Five minutes after this injection, the livers were harvested from the saline- and EGF-treated animals. I analyzed the EGF/EGFR signaling pathways using Western blots with total liver tissue lysates. In agreement with previous studies done in cell culture [40-42] and animal livers [43-45], starvation abolished phosphorylation of the following targets in the liver tissues of all saline-treated animals: EGFR at Tyr1068; the EGF/EGFR-downstream targets AKT at Ser473; STAT3 at Tyr705; STAT5 at Tyr694; and ERK at Thr202/Tyr204 (Figs. 2A~2E). However, the EGF treatments rapidly induced EGFR phosphorylation in the livers of both starved *control* and A/A^{Hep} mice. However, the EGFR phosphorylation levels of A/A^{Hep} livers were significantly lower than were those in the control livers. This difference is explained by a reduced level of EGFR protein in A/A^{Hep} livers compared to that in the control livers (left graph in Fig. 2A). With the exception of ERK phosphorylation (Fig. 2E), the phosphorylation levels of AKT, STAT3, and STAT5 were also significantly lower in A/A^{Hep} livers than they were in control livers (Figs. 2B~2D). These data suggest that eIF2α phosphorylation may be required to keep the EGFR expression level normal, and to maintain activity of the EGF-dependent EGFR signaling pathways in hepatocytes.

eIF2α phosphorylation-deficient primary hepatocytes are susceptible to oxidative stress

Several groups have reported that EGFR can be activated by oxidative stress [8-13, 18] (Fig.3). In contrast, the inhibition or genetic disruption of EGFR is involved in induction of oxidative stress and cytotoxicity *in vitro* and *in vivo* [46, 47]. Previous report suggests that eIF2α phosphorylation protects hepatocytes from oxidative stress [37]. Therefore, I measured the ROS-scavenging activity and oxidative stress-mediated cell death in P-eIF2α-deficient primary hepatocytes. I compared these features to those of control hepatocytes. There was no significant difference between the *Cont.* and *A/A*^{Hep} hepatocytes (under mock conditions) with regard to the microscopic evaluation of dihydroethidium (DHE) fluorescence in the detection of superoxides (Fig. 4A). However, when accumulated ROS levels were compared in menadione (Men) or hydrogen peroxide (H_2O_2)-treated conditions, the DHE fluorescence intensities were significantly higher in the *A/A*^{Hep} hepatocytes than they were in the *Cont.* although treatment with antioxidant N-acetylcysteine (NAC) removed the difference (Fig. 4A), suggesting that P-eIF2α-deficient primary hepatocytes have reduced ROS-scavenging activity than do control hepatocytes. I next investigated the influence of eIF2α phosphorylation on Menadione or H_2O_2-induced cell death. Menadione or H_2O_2 treatment reduced the number of crystal violet stained cells in a dose-dependent manner (Fig. 4B). However, menadione or H_2O_2 treatment caused larger reductions in the cell viability of eIF2α phosphorylation-deficient *A/A*^{Hep} hepatocytes than it did in control cells (Fig. 4B). Cell death analysis was performed using the Hoechst 33258/propidium iodide (PI) staining procedure. The *A/A*^{Hep} hepatocytes also demonstrated more cell death than did the control hepatocytes in menadione or H_2O_2 treated conditions (Fig. 4C). Therefore, eIF2α phosphorylation-deficient primary hepatocytes were more susceptible to oxidative stress (than were control cells) because of reduced ROS-scavenging activity.

EGFR knockdown reduces ROS-scavenging activity and increases vulnerability to oxidative stress

I previously showed that vulnerability to oxidative stress in *A/A*^{Hep} primary hepatocytes is related to decreasing EGFR protein levels. Therefore, I knocked down the EGFR gene in both immortalized mouse embryonic hepatocyte cell lines [37, 38] (Fig.6), and in the mouse hepatocyte cell line AML12 (Fig.7). I then assessed these cells with regard to their ROS-scavenging activity and ROS-mediated cell death. First, I observed the concentrations and time-dependent changes of EGFR and eIF2α phosphorylation in both cell lines (Fig.3). With regard to menadione and H_2O_2 treatments in immortalized hepatocytes, the activation of eIF2α phosphorylation was rapid and persistent in all tested conditions (of differing concentrations and times) (Fig. 3A and 3C). However, the induction of eIF2α phosphorylation in the drug-treated AML12 cells was observed after 2 hours of treatment, but not at any other time points (Fig. 3B and 3D). The EGFR phosphorylation gradually increased in a concentration- and time-dependent manner during drug treatment (Fig. 3A~3C), except for the time-dependent treatments in AML12 cells (Fig. 3D). Similar to eIF2α phosphorylation, the EGFR phosphorylation was the highest after 2 hours of treatment. After this, the EGFR phosphorylation progressively decreased at increased treatment times in AML12 cells (Fig. 3D). Therefore, these results indicate that oxidative stressors induce EGFR and eIF2α phosphorylation in a similar concentration- and time-dependent manner. However, there is no evidence that eIF2α phosphorylation regulates that of EGFR yet.

Next, in order to examine whether the level of EGFR expression can affect a cell's antioxidant capacity, I established EGFR knockdown cell lines. These knockdown cell lines were created by transducing EGFR targeting shRNA-expressing lentiviruses and following puromycin selection in both immortalized mouse embryonic hepatocytes (Fig. 6A) and AML12 cells (Fig. 7A). Among the established EGFR knockdown cell lines, the cell lines with the lowest expression of EGFR protein were chosen for further experiments. These included the

shEGFR-83 cell line for immortalized hepatocytes (Fig. 6A) and the shEGFR-81 cell line for AML12 cells (Fig. 7A). In order to assess the ROS-scavenging activity of the EGFR knockdown cell lines, the levels of accumulated ROS were compared to the fluorescence intensity of an oxidant-sensing probe DCF-DA in H_2O_2-treated shNC control or shEGFR-83 cell lines. Under H_2O_2-treated conditions, the fluorescence intensity of shEGFR-83 cells was significantly higher than that of shNC control cells (Fig. 6B). However, there was no significant difference in the fluorescence intensity between them before H_2O_2 treatment or after H_2O_2 and N-acetyl-L-cysteine (NAC) co-treatment. In addition, the fluorescent microscopic examination of menadione-treated cells (using a superoxide indicator dihydroethidium (DHE)) revealed that DHE fluorescence in the EGFR knockdown cells (shEGFR) was stronger than that in shNC control cells (Fig. 6C). These results indicate that EGFR protein levels are important to maintain a cell's hydrogen peroxide- or superoxide-scavenging activity.

Having observed that EGFR knockdown cells have reduced ROS-scavenging activity, I next examined whether knockdown of EGFR increases a cell's vulnerability to oxidative stress. To do so, I applied the crystal violet assay and Hoechst 33258/propidium iodide (PI) staining analysis to compare cell death between EGFR knockdown cells and controls (Fig. 6D and 6E, Fig. 4A and 4B, and Fig. 7). As expected, the crystal violet assay showed that the shEGFR-83 cells had poorer cell viability than did shNC control cells under menadione or H_2O_2 treatment although the cell viability of shNC control cells was also reduced in a dose-dependent manner in these treatments. However, the levels in the shEGFR-83 cells were similar to those in shNC control cells in NAC-treated conditions. The cell death analysis (using the Hoechst 33258/propidium iodide (PI) staining procedure) also revealed that shEGFR-83 cells had a higher rate of cell death than did the shNC control cells in menadione or H_2O_2 treated conditions (Fig. 6E). However, the levels in the shEGFR-83 cells were similar to those in shNC control cells in NAC-treated conditions. I obtained similar results in the shEGFR-81 cell line of AML12 cells (Fig. 7B and 7C). The shEGFR-81 cells were more susceptible to

menadione- or H_2O_2-mediated oxidative stress than were shNC control cells. These cell death analyses suggested that the EGFR protein is important to alleviate oxidative stress-mediated cell death. Collectively, those experiments suggest that attenuated EGFR expression reduces cellular ROS-scavenging activity, which then increases cells' vulnerability to oxidative stress.

EGFR overexpression increases ROS-scavenging activity and alleviates ROS-mediated cell death in eIF2α phosphorylation-deficient primary hepatocyte

I next investigated whether transient enforced expression of EGFR in p-eIF2α deficient primary hepatocytes can increase cellular ROS-scavenging activity and therefore reduce their sensitivity to oxidative stress. Primary hepatocytes purified from livers of hepatocyte specific p-eIF2α deficient (A/A^{Hep}) mice were infected with C-terminal Flag-tagged EGFR expressing recombinant adenovirus (Ad-EGFR-Flag) or control adenovirus (Ad-Vec). As expected, immunofluorescence analysis against anti-Flag antibody demonstrated that EGFR-Flag proteins were expressed in almost all A/A^{Hep} primary hepatocytes infected by Ad-EGFR-Flag, but not in those infected by Ad-Vec (Fig. 9A). Therefore, Western blot analysis showed that the total amount of EGFR proteins was strongly higher in the Ad-EGFR-Flag infected cell lysates than it was in the Ad-Vec infected cell lysates (Fig. 9B). I next examined whether the enforced expression of EGFR can upregulate cellular ROS-scavenging activity in p-eIF2α deficient (A/A^{Hep}) primary hepatocytes. Microscopic observation of dihydroethidium (DHE) fluorescence revealed that there was no significant difference in the fluorescence intensity between Ad-Vec infected hepatocytes and Ad-EGFR-Flag infected hepatocytes under mock conditions (Fig. 9C). However, when the accumulated ROS levels were compared in menadione (Men) or hydrogen peroxide (H_2O_2)-treated conditions, the DHE fluorescence intensities were significantly lower in the Ad-EGFR-Flag infected hepatocytes than in the Ad-Vec infected hepatocytes. The levels in the Ad-EGFR-Flag infected hepatocytes were similar to those in NAC-treated hepatocytes (Fig. 9C). These findings suggest that the enforced

expression of EGFR potentiates cellular ROS-scavenging activity of p-eIF2α deficient (*A/A*^{Hep}) primary hepatocytes. In line with these results, the enforced expression of EGFR increased cell viability in menadione (Men) or hydrogen peroxide (H_2O_2)-treated *A/A*^{Hep} primary hepatocytes (Fig. 9D and Fig. 8). Moreover, the EGFR-Flag expressing *A/A*^{Hep} primary hepatocytes demonstrated less cell death than did the *A/A*^{Hep} primary hepatocytes under oxidative stress conditions (Fig. 9E). Based on these observations, I conclude that EGFR proteins are required to maintain ROS-scavenging activity in hepatocytes. These proteins are also important to attenuate oxidative stress-mediated cell death.

In this study, I showed that hepatocyte-specific eIF2α phosphorylation-deficient mice have significantly reduced expression of the EGF receptor (EGFR) and altered EGFR-mediated signaling pathways. Moreover, the eIF2α phosphorylation–deficiency or reduced expression of the EGFR decreased ROS-scavenging activity and increased ROS-mediated cell death in hepatocytes. However, the drawbacks were alleviated by enforced expression of EGFR in p-eIF2α deficient primary hepatocytes. Therefore, I concluded that reduced EGFR level in eIF2α phosphorylation–deficient hepatocytes is one of critical factors responsible for a cell's susceptibility to oxidative stress. Furthermore, vulnerability to oxidative stress in hepatocytes that have reduced EGFR level or EGFR activity might be the underlying mechanism of hepatotoxicity induced by several EGFR inhibitors (e.g., erlotinib, lapatinib, and gefitinib) used for the treatment of non-small cell lung cancer and pancreatic cancer [48, 49], since most EGFR inhibitors undergo intense metabolism by cytochrome P450 enzymes in hepatocytes [50, 51] which produces reactive metabolites [52]. However, further studies are required to verify whether the hepatotoxicity is related to oxidative stress susceptibility in EGFR inhibitor-treated hepatocytes.

.

Figures

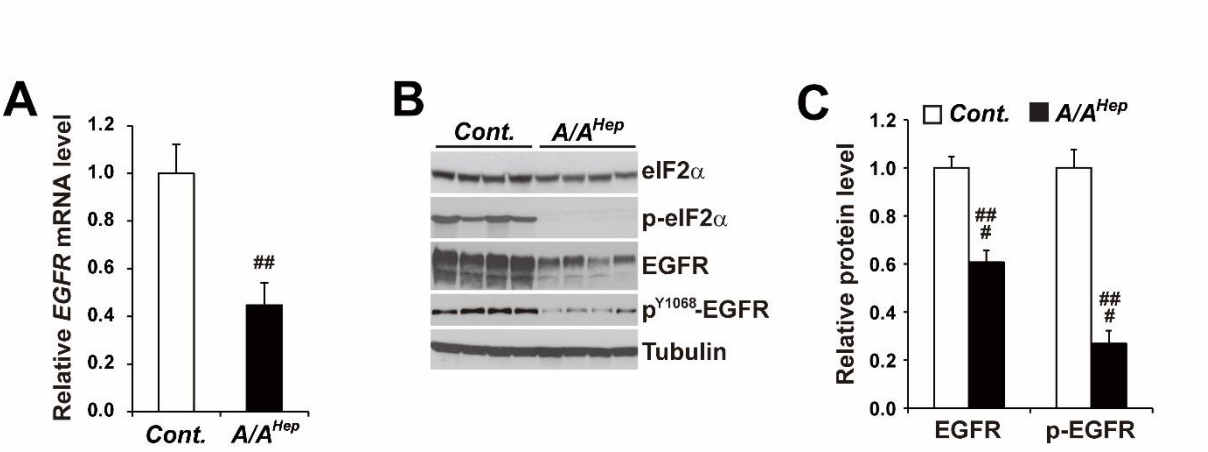

Figure. 1. Expression levels of EGFR mRNA and protein are reduced in liver tissues of hepatocyte-specific eIF2α phosphorylation-deficient mice.

(A) Quantitative real-time PCR analysis of the expression of *Egfr* mRNAs in liver tissues from 3-month-old *Cont.* and *A/A*^{Hep} mice. Data are expressed as means ± SEM (n = 6 mice per group); $^{\#\#}p < 0.01$; *Cont.* vs *A/A*^{Hep}. (B) Western blot analysis of eIF2α, p-eIF2α, EGFR, p-EGFR, and tubulin in liver tissues from 3-month-old *Cont.* and *A/A*^{Hep} mice. The efficiency of deletion of *floxed eIF2α fTg* by Cre recombinase in *A/A*^{Hep} livers was determined based on the existence of phosphorylated eIF2α proteins [37]. (C) Densitometric quantification of EGFR and p-EGFR protein expression levels in (B). Values were normalized against tubulin levels. Data are expressed as means ± SEM (n = 4 mice per group); $^{\#\#\#}p < 0.001$; *Cont.* vs *A/A*^{Hep}.

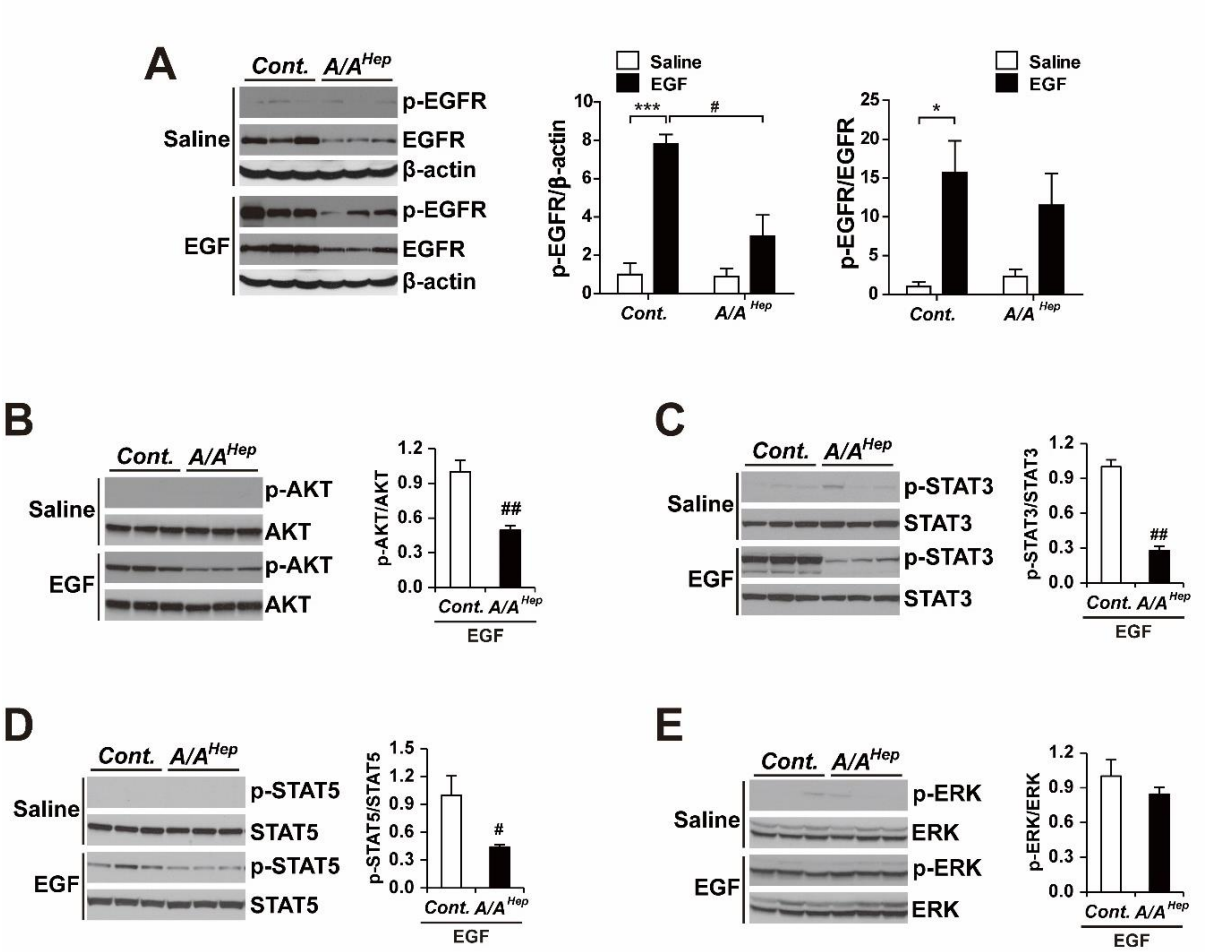

Figure. 2. EGFR signaling pathways are altered in liver tissues of hepatocyte-specific eIF2α phosphorylation-deficient mice.

For EGFR signaling pathway analysis, fasted and anesthetized *Cont.* and *A/A^{Hep}* mice were administered saline or recombinant murine EGF (0.5 μg/g) via the vena cava. The livers were removed five minutes after this injection. The liver lysates were subjected to SDS-PAGE, followed by immunoblot analyses using antibodies specific for p-EGFR, EGFR, p-eIF2α, eIF2α and β-actin in (A), p-AKT and AKT in (B), p-STAT3 and STAT3 in (C), p-STAT5 and STAT5 in (D), and p-ERK and ERK in (E). The ratios of p-EGFR/ β-actin and p-EGFR/EGFR in (A), p-AKT/AKT in (B), p-STAT3/STAT3 in (C), p-STAT5/STAT5 in (D), and p-ERK/ERK in (E) were densitometrically quantified. Data are expressed as means ± SEM (n = 3 mice per group); *p < 0.05 and ***p < 0.001; Saline vs EGF and $^{\#}$p < 0.05 and $^{\#\#}$p < 0.001; *Cont.* vs *A/A^{Hep}*.

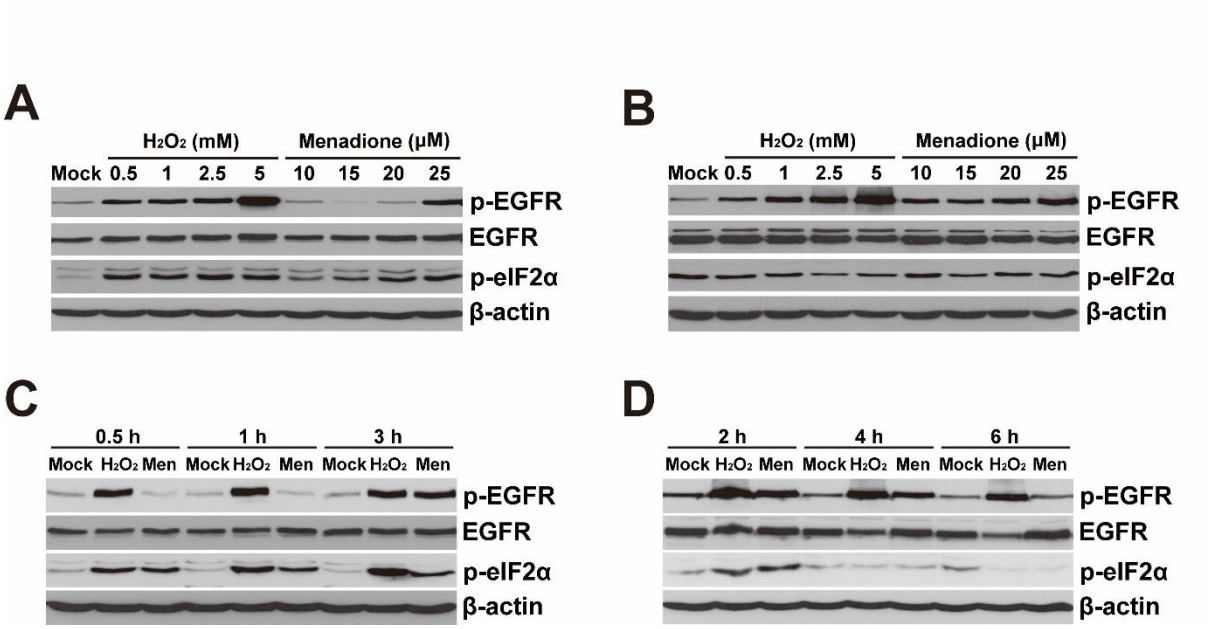

Figure 3. Concentration and time-dependent change of EGFR and eIF2α phosphorylation against reactive oxygen species.

(A, B) Immortalized embryonic hepatocytes (A) and AML12 cells (B) were treated with hydrogen peroxide (H_2O_2) or menadione at indicated concentration for 6 hrs. (C, D) The immortalized embryonic hepatocytes (C) and AML12 cells (D) were treated with hydrogen peroxide (2.5 mM) or menadione (20 μM) for the indicated times. The cell lysates were subjected to SDS-PAGE, followed by immunoblot analyses using antibodies specific for p-EGFR, EGFR, p-eIF2α, eIF2α, and β-actin.

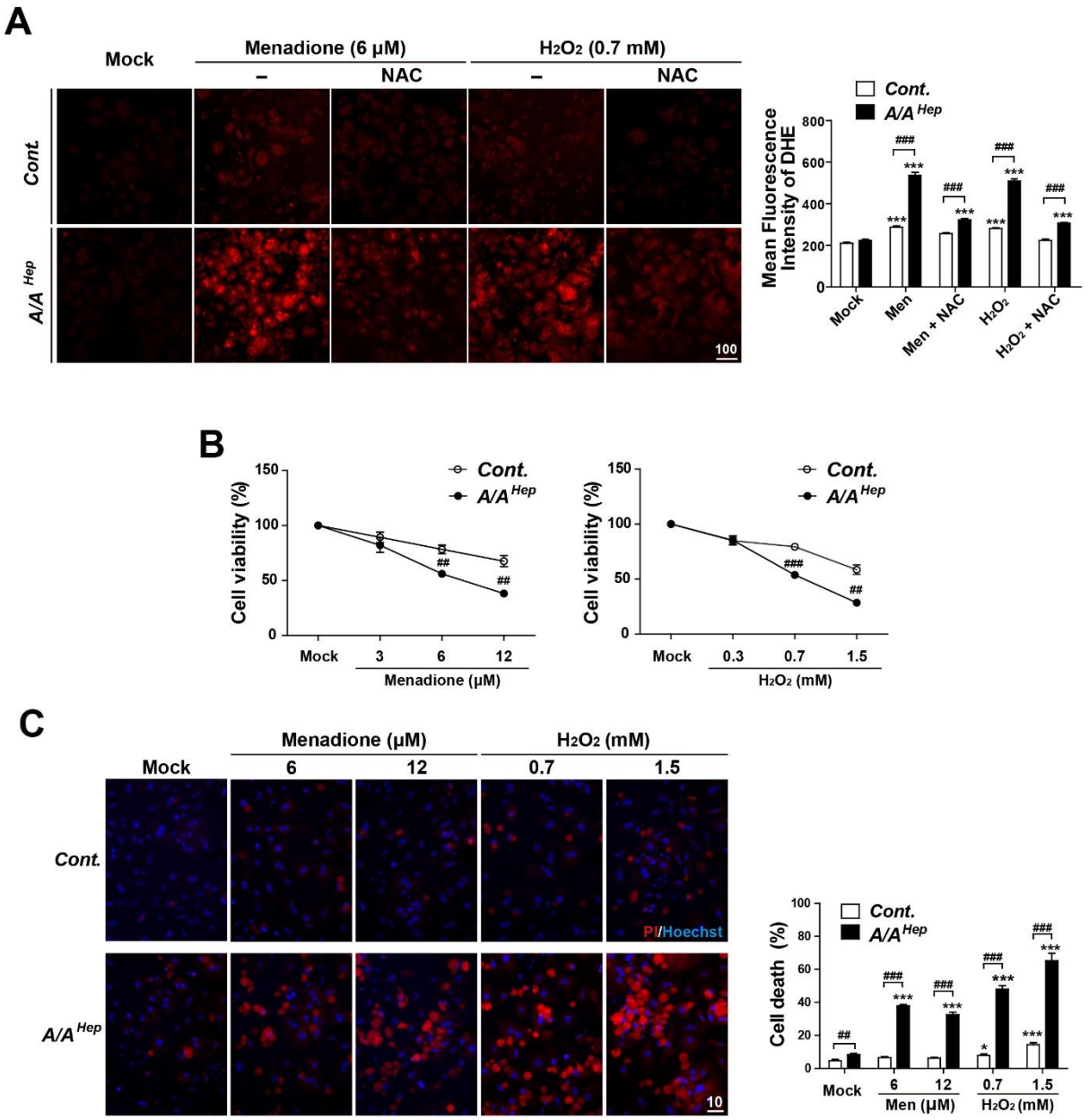

Figure 4. eIF2α phosphorylation-deficient primary hepatocyte has reduced ROS-scavenging activity, which may increase vulnerability to oxidative stress.

(A) Primary hepatocytes isolated from *Cont.* and *A/A*^{Hep} mice were treated with menadione (6 μM), menadione (6 μM) plus N-acetylcysteine (NAC, 1 mM), hydrogen peroxide (H_2O_2, 0.7 mM), or hydrogen peroxide (H_2O_2, 0.7 mM) plus N-acetylcysteine (NAC, 1 mM) for 16 hrs. Accumulated intracellular ROS were observed by fluorescence microscopy of cells stained with dihydroethidium (DHE), reflecting ROS levels. The representative images are shown (scale bar = 100 μm). For graphs, the mean fluorescence intensities (MFI) of DHE staining were measured using image analysis software. The data are expressed as means ± SEMs of

three independent experiments. ***p < 0.001; Mock vs Chemicals in the same genotype, $^{###}$p < 0.001; *Cont.* vs *A/A^{Hep}.* (B) Primary hepatocytes isolated from *Cont.* and *A/A^{Hep}* mice were treated with menadione or hydrogen peroxide (H_2O_2) at indicated concentrations for 30 hrs. The cell viability was determined using the crystal violet assay. The data are expressed as means ± SEMs of three independent experiments. $^{##}$p < 0.01 and $^{###}$p < 0.001; *Cont.* vs *A/A^{Hep}*. (C) The primary hepatocytes isolated from *Cont.* and *A/A^{Hep}* mice were treated with menadione or hydrogen peroxide (H_2O_2) at indicated concentrations for 24 hrs. Cell death (apoptotic and necrotic cells) was determined by double staining with Hoechst 33258 and propidium iodide (PI). Representative images are shown (scale bar = 10 μm). At least 500 cells were counted. Cell death is expressed as a percentage of total cells. The data are expressed as means ± SEMs of three independent experiments. *p < 0.05 and ***p < 0.001; Mock vs Chemicals in the same genotype, $^{##}$p < 0.01 and $^{###}$p < 0.001; *Cont.* vs *A/A^{Hep}*.

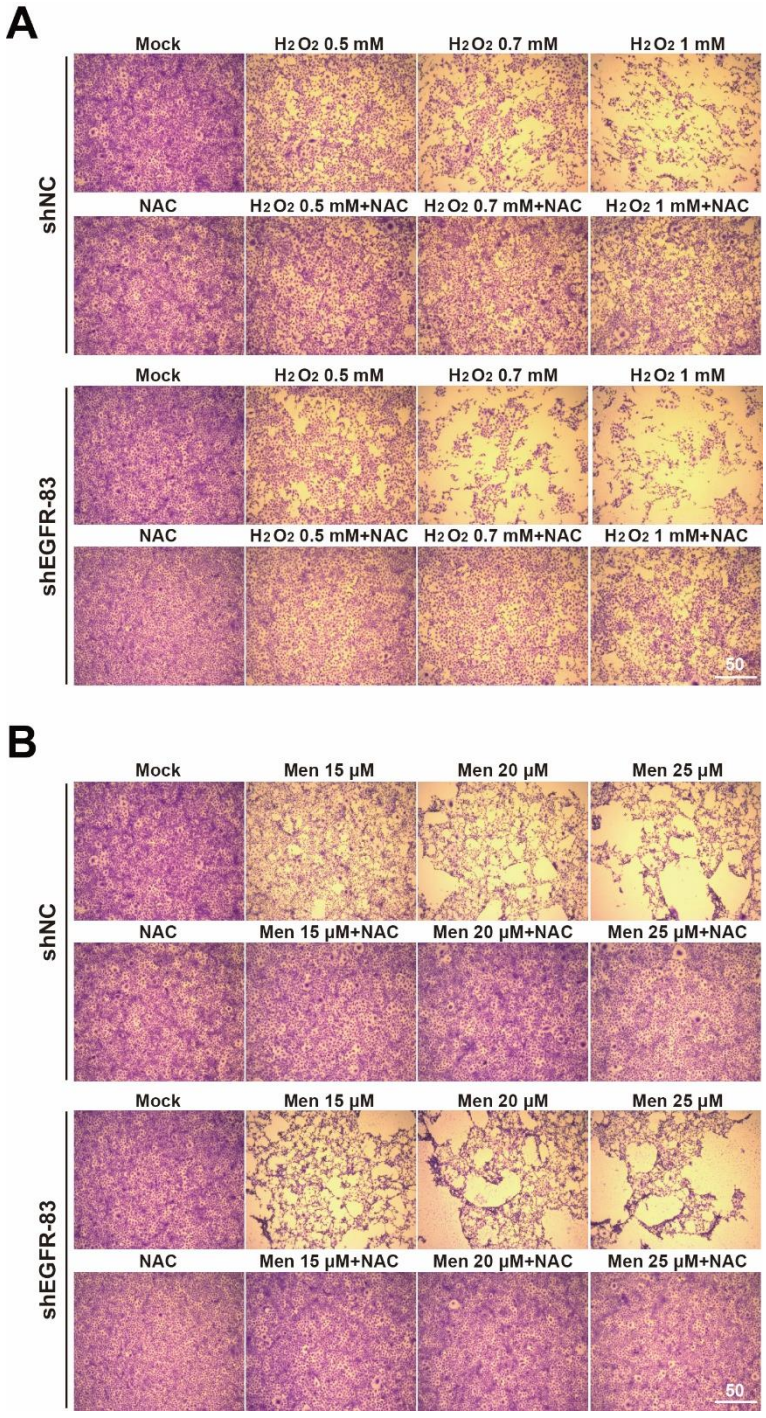

Figure 5. EGFR knockdown enhances susceptibility to reactive oxygen species in immortalized embryonic hepatocytes.

(A and B) The shNC and shEGFR-83 cell lines were treated with hydrogen peroxide (H_2O_2) or menadione at indicated concentrations with/without NAC (1mM) for 7 hrs. The remaining cells were stained with crystal violet staining solution (scale bar = 50 μm).

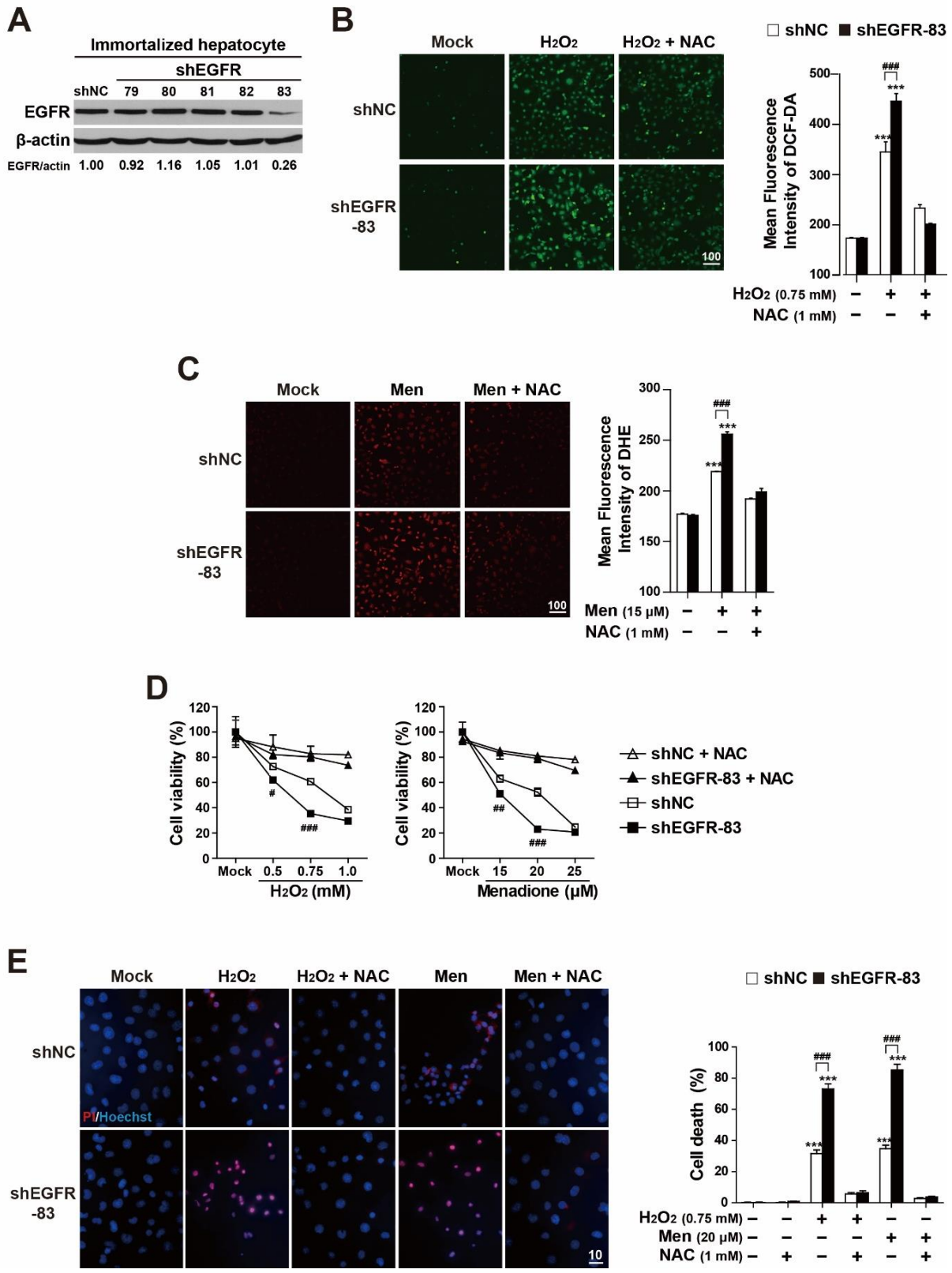
A
Immortalized hepatocyte
shEGFR
shNC 79 80 81 82 83
EGFR
β-actin
EGFR/actin 1.00 0.92 1.16 1.05 1.01 0.26
B
Mock
H2O2
H2O2 + NAC
shNC
shEGFR -83
100
□ shNC ■ shEGFR-83
Mean Fluorescence Intensity of DCF-DA
H2O2 (0.75 mM) – + +
NAC (1 mM) – – +
C
Mock
Men
Men + NAC
shNC
shEGFR -83
100
Mean Fluorescence Intensity of DHE
Men (15 μM) – + +
NAC (1 mM) – – +
D
Cell viability (%)
Mock 0.5 0.75 1.0
H2O2 (mM)
Mock 15 20 25
Menadione (μM)
shNC + NAC
shEGFR-83 + NAC
shNC
shEGFR-83
E
Mock
H2O2
H2O2 + NAC
Men
Men + NAC
shNC
shEGFR -83
PI/Hoechst
10
□ shNC ■ shEGFR-83
Cell death (%)
H2O2 (0.75 mM) – – + + – –
Men (20 μM) – – – – + +
NAC (1 mM) – + – + – +

Figure 6. EGFR depletion enhances susceptibility to reactive oxygen species.

(A) From immortalized embryonic hepatocytes stably expressing five EGFR shRNAs (79~83) or shNC, the cell lysates were subjected to SDS-PAGE, followed by immunoblot analyses using antibodies specific for EGFR and β-actin. For the EGFR/β-actin ratio, densitometry scanning was performed and quantified with NIH Image software. (B) The shNC and shEGFR-83 cell lines were treated with hydrogen peroxide (H_2O_2, 0.75 mM) or hydrogen peroxide (H_2O_2, 0.7 mM) plus N-acetylcysteine (NAC, 1 mM) for 4 hrs. (C) The shNC and shEGFR-83 cell lines were treated with menadione (6 μM), or menadione (15 μM) plus N-acetylcysteine (NAC, 1 mM) for 3 hrs. The accumulated intracellular ROS was observed by fluorescence microscopy of cells stained with DCF-DA in Fig. 4B and dihydroethidium (DHE) (C), reflecting ROS levels. Representative images are shown (scale bar = 100 μm). The mean fluorescence intensities (MFI) of DCF-DA or DHE staining were measured using image analysis software. The data are expressed as means ± SEMs of three independent experiments. ***$p < 0.001$; Mock vs Chemicals in the same genotype, $^{###}p < 0.001$; shNC vs shEGFR. (D) The shNC and shEGFR-83 cell lines were treated with hydrogen peroxide (H_2O_2) or menadione at indicated concentrations with/without NAC (1 mM) for 7 hrs. Cell viability was determined using the crystal violet assay. The data are expressed as means ± SEMs of three independent experiments. $^{#}p < 0.05$, $^{##}p < 0.01$ and $^{###}p < 0.001$; shNC vs shEGFR. (E) The shNC and shEGFR-83 cell lines were treated with hydrogen peroxide (H_2O_2, 0.75 mM), menadione (15 μM), H_2O_2 (0.75 mM) plus NAC (1 mM) or menadione (15 μM) plus NAC (1 mM) for 7 hrs. Cell death (apoptotic and necrotic cells) was determined by double staining with Hoechst 33258 and propidium iodide (PI). Representative images are shown (scale bar = 10 μm). At least 500 cells were counted, and cell death is expressed as a percentage of total cells. The data are expressed as the means ± SEMs of three independent experiments. ***$p < 0.001$; Mock vs Chemicals in the same genotype, $^{###}p < 0.001$; shNC vs shEGFR.

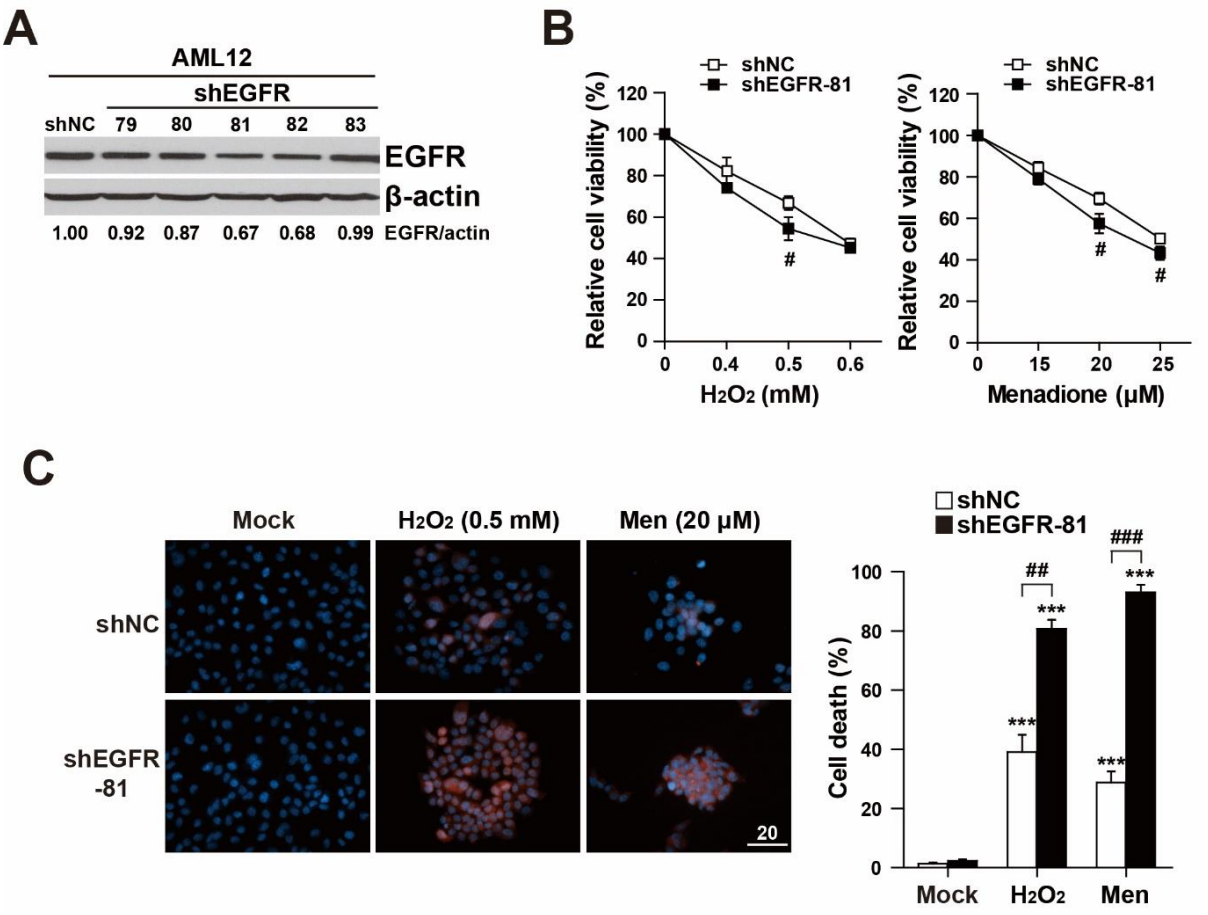

Figure 7. EGFR knockdown enhances susceptibility to reactive oxygen species in AML12 cells.

(A) From AML12 cells stably expressing five EGFR shRNAs (79~83) or shNC, the cell lysates were subjected to SDS-PAGE, followed by immunoblot analyses using antibodies specific for EGFR and β-actin. For the EGFR/β-actin ratio, densitometry scanning was performed and quantified using NIH Image software. (B) AML12 shNC and AML12 shEGFR-81 cell lines were treated with menadione or hydrogen peroxide (H_2O_2) at indicated concentration for 7 hrs. Cell viability was determined using the crystal violet assay. The data are expressed as means ± SEMs of three independent experiments. $^{\#}p < 0.05$; shNC vs shEGFR (C) AML12 shNC and AML12 shEGFR-81 cell lines were treated with hydrogen peroxide (H_2O_2, 0.5 mM) or menadione (20 μM) for 7 hrs. Cell death (apoptotic and necrotic cells) was determined using double staining with Hoechst 33258 and propidium iodide (PI). Representative images are shown (scale bar = 20 μm). At least 500 cells were counted, and cell death is expressed as a percentage of total cells. The data are expressed as means ± SEMs of three independent experiments. ***$p < 0.001$; Mock vs Chemicals in the same group, $^{\#\#}p < 0.01$ and $^{\#\#\#}p < 0.001$; shNC vs shEGFR.

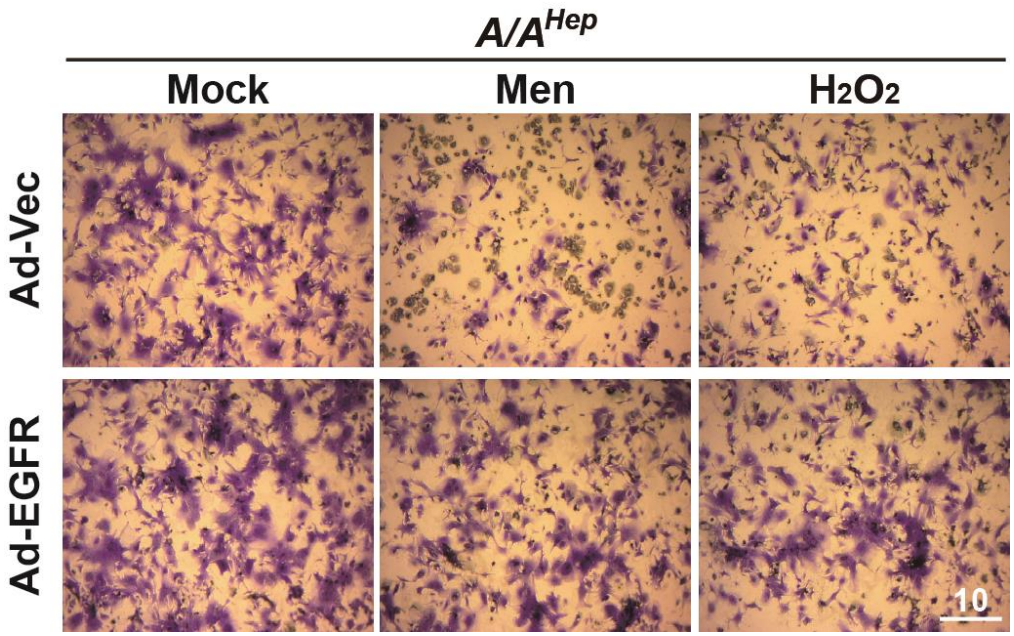

Figure 8. EGFR overexpression reduces the susceptibility of eIF2α phosphorylation-deficient primary hepatocytes to reactive oxygen species.

The Ad-EGFR-Flag or Ad-Vec infected *A/A*^{Hep} primary hepatocytes were treated with menadione (6 μM) or hydrogen peroxide (H_2O_2, 0.7 mM) for 30 hours. The remaining cells were stained with crystal violet staining solution (scale bar = 10 μm).

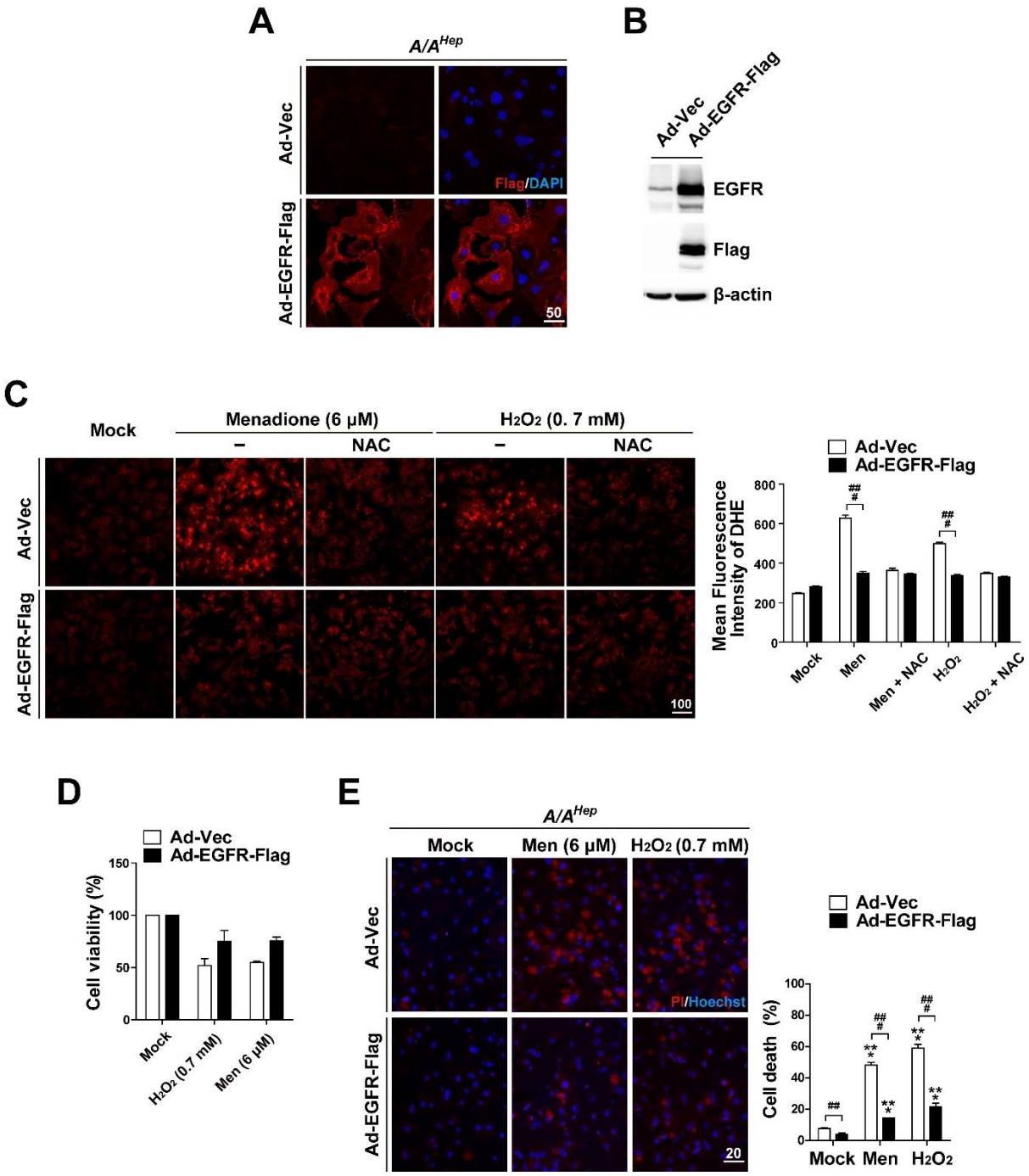

Figure 9. EGFR overexpression reduces the susceptibility of eIF2α phosphorylation-deficient primary hepatocytes to reactive oxygen species.

(A) Primary hepatocytes isolated from *A/A*^{Hep} mice were infected with recombinant adenoviruses (100 multiplicity of infection) expressing EGFR-Flag (Ad-EGFR-Flag) or empty vector controls (Ad-Vec) for 12 hrs. The cells were fixed, stained with anti-Flag monoclonal antibody and DAPI, and examined by fluorescence microscopy (scale bar = 50 μm). (B) From

Ad-EGFR-Flag or Ad-Vec infected *A/A*^{Hep} primary hepatocytes, the cell lysates were subjected to SDS-PAGE, followed by immunoblot analyses using antibodies specific for EGFR, Flag, and β-actin. (C) The Ad-EGFR-Flag or Ad-Vec infected *A/A*^{Hep} primary hepatocytes were treated with menadione (6 μM), menadione (6 μM) plus N-acetylcysteine (NAC, 1 mM), hydrogen peroxide (H_2O_2, 0.7 mM), or hydrogen peroxide (H_2O_2, 0.7 mM) plus N-acetylcysteine (NAC, 1 mM) for 20 hrs. The accumulated intracellular ROS were observed using fluorescence microscopy of the cells stained with dihydroethidium (DHE), reflecting ROS levels. Representative images are shown (scale bar = 100 μm). The mean fluorescence intensities (MFI) of DHE staining were measured using image analysis software. The data are expressed as the means ± SEMs of three independent experiments. . $^{**}p < 0.01$ and $^{***}p < 0.001$; Mock vs Chemicals in the same genotype, $^{###}p < 0.001$; Ad-Vec vs Ad-EGFR-Flag. (D and E) The Ad-EGFR-Flag or Ad-Vec infected *A/A*^{Hep} primary hepatocytes were treated with menadione (6 μM) or hydrogen peroxide (H_2O_2, 0.7 mM) for 30 hours in (D) and 18 hours in (E). Cell viability was determined using the crystal violet assay. The data are expressed as means ± SEMs of three independent experiments. Cell death (apoptotic and necrotic cells) was determined by double staining with Hoechst 33258 and propidium iodide (PI). Representative images are shown (scale bar = 20 μm). At least 500 cells were counted, and cell death is expressed as a percentage of total cells. The data are expressed as means ± SEMs of three independent experiments. $^{*}p < 0.05$, $^{**}p < 0.01$, and $^{***}p < 0.001$; Mock vs Chemicals in the same group, $^{##}p < 0.01$ and $^{###}p < 0.001$; Ad-Vec vs Ad-EGFR-Flag.

References

1. Berasain C, Avila MA: **The EGFR signalling system in the liver: from hepatoprotection to hepatocarcinogenesis**. *J Gastroenterol* 2014, **49**(1):9-23.
2. Schneider MR, Wolf E: **The epidermal growth factor receptor ligands at a glance**. *J Cell Physiol* 2009, **218**(3):460-466.
3. Sato K: **Cellular functions regulated by phosphorylation of EGFR on Tyr845**. *Int J Mol Sci* 2013, **14**(6):10761-10790.
4. Carpenter G, Cohen S: **Epidermal growth factor**. *J Biol Chem* 1990, **265**(14):7709-7712.
5. Citri A, Yarden Y: **EGF-ERBB signalling: towards the systems level**. *Nat Rev Mol Cell Biol* 2006, **7**(7):505-516.
6. Jorissen RN, Walker F, Pouliot N, Garrett TP, Ward CW, Burgess AW: **Epidermal growth factor receptor: mechanisms of activation and signalling**. *Exp Cell Res* 2003, **284**(1):31-53.
7. Liebmann C: **EGF receptor activation by GPCRs: an universal pathway reveals different versions**. *Mol Cell Endocrinol* 2011, **331**(2):222-231.
8. Chiarugi P, Buricchi F: **Protein tyrosine phosphorylation and reversible oxidation: two cross-talking posttranslation modifications**. *Antioxid Redox Signal* 2007, **9**(1):1-24.
9. Kim D, Dai J, Fai LY, Yao H, Son YO, Wang L, Pratheeshkumar P, Kondo K, Shi X, Zhang Z: **Constitutive activation of epidermal growth factor receptor promotes tumorigenesis of Cr(VI)-transformed cells through decreased reactive oxygen species and apoptosis resistance development**. *J Biol Chem* 2015, **290**(4):2213-2224.
10. Abdelmohsen K, Gerber PA, von Montfort C, Sies H, Klotz LO: **Epidermal growth factor receptor is a common mediator of quinone-induced signaling leading to phosphorylation of connexin-43: role of glutathione and tyrosine phosphatases**. *J Biol Chem* 2003, **278**(40):38360-38367.
11. Filosto S, Khan EM, Tognon E, Becker C, Ashfaq M, Ravid T, Goldkorn T: **EGF receptor exposed to oxidative stress acquires abnormal phosphorylation and aberrant activated conformation that impairs canonical dimerization**. *PLoS One* 2011, **6**(8):e23240.
12. Weng MS, Chang JH, Hung WY, Yang YC, Chien MH: **The interplay of reactive oxygen species and the epidermal growth factor receptor in tumor progression and drug resistance**. *J Exp Clin Cancer Res* 2018, **37**(1):61.

13. Gamou S, Shimizu N: **Hydrogen peroxide preferentially enhances the tyrosine phosphorylation of epidermal growth factor receptor**. *FEBS Lett* 1995, **357**(2):161-164.
14. Heppner DE, van der Vliet A: **Redox-dependent regulation of epidermal growth factor receptor signaling**. *Redox Biol* 2016, **8**:24-27.
15. Paulsen CE, Truong TH, Garcia FJ, Homann A, Gupta V, Leonard SE, Carroll KS: **Peroxide-dependent sulfenylation of the EGFR catalytic site enhances kinase activity**. *Nat Chem Biol* 2011, **8**(1):57-64.
16. Lee SR, Kwon KS, Kim SR, Rhee SG: **Reversible inactivation of protein-tyrosine phosphatase 1B in A431 cells stimulated with epidermal growth factor**. *J Biol Chem* 1998, **273**(25):15366-15372.
17. Sham D, Wesley UV, Hristova M, van der Vliet A: **ATP-mediated transactivation of the epidermal growth factor receptor in airway epithelial cells involves DUOX1-dependent oxidation of Src and ADAM17**. *PLoS One* 2013, **8**(1):e54391.
18. Wang X, McCullough KD, Franke TF, Holbrook NJ: **Epidermal growth factor receptor-dependent Akt activation by oxidative stress enhances cell survival**. *J Biol Chem* 2000, **275**(19):14624-14631.
19. Chowdhry S, Zhang Y, McMahon M, Sutherland C, Cuadrado A, Hayes JD: **Nrf2 is controlled by two distinct beta-TrCP recognition motifs in its Neh6 domain, one of which can be modulated by GSK-3 activity**. *Oncogene* 2013, **32**(32):3765-3781.
20. Ma Q: **Role of nrf2 in oxidative stress and toxicity**. *Annu Rev Pharmacol Toxicol* 2013, **53**:401-426.
21. Brunet A, Bonni A, Zigmond MJ, Lin MZ, Juo P, Hu LS, Anderson MJ, Arden KC, Blenis J, Greenberg ME: **Akt promotes cell survival by phosphorylating and inhibiting a Forkhead transcription factor**. *Cell* 1999, **96**(6):857-868.
22. Sadidi M, Lentz SI, Feldman EL: **Hydrogen peroxide-induced Akt phosphorylation regulates Bax activation**. *Biochimie* 2009, **91**(5):577-585.
23. Hagenbuchner J, Kuznetsov A, Hermann M, Hausott B, Obexer P, Ausserlechner MJ: **FOXO3-induced reactive oxygen species are regulated by BCL2L11 (Bim) and SESN3**. *J Cell Sci* 2012, **125**(Pt 5):1191-1203.
24. Wang XT, McCullough KD, Wang XJ, Carpenter G, Holbrook NJ: **Oxidative stress-induced phospholipase C-gamma 1 activation enhances cell survival**. *J Biol Chem* 2001, **276**(30):28364-28371.
25. Morita M, Matsuzaki H, Yamamoto T, Fukami Y, Kikkawa U: **Epidermal growth factor receptor phosphorylates protein kinase C {delta} at Tyr332 to form a trimeric complex with p66Shc in the H2O2-stimulated cells**. *J Biochem* 2008, **143**(1):31-38.

26. Goldkorn T, Balaban N, Matsukuma K, Chea V, Gould R, Last J, Chan C, Chavez C: **EGF-Receptor phosphorylation and signaling are targeted by H2O2 redox stress**. *Am J Respir Cell Mol Biol* 1998, **19**(5):786-798.
27. Carballo M, Conde M, El Bekay R, Martin-Nieto J, Camacho MJ, Monteseirin J, Conde J, Bedoya FJ, Sobrino F: **Oxidative stress triggers STAT3 tyrosine phosphorylation and nuclear translocation in human lymphocytes**. *J Biol Chem* 1999, **274**(25):17580-17586.
28. Miklossy G, Hilliard TS, Turkson J: **Therapeutic modulators of STAT signalling for human diseases**. *Nat Rev Drug Discov* 2013, **12**(8):611-629.
29. Rodriguez-Fragoso L, Melendez K, Hudson LG, Lauer FT, Burchiel SW: **EGF-receptor phosphorylation and downstream signaling are activated by benzo[a]pyrene 3,6-quinone and benzo[a]pyrene 1,6-quinone in human mammary epithelial cells**. *Toxicol Appl Pharmacol* 2009, **235**(3):321-328.
30. Sonenberg N, Hinnebusch AG: **Regulation of translation initiation in eukaryotes: mechanisms and biological targets**. *Cell* 2009, **136**(4):731-745.
31. Proud CG: **eIF2 and the control of cell physiology**. *Semin Cell Dev Biol* 2005, **16**(1):3-12.
32. Wek RC, Jiang HY, Anthony TG: **Coping with stress: eIF2 kinases and translational control**. *Biochem Soc Trans* 2006, **34**(Pt 1):7-11.
33. Liu L, Wise DR, Diehl JA, Simon MC: **Hypoxic reactive oxygen species regulate the integrated stress response and cell survival**. *J Biol Chem* 2008, **283**(45):31153-31162.
34. Rajesh K, Krishnamoorthy J, Kazimierczak U, Tenkerian C, Papadakis AI, Wang S, Huang S, Koromilas AE: **Phosphorylation of the translation initiation factor eIF2alpha at serine 51 determines the cell fate decisions of Akt in response to oxidative stress**. *Cell Death Dis* 2015, **6**:e1591.
35. Lewerenz J, Maher P: **Basal levels of eIF2alpha phosphorylation determine cellular antioxidant status by regulating ATF4 and xCT expression**. *J Biol Chem* 2009, **284**(2):1106-1115.
36. Han J, Back SH, Hur J, Lin YH, Gildersleeve R, Shan J, Yuan CL, Krokowski D, Wang S, Hatzoglou M *et al*: **ER-stress-induced transcriptional regulation increases protein synthesis leading to cell death**. *Nat Cell Biol* 2013, **15**(5):481-490.
37. Choi WG, Han J, Kim JH, Kim MJ, Park JW, Song B, Cha HJ, Choi HS, Chung HT, Lee IK *et al*: **eIF2alpha phosphorylation is required to prevent hepatocyte death and liver fibrosis in mice challenged with a high fructose diet**. *Nutr Metab (Lond)* 2017, **14**:48.

38. Back SH, Scheuner D, Han J, Song B, Ribick M, Wang J, Gildersleeve RD, Pennathur S, Kaufman RJ: **Translation attenuation through eIF2alpha phosphorylation prevents oxidative stress and maintains the differentiated state in beta cells**. *Cell Metab* 2009, **10**(1):13-26.
39. Oh HY, Namkoong S, Lee SJ, Por E, Kim CK, Billiar TR, Han JA, Ha KS, Chung HT, Kwon YG *et al*: **Dexamethasone protects primary cultured hepatocytes from death receptor-mediated apoptosis by upregulation of cFLIP**. *Cell Death Differ* 2006, **13**(3):512-523.
40. Kitade M, Factor VM, Andersen JB, Tomokuni A, Kaji K, Akita H, Holczbauer A, Seo D, Marquardt JU, Conner EA *et al*: **Specific fate decisions in adult hepatic progenitor cells driven by MET and EGFR signaling**. *Genes Dev* 2013, **27**(15):1706-1717.
41. Musallam L, Ethier C, Haddad PS, Bilodeau M: **Role of EGF receptor tyrosine kinase activity in antiapoptotic effect of EGF on mouse hepatocytes**. *Am J Physiol Gastrointest Liver Physiol* 2001, **280**(6):G1360-1369.
42. Guren TK, Odegard J, Abrahamsen H, Thoresen GH, Susa M, Andersson Y, Ostby E, Christoffersen T: **EGF receptor-mediated, c-Src-dependent, activation of Stat5b is downregulated in mitogenically responsive hepatocytes**. *J Cell Physiol* 2003, **196**(1):113-123.
43. Ostrowski J, Woszczynski M, Kowalczyk P, Trzeciak L, Hennig E, Bomsztyk K: **Treatment of mice with EGF and orthovanadate activates cytoplasmic and nuclear MAPK, p70S6k, and p90rsk in the liver**. *J Hepatol* 2000, **32**(6):965-974.
44. Quesnelle KM, Boehm AL, Grandis JR: **STAT-mediated EGFR signaling in cancer**. *J Cell Biochem* 2007, **102**(2):311-319.
45. Fan QW, Cheng CK, Gustafson WC, Charron E, Zipper P, Wong RA, Chen J, Lau J, Knobbe-Thomsen C, Weller M *et al*: **EGFR phosphorylates tumor-derived EGFRvIII driving STAT3/5 and progression in glioblastoma**. *Cancer Cell* 2013, **24**(4):438-449.
46. Orcutt KP, Parsons AD, Sibenaller ZA, Scarbrough PM, Zhu Y, Sobhakumari A, Wilke WW, Kalen AL, Goswami P, Miller FJ, Jr. *et al*: **Erlotinib-mediated inhibition of EGFR signaling induces metabolic oxidative stress through NOX4**. *Cancer Res* 2011, **71**(11):3932-3940.
47. Schreier B, Rabe S, Schneider B, Bretschneider M, Rupp S, Ruhs S, Neumann J, Rueckschloss U, Sibilia M, Gotthardt M *et al*: **Loss of epidermal growth factor receptor in vascular smooth muscle cells and cardiomyocytes causes arterial hypotension and cardiac hypertrophy**. *Hypertension* 2013, **61**(2):333-340.
48. Kim MK, Yee J, Cho YS, Jang HW, Han JM, Gwak HS: **Risk factors for erlotinib-**

induced hepatotoxicity: a retrospective follow-up study. *BMC Cancer* 2018, **18**(1):988.

49. Paech F, Bouitbir J, Krahenbuhl S: **Hepatocellular Toxicity Associated with Tyrosine Kinase Inhibitors: Mitochondrial Damage and Inhibition of Glycolysis**. *Front Pharmacol* 2017, **8**:367.
50. Rakhit A, Pantze MP, Fettner S, Jones HM, Charoin JE, Riek M, Lum BL, Hamilton M: **The effects of CYP3A4 inhibition on erlotinib pharmacokinetics: computer-based simulation (SimCYP) predicts in vivo metabolic inhibition**. *Eur J Clin Pharmacol* 2008, **64**(1):31-41.
51. Li J, Zhao M, He P, Hidalgo M, Baker SD: **Differential metabolism of gefitinib and erlotinib by human cytochrome P450 enzymes**. *Clin Cancer Res* 2007, **13**(12):3731-3737.
52. Haouzi D, Lekehal M, Moreau A, Moulis C, Feldmann G, Robin MA, Letteron P, Fau D, Pessayre D: **Cytochrome P450-generated reactive metabolites cause mitochondrial permeability transition, caspase activation, and apoptosis in rat hepatocytes**. *Hepatology* 2000, **32**(2):303-311.

CHAPTER 2

eIF2α phosphorylation is a critical event for autophagosome maturation upon ER stress

Abstract

Endoplasmic reticulum (ER) stress caused by an accumulation of improperly folded proteins can trigger the unfolded protein response (UPR) to restore ER homeostasis. UPR-mediated restoration of ER homeostasis can be achieved by diverse signaling pathways to increase ER protein-folding capacity and reduce misfolded protein accumulation in the ER. The UPR can activate degradation systems such as the autophagy lysosome system and the ubiquitin proteasome system to remove misfolded ER proteins. In response to ER stress, the eukaryotic translation initiation factor 2 alpha subunit (eIF2α) suppresses the translation of general mRNA, to reduce the accumulation of misfolded proteins in the ER. To investigate the role of eIF2α phosphorylation in autophagy induced by ER stress, I used a hepatocyte-specific eIF2α phosphorylation-deficient mouse model. Upon treatment with tunicamycin, an ER stress inducer, deficiency in eIF2α phosphorylation produced an abnormal ER structure and defective mitochondrial dynamics. Interestingly, the deficiency in eIF2α phosphorylation downregulated the expression of autophagy genes but caused a marked accumulation of LC3, an autophagosome marker, and P62/sequestosome-1, a selective autophagy substrate, in ER-stressed hepatocytes. In addition, during ER stress, eIF2α phosphorylation-deficient hepatocytes displayed an accumulation of LC3/P62-positive autophagic vesicles but decreased co-localization between LC3 and LAMP1, which suggests that eIF2α phosphorylation is not necessary for autophagosome formation but is required for autophagosome maturation, including the fusion of the autophagosome with a late endosome or lysosome. eIF2α phosphorylation deficiency disrupts lysosome positioning as well as lysosome functionality which can affect autophagic flux upon ER stress. Importantly, Qa-SNARE syntaxin 17 (STX17), which is required for autophagosomal fusion with lysosomes, was not co-localized with LC3-positive vesicles in eIF2α phosphorylation-deficient hepatocytes during ER stress. Accordingly, at the late stage of ER stress, the mis-localization of STX17 could be responsible for blocking autophagic flux in eIF2α phosphorylation-deficient

hepatocytes. Lastly, I observed that eIF2α phosphorylation was responsible for maintaining the expression of lysosomal genes and autophagosome-lysosome fusion related genes, which are the target genes of the master autophagy regulators TFEB and TFE3, during ER stress. Therefore, TFEB overexpression could restore lysosome functionality and mitochondrial dynamics in eIF2α phosphorylation-deficient primary hepatocytes upon ER stress. In other words, TFEB overexpression promotes autophagosome-lysosome fusion in eIF2α phosphorylation-deficient primary hepatocytes upon ER stress. Collectively, these observations suggest that eIF2α phosphorylation is an important event in modulating autophagy to ameliorate ER stress.

Therefore, it is possible that ER stress-mediated liver damage in the eIF2α phosphorylation-deficient mouse model could be caused by the impairment of lysosomal degradation. Alternatively, modulating TFEB activity which stimulates autophagy, lysosomal and mitochondrial biogenesis, lysosomal motility, and SNARE-mediated fusion, is an attractive therapeutic avenue for diseases related to defects in the autophagy-lysosomal pathway.

Introduction

The endoplasmic reticulum (ER) is an intracellular organelle that consists of a vast tubular network in which secretory and integral membrane proteins are synthesized and folded [1-3]. Nascent proteins are transported through the ER translocon to secretory pathways [4]. The ER is responsible for protein translocation, protein folding, and post-translational modification including disulfide bond formation and N-linked glycosylation [1]. Properly folded and modified proteins are exported to the Golgi apparatus, in which most of the post-translational modifications are completed [1,5]. Proper function of the ER is perturbed when the influx of nascent proteins exceeds the folding and processing capacity of the ER [6]. ER stress caused by an accumulation of unfolded proteins in the ER lumen can activate multiple signaling pathways, including the unfolded protein response (UPR), ER-associated protein degradation, and autophagy [7], to restore cellular homeostasis.

The UPR is triggered to increase the folding and degradation capacity of the ER [5]. The UPR is distinguished by the action of three ER resident transmembrane proteins: PERK (protein kinase RNA-like endoplasmic reticulum kinase), IRE1α (inositol-requiring enzyme-1α), and ATF6α (activating transcription factor 6) [1]. Activated PERK prevents the accumulation of newly synthesized unfolded proteins by attenuating their mRNA translation through the functional regulation of the eukaryotic translation initiation factor 2 complex [8]. Eukaryotic translation initiation factor 2 alpha (eIF2α) is a subunit of the trimeric eIF2 complex that mediates delivery of the initiator methionyl-tRNA to the ribosome at the initiation of translation of cytoplasmic mRNA in eukaryotic cells [9]. In mammals, eIF2α is phosphorylated on residue serine 51 by the four eIF2α protein kinases, PERK, GCN2, PKR, and HRI, in response to various cellular stresses [10, 11]. During ER stress, PERK-mediated phosphorylation of eIF2α suppresses the translation of general mRNA. In addition, eIF2α phosphorylation facilitates the selective translation of the ATF4 transcription factor, which can activate autophagy by inducing genes involved in several ATG proteins, amino acid biosynthesis, and transporters [12].

Furthermore, eIF2α phosphorylation is also required to activate the ER stress sensor ATF6α by facilitating its intramembrane proteolysis 21917591 [13, 14] and to ensure maximal induction of spliced X-box-binding protein 1 (XBP1s) by stabilizing its mRNA [15]; XBP1s is a transcription factor that promotes the induction of UPR genes, which enhance ER processing capacity (protein folding and degradation) and alleviate cellular injury [16]. Thus, eIF2α phosphorylation during cellular stress is responsible for transcriptional and translational reprogramming that protects the stressed cells.

IRE1 has a serine/threonine kinase and endoribonuclease domain. An accumulation of unfolded proteins triggers autophosphorylation of IRE1α's cytosolic kinase domain, and downstream activation of c-Jun N-terminal kinase causes Bcl-2 phosphorylation, followed by segregation of beclin-1 and activation of the phosphoinositide-3-kinase (PI3K) complex which is important for the formation of an isolation membrane (also called a phagophore) [8, 17, 18]. In addition, IRE1 -mediated XBP1 mRNA splicing triggers the induction of autophagic signaling through the transcriptional regulation of beclin-1 [19, 20]. ATF6α is transcription factor that contains a basic leucine zipper motif in its cytosolic domain [21]. Under resting conditions, when Golgi-localization sequences in the luminal domain of ATF6α are masked by binding to the chaperone BIP, ATF6α localizes at the ER [22]. However, ER stress induces the dissociation of ATF6α from BIP, resulting in the translocation of ATF6α to the Golgi compartment. Sequentially, the luminal domain of ATF6α is cleaved by site-1 protease (S1P) and site-2 protease (S2P), and its cytoplasmic domain is released [23, 24]. The cleaved cytosolic domain of ATF6α translocates into the nucleus, where it activates the transcription of target genes such as GRP78/BIP, CHOP, and XBP-1 [21]. In that way, ATF6α indirectly regulates autophagy.

Acute or prolonged ER stress is causally linked to various pathologies including neurodegenerative diseases, obesity, and diabetes [25, 26]. Several studies have reported a link between UPR signaling pathways and autophagy [27]. Autophagy is a cellular catabolic process that delivers proteins and organelles to lysosomes for degradation and recycling [28].

This mechanism plays a critical role in maintaining cellular homeostasis and preserving cell viability during ER stress through the catabolic lysis of aggregated proteins, unfolded proteins, and damaged subcellular organelles [7].

The autophagy process involves sequential stages: autophagy induction, autophagosome nucleation, elongation, completion, lysosomal fusion, degradation, and recycling [7,29]. Upon autophagy induction by several stimuli, autophagy initiation starts with the activation of the ULK1/2 complex and the Class Ⅲ PI3K complex Ⅰ [30]. This complex generates PtdIns3P at the surface of the ER membrane, which is considered a prominent membrane source for building phagophores [29, 31]. Membrane formation requires a unique subset of proteins called autophagy-related (ATG) proteins during autophagy [32]. ATG components are recruited to the pre-autophagosomal structures [33]. The ATG conjugation system consists of the ATG2-ATG18 complex, the ATG12 conjugation system, and the LC3 (mammalian ATG8)-PE conjugation system [32]. These ATG conjugation systems are important in mediating the elongation and maturation of the phagophore [34, 35]. Subsequently, LC3I is covalently linked to PE at the phagophore membrane, which facilitates the conversion of cytosolic LC3I to membrane-bound LC3II [36]. The lipidated LC3II remains anchored to the elongating phagophore, which is essential for autophagosome formation [35]. Cargo recognition occurs during phagophore elongation. Cytoplasmic constituents are sequestered by the phagophore or isolation membrane [31]. P62/SQSTM1, an autophagic receptor, has one domain to interact with the ubiquitin-labeled cargo and another domain to interact with LC3II at the phagophore membrane [29]. The phagophore continues elongating around the cargo, giving rise to the double-membrane vesicle called the autophagosome [29]. The completed autophagosomes fuse with lysosomes, producing autolysosomes that deliver the cargo into the lysosomal compartment [37].

The molecular machinery for the final step of autophagy, autolysosome formation, includes soluble N-ethylmaleimide-sensitive factor attachment protein receptors (SNAREs),

small GTPases, the HOPS (homotypic fusion and protein sorting) complex, and other tethering factors [38]. RAB GTPases and the RAB7A effector enable recruitment of the HOPS complex to the lysosome membrane [39]. Intracellular membrane fusion occurs in a specific manner such that conserved SNARE proteins are responsible for vesicle docking and membrane fusion [40]. The C-terminal tail of Qa-SNARE syntexin17 (STX17) is required for its ER localization, and the N-terminal domain regulates its transport from the ER into the ER-Golgi intermediate compartment [41]. Upon autophagy induction, STX17 is recruited to the outer membranes of completed autophagosomes but not to isolation membranes [42]. Thus, the late recruitment of STX17 to the autophagosome can prevent premature fusion with the lysosome [42]. Interestingly, Stx17 transcript knockdown results in an accumulation of autophagosomes without catabolic lysis [42]. In SNARE-mediated membrane fusion, Qa-SNARE STX17 and Qbc-SNARE SNAP29 preform the helix-bundle on the autophagosome and then assemble a complex with lysosome-localized R-SNAREs, such as VAMP7 and VAMP8, leading to the degradation of the enclosed materials [42]. Normally, the distribution of the lysosome depends on transportation driven by microtubule motors. Lysosomes are clustered in perinuclear-enriched regions across microtubule tracks, but autophagosomes are scattered in peripheral regions of the cytoplasm [43]. Upon autophagy, autophagosomes are transported to perinuclear regions in a dynein-mediated manner that facilitates autophagosome-lysosome fusion to achieve autophagic degradation [44].

The transcription factors TFEB and TFE3 are master regulators of autophagy-lysosomal pathway genes [45]. TFEB and TFE3 directly bind the coordinated lysosomal expression and regulation (CLEAR) element in the promoter of lysosomal and autophagy-related genes [46]. Lysosomes are the cellular degradative compartment for maintaining cellular homeostasis, and endocytosis is the dynamic process that delivers intracellular materials and damaged organelles into lysosomes [47]. Importantly, mTORC1 determines the intracellular localization and activation of TFEB and TFE3. When nutrients are abundant, mTORC1 is recruited to the lysosomal surface and is activated, which promotes cellular

processes, such as protein synthesis and proliferation [46]. MTORC1 directly phosphorylates TFEB and TFE3 and leads to cytosolic retention of TFEB and TFE3 [48]. On the contrary, under autophagy induction, mTORC1 is inactivated and lysosomal calcium release via mucolipin-1 (MCOLN1) induces the activation of calcineurin, which dephosphorylates TFEB and TFE3, promoting their nuclear translocation [49]. The ability of TFEB and TFE3 to stimulate autophagy is of great importance because it reveals the transcriptional regulation of a cellular degradative pathway [45]. TFEB and TFE3 are activated in response to mitochondrial and ER stress, which suggests that they have an important role in cellular adaptations to stress [46]. Similar to mitochondrial and ER stress conditions, the nuclear translocation of TFEB and TFE3 promotes mitochondrial biogenesis by inducing the expression of PGC-1α (peroxisome proliferator-activated receptor-γ coactivator-1α) [46,50,51]. In addition, a recent report suggests that TFE3 targets include not only lysosomal and autophagy-related genes but also ATF4, which is responsible for the expression of genes involved in amino acid biosynthesis and transport and apoptosis [52-54]. Thus, TFEB and TFE3 play an important role in the cellular response to ER stress.

In this study, I demonstrate that eIF2α phosphorylation is a critical contributor to the activation of three canonical UPR branches that regulate autophagy pathways during ER stress. Those observations show that eIF2α phosphorylation deficiency disrupts autophagy flux by inhibiting autophagosome-lysosome fusion in response to ER stress Furthermore, I reveal that eIF2α phosphorylation regulates the autophagy-lysosome pathway by affecting the nuclear translocation of TFEB in the cellular adaptation to ER stress.

Materials and Methods

Reagents

Tunicamycin (Tm, MP-654380) was purchased from EMD Millipore. Bafilomycin (Baf, #11038) was purchased from Cayman chemical. Leupeptin (Leup, #1167) was purchased from Tocris Bioscience. Lysotracker-Red DND-99 (L7528), Mitotracker-Red CMXRos (M7512), and JC-1 Dye (#T3168) were purchased from Thermo Fisher Scientific. Magic Red Cathepsin B assay (#937) and Magic Red Cathepsin L assay (#941) were purchased from ImmunoChemistry Technologies.

Antibodies

From Cell signaling Technology: ATF4 (#11815S), Flag-DYKDDDDK-Tag(#14793S), IRE1α (#3294), LC3A/B (#4108S), PERK (#3192S). From Santa Cruz Biotechnology: Chop (sc-7351), Cathepsin B (sc-6293), Cathepsin D (sc-6486), Total eIF2α (sc-133132), Dynactin-1 (sc-365274), Lamin A/C (sc-6215). From Sigma-Aldrich: β-actin (A5441), Flag(F1804), LC3B (L7543), Syntaxin 17 (HPA001204), TFE3 (HPA023881). From New east bioscience: Rab7 (#21069). From Novus Biological: Vamp7 (NBP2-32232). From Abcam: ATG5 (ab78073), phospho-eIF2α (ab32157), Vamp8 (ab76021). From Abnova: P62/SQSTM1 (H00008878-M01). From Assay designs: KDEL (SPA-827). From Bethyl: TFEB (A303-673A). From Biolegend: XBP1s (#619502). From Clontech: GFP (#632381), RFP (#632392). From DSHB: LAMP1 (1D4B-C), LAMP2 (ABL-93-C). From MBL: Ubiquitin (D058-3).

HRP-conjugated secondary antibodies were purchased from Thermo Fisher Scientific (anti-mouse; NCI1430KR) or Jackson ImmunoResearch. (anti-Rabbit; #111-035-003, anti-mouse; #751-036-151, anti-goat; #305-035-003, anti-Rat; #112-035-003)

Animals

All mice were housed at 22 ± 2 °C in 55 ± 5% relative humidity with 12 h/12 h, light/dark cycles, and provided with free access to water and standard rodent chow (Purina; Cargill Inc., USA). Mice were maintained in specific pathogen-free housing conditions. All animal care and procedures were conducted in accordance with the guidelines approved from the University of Ulsan Animal Care and Use Committee (UOUACUC) (No. SHB-17-020).

Rescued homozygous *eIF2α S51A* mice, ***A/A;fTg/0 mice*** were created by introducing a transgene (fTg, LoxP-meIF2α-LoxP-EGFP) encoding constitutively expressing wild-type of eIF2α flanked by LoxP sites into an eIF2α S51A knock-in background. These mice were then bred to mice expressing CRE recombinase under the control of an albumin promoter for hepatocyte-specific transgene deletion. The transgenic construct (fTg) was designed to

coordinately induce green fluorescence protein (EGFP) expression as deletion reporter upon Cre recombinase-mediated deletion of the transgene.

A/A;fTg/0;CreHep/0 (A/A^{Hep}) mice were obtained by crossing *A/A;fTg/fTg (A/A-fTg*) mice with *S/A;Cre^{Hep}/0 (S/A-Cre^{Hep})* mice*.* To delete a transgene in hepatocytes, heterozygous *eIF2*α *S51A* mice carrying a hepatocyte specific Cre expressing (*Hep-Cre)* transgenic mice were bred with transgenic homozygous ***eIF2α S51A*** mice (***A/A;fTg/fTg***). The *Hep-Cre* transgene led to a hepatocyte-specific deletion, starting from a late gestation and leading to nearly complete deletion in adult mice.

Animal experiments

Tunicamycin (Tm, 1 mg/kg body weight) in 150 mM dextrose was injected intraperitoneally into mice to induce ER stress. Based on established humane endpoints, the liver tissues from the anesthetized mice were isolated at the indicated times.

For adenovirus injection, 2 to 3 -month-old female mice were used. Mice were administered by recombinant adenoviruses expressing RFP-LC3B at a dose of 2.0 x10^9 IFU /100ul per mouse. On five days after administration, the organs were collected at indicated time after intraperitoneal injection of tunicamycin (1mg/kg).

Generation of Recombinant Adenoviruses

Recombinant adenoviruses expressing RFP-LC3B, hTFEB-Flag or hTFEB(S211)-Flag were generated by the AdEasy vector system according to the manufacturer's instructions (Agilent Technologies, USA). In brief, *Pme I*-dizested and linearized RFP-LC3B, hTFEB-Flag or hTFEB(S211)-Flag expressing shuttle vectors were then electrophoresed into BJ5183 cells containing the adenoviral vector Adeasy to generate recombinant adenoviral plasmids respectively. The recombinants were amplified in HEK-293A cells and purified by CsCl (Sigma-Aldrich) gradient centrifugation. Viral preparations were collected and desalted, and titers were determined using the AdEasy Viral Titer Kit (Agilent Technologies) according to the manufacturer's instructions. The efficiency of adenoviral infection was assessed by immunofluorescence detection.

Cell culture

Immortalized wild-type (*S/S^{Hep}*) and eIF2α S51A homozygous mutant (*A/A^{Hep}*) hepatocytes were cultured in Medium 199 (WelGENE) supplemented with 10% Fetal Bovine Serum (WelGENE) and 1% penicillin-streptomycin (Gibco). The cells were grown in 5% CO_2 incubator at 37 °C.

Primary mouse hepatocyte isolation

Primary mouse hepatocytes were isolated from the liver of ***S/A;fTg/0 (Cont.)*** and ***A/A;fTg/0;CreHep/0 (A/AHep)*** mice on the two-step collagenase perfusion technique.

The liver was perfused with warm perfusion buffer and digested by Collagenase Ⅳ (From Sigma Aldrich: #C5138). Isolated hepatocytes were plated on 0.01% Collagen-coated plates with/without round coverslips and cultured in Medium 199 (WelGENE) containing 10% Fetal Bovine Serum (WelGENE) and Penicillin/Streptomycin (Gibco). After 2 h of incubation, the culture medium was replaced with new FBS-free medium to remove unattached cells. After 12 h, the isolated cells were treated with indicated chemicals in fresh Medium 199 containing 10% FBS and MEM non-essential amino acids solution (Gibco).

Western blot analysis

Liver tissues and cells were homogenized in Nonidet P-40 Lysis buffer (1% NP-40, 50 mM Tris-Cl pH 7.5, 150 mM NaCl, 0.05% SDS, 0.5 mM Na-vanadate, 100 mM NaF, 50 mM -glycerophosphate) which was supplemented with Halt Protease inhibitor cocktail (Thermo Fisher Scientific). The homogenates were centrifuged at 12,000 g for 15 min at 4 °C and supernatants were collected. Liver nuclear extracts were prepared by using an NE-PER™ Nuclear and cytoplasmic Extraction Kit (Thermo Fisher Scientific). The protein concentration was determined by using a BCA protein assay kit (Thermo Fisher Scientific). Cellular proteins (60 μg) were resolved on SDS-polyacrylamide gels and transferred to nitrocellulose (NC) or polyvinylidene difluoride (PVDF) membrane. The membranes were blocked for 1 h at room temperature with 5% skim milk or 5% BSA in Tris buffered saline-Tween 20 buffer (TBS-T: 0.1% Tween 20, 20 mM Tris-Cl pH 7.5 and 150 mM NaCl). The membranes were then incubated with the indicated primary antibodies overnight at 4 °C and then horseradish peroxidase-conjugated secondary antibodies (1:5000). The primary antibodies were used at a dilution ranging from 1:200 to 1:2000 in Western blot analysis.

Immunoprecipitation

S/S and *A/A* Hepatocytes which overexpress Flag-STX17 were collected in lysis buffer (50 mM Tris-Cl pH 7.4, 150 mM NaCl, 1 mM EDTA, 1% Triton X-100) plus protease and phosphatase inhibitor cocktail (Thermo Scientific). Supernatants were immunoprecipitated with anti-Flag magnetic bead (Sigma-Aldrich) overnight at 4 °C. After the resin was washed three times in TBS buffer (50 mM Tris-Cl, 150 mM NaCl pH 7.4), it was collected in the magnetic separator. Individual proteins were detected by Western blot analysis.

Quantitative RT-PCR.

Total RNAs were isolated from liver tissues and primary hepatocytes by using Trizol reagent (Quagen). For mRNA expression analysis, cDNAs were generated from 100 ng of total RNA by using High-Capacity cDNA RT kit (Life Technologies). Quantitative real-time polymerase chain reaction (qRT-PCR) was carried out to detect the expression levels of indicated RNAs with StepOnePlus Real Time system (Applied Biosystems) by using the SYBR green PCR master mix (Enzynomics). The specificity of each primer pair was confirmed by using melting curve analysis. Relative copy numbers, compared to the β-actin gene, were calculated using $2^{-\Delta\Delta Ct}$.

Primer sequences are given in the Table-1.

Immunofluorescence

Isolated primary hepatocytes were plated on 0.01% collagen-coated plates with/without round coverslips. The cells were treated with the indicated chemicals and then fixed with 3.5% paraformaldehyde (PFA) in PBS for 15min at room temperature or ice-cold methanol at -20 °C. The PFA fixed samples were permeabilized with 0.1% Triton X-100 in PBS for 4 min. After washed two times in PBS, the cells on coverslips were blocked with 2.5% normal horse serum blocking solution (VECTOR laboratories) for 1 h at room temperature. Next, the coverslips were incubated with primary antibodies diluted in 1% BSA overnight at 4 °C. The next day, the coverslips were rinsed two times with PBS for 5 min and incubated with fluorescence conjugated secondary antibodies for 2 h at room temperature in the dark. After washed three times in PBS, the coverslips were mounted on a slide glass by using antifade reagent (Invitrogen).

For immunofluorescence analyses of vibratome sections, mice were anesthetized with 2,2,2-Tribromoethanol and perfused with phosphate-buffered saline (PBS, pH 7.4) and liver tissues were collected. The liver tissues were fixed with 4% PFA in PBS overnight at 4 °C. The sections were sliced to thickness of 40 μm by using a vibratome (VT1000P; Leica Microsystems), and then washed several times in PBS. The sections were permeabilized with 0.1% Triton-X100 in PBS for 30 min at room temperature. Antigen retrieval was achieved by heating the sections in 10 mM sodium citrate and 0.05% Tween 20 solution (pH 8.5) for 30 min and followed by cooling for 20 min at room temperature. The sections were washed three times with dH_2O. Following steps were performed as described above.

For immunofluorescence analyses of paraffin sections, paraffin sections (4 μm thickness) were deparaffinized and rehydrated as standard procedures. Antigen retrieval and immunostaining were performed as described above.

In fluorescence images of living cells, Pearson correlation coefficients (Rr) and intensity spatial profiles were measured by using FV10-ASW software (Olympus).

All fluorescence images were captured with a cooled charge-coupled device camera and a confocal laser scanning microscope (FV1200-OSR microscope, Olympus).

Live cell fluorescence microscopy

Live cell imaging can directly visualize cellular biological phenomena. Primary hepatocytes were plated on collagen coated 35 mm cover-glass bottom dishes (SPL). After treatment of specific chemicals for indicated times, the cells were stained with indicated fluorescent probes for live cell imaging in DMEM without phenol red (Gibco).

For viable lysosomal labeling in live cells, primary hepatocytes were incubated with Lysotracker-Red DND-99 (400 nM) for 30 min at 37 °C. For Mitochondria-specific probe labeling, primary hepatocytes were stained with Mitotracker-Red CMXRos (50 nM) and 4 μg/ml Hoechst 33258 (Sigma-Aldrich) for 30 min at 37 °C. For monitoring mitochondrial membrane potential, primary hepatocytes were incubated with JC-1 (2.5 μM) for 30 min in 37 °C. Fluorescence images of living cells were obtained by using an FV1200-OSR confocal laser microscope (Olympus). Mean fluorescence intensity (MFI) was measured by using FV10-ASW software (Olympus).

Cathepsin B and cathepsin L activity assay

Intracellular cathepsin B and cathepsin L activities were detected by Magic Red Cathepsin B assay and Magic Red Cathepsin L assay kits (ImmunoChemistry Technologies, LLC.).

Primary hepatocytes were plated on collagen coated 35 mm cover-glass bottom dishes (SPL). After treatment of indicated chemicals, cells were stained with Cathepsin B substrate [MR-$(RR)_2$] or Cathepsin L substrate [MR-$(FR)_2$] for 30 min at 37 °C, according to the manufacturer's instruction. Fluorescence and differential interference contrast (DIC) images of living cells were obtained by using an FV1200-OSR confocal laser microscope (Olympus). Mean fluorescence intensity (MFI) was measured by using FV10-ASW software (Olympus).

Immunohistochemistry

Liver tissues were isolated, fixed with 4% paraformaldehyde, and embedded in paraffin. Paraffin sections (4 μm) were deparaffinized and rehydrated by following standard procedures. The sections were permeabilized with 0.1% Triton-X100 in PBS for 30 min at room temperature. Antigen retrieval was achieved by heating the sections in 10 mM sodium citrate

and 0.05% Tween 20 solution (pH 8.5) for 30 min and followed by cooling for 20 min at room temperature. The sections were washed three times with dH_2O. To quench endogenous peroxidase activity, the sections were incubated with 3% hydrogen peroxide in methanol for 30 min at room temperature. After being washed three times with dH_2O and then PBS, the sections were blocked with 2.5% normal horse serum blocking solution (VECTOR laboratories) for 1 h at room temperature. The sections were incubated with diluted primary antibodies in PBS with 1% BSA for overnight at 4 °C. The next day, the sections were rinsed twice with 2% BSA in PBS-T (0.05% tween 20) for 5 min and then incubated with peroxidase conjugated anti-mouse or rabbit secondary antibody (VERCOR laboratories) for 30 min at room temperature. Peroxidase substrate DAB solution (VECTOR laboratories) was used as chromogen, resulting in a reddish-brown reaction product within 5 min. The sections were then counterstained with Mayer's hematoxylin (Sigma Aldrich). The images of the liver sections were captured by using a whole slide imaging system (DotSlide; Olympus) at the UNIST-Olympus Biomed Imaging Center.

Transmission Electron Microscopy

Mice were anesthetized with 2,2,2-Tribromoethanol and the liver was perfused with phosphate-buffered saline (PBS, pH 7.4) to remove any remaining blood. This was followed by perfusion with fixation solution (2% paraformaldehyde and 2.5% glutaraldehyde in 0.1 M phosphate buffer (PB)) for 10 min. After perfusion, the livers were removed and cut into 1-2 mm thick slices, which were further fixed by the fixation solution for overnight at 4 °C. After being washed in 0.1 M phosphate buffer, the liver slices were post-fixed with 1% osmium tetroxide in PB for 1 h at 4 °C. Next the samples were dehydrated with a series of the graded ethyl alcohol solution, which was exchanged with acetone in the next stage, and the samples were next embedded in EPON 812. Ultrathin sections (70~80 nm) were obtained by an ultramicrotome (Leica Ultracut UCT). Ultrathin sections were double stained with uranyl acetate and lead citrate. Finally, they were examined in a transmission electron microscope (JEM-1010) at 60 kV. [111]

Statistical analysis.

All data are presented as mean ± SEM. The statistical significance of differences between groups was evaluated by using Student's t test or the ANOVA one way test (Tukey's test). $P < 0.05$ was considered significant. $^{*, \#, \&}P < 0.05$, $^{**, \#\#, \&\&}P < 0.01$, $^{***, \#\#\#, \&\&\&}P < 0.001$.

Table-1. Primer List

Gene name	5' oligonucelotide	3' oligonucelotide	Usage
Atg5	AGCCAGGTGATGATTCACGG	GGCTGGGGGACAATGCTAA	qRT-PCR
Atg7	GTTCGCCCCCTTTAATAGTGC	TGAACTCCAACGTCAAGCGG	qRT-PCR
Atg12	GGAGACACTCCTATAATGAAA	ATAAATAAACAACTGTTCCGA	qRT-PCR
LC3b	CGTCCTGGACAAGACCAAGT	ACCATGTACAGGAAGCCGTC	qRT-PCR
P62	GCTGCCCTATACCCACATCT	CGCCTTCATCCGAGAAAC	qRT-PCR
Nbr1	TTCCAGGAAGACTACAATTC	ATGCAATTCTTCCTTCTTAG	qRT-PCR
Mcoln1	GCTGGGTTACTCTGATGGGTC	CCACCACGGACATAGGCATAC	qRT-PCR
Lamp-1	ACCTGTCGAGTGGCAACTTCA	GGGCACAAGTGGTGGTGAG	qRT-PCR
Lamp-2a	GCAGTGCAGATGAAGACAAC	AGTATGATGGCGCTTGAGAC	qRT-PCR
Lamp-2b	GGTGCTGGTCTTTCAGGCTTGATT	ACCACCCAATCTAAGAGCAGGACT	qRT-PCR
Lamp-2c	ATGTGCTGCTGACTCTGACCTCAA	TGGAAGCACGAGACTGGCTTGATT	qRT-PCR
Limp-1	GAAGCAGGCCATTACCCATGA	TGACTTCACCTGGTCTCTAAACA	qRT-PCR
Limp-2	TGTTGAAACGGGAGACATCA	TGGTGACAACCAAAGTCGTG	qRT-PCR
Cathepsin B (CtsB)	TCCTTGATCCTTCTTTCTTGCC	ACAGTGCCACACAGCTTCTTC	qRT-PCR
Cathepsin D (CtsD)	CTGAGTGGCTTCATGGGAAT	CCTGACAGTGGAGAAGGAGC	qRT-PCR
Cathepsin L (CtsL)	ATCAAACCTTTAGTGCAGAGTG	CTGTATTCCCCGTTGTGTAGC	qRT-PCR
Cathepsin F (CtsF)	GCAACTTCTCAGCACAGATGGCAA	GAACTGCATGCCGAAGGCGTTAAT	qRT-PCR
Cathepsin H (CtsH)	TACAACAAGGGCATCATGGA	TTCTTGACGAATGCAACAGC	qRT-PCR
Cathepsin K (CtsK)	GGGCCAGGATGAAAGTTGTA	CACTGCTCTCTTCAGGGCTT	qRT-PCR
Cathepsin O (CtsO)	TGGTGGCAGATTCACAGTACCCAT	AGTGCTCTGGCCATTTCATCCTCT	qRT-PCR
Cathepsin S (CtsS)	ACCTACCAAGTGGGCATGAACGAT	TCGGGAAATTCTCAGAGCACCCAT	qRT-PCR
Cathepsin Z (CtsZ)	TGTCATTGACTGTGGCAATGCTGG	TGCAGGTCCCACACTGGTTAAACT	qRT-PCR
DCTN1	AAATGGGTGGGCGTGATTCTG	ACTGGCGTACAAAGATGCCG	qRT-PCR
Rab7	AAGCCACAATAGGAGCGGAC	AGACTGGAACCGTTCTTGACC	qRT-PCR
Syntaxin 8 (Stx8)	CCGAGAGAGACTGCTCCTG	CCTCGCTTTGCTTCTTCGC	qRT-PCR
Syntaxin 17 (Stx17)	TCACTAAGATCGTGATCCCAACA	TCTGCACCGCTGATACTTCTC	qRT-PCR
Vit1b	GCCTCCTCCGAGCATTTCG	GTGCATATCGTAGTTCTTCCTCC	qRT-PCR
Vamp3	CCACTGGCAGTAATCGAAGAC	GCGGTCATCTAGCTCCGAGA	qRT-PCR
Vamp7	GACAACTTACGGTTCAAGAGCA	TCTCCACGTTGAGCAACTAAATC	qRT-PCR
Vamp8	AGTGGGAGTGCCGGAAATG	TGAAGTGTTCAGACGTGGCTT	qRT-PCR
SNAP29	AGGTTTACCCAAAGAACTCGACC	TGGCCTAATCCCACGGACA	qRT-PCR
Vps8	CCTCAGGTGGATACCCCTCC	CCAGAACGAAAGACTCATCTTCA	qRT-PCR
Vps11	AAAAGAGAGACGGTGGCAATC	AGCCCAGTAACGGGATAGTTG	qRT-PCR
Vps16	ATGGACTGTTACACTGCGAAC	CCACCAGGCAATCCTTGAG	qRT-PCR
Vps18	AGTACGAGGACTCATTGTCCC	TGGGCACTTACATACCCAGAAT	qRT-PCR
Vps33a	TACGGGCGAGTGAACCTGAA	ACTCATCCCACACTATTGCCTT	qRT-PCR
Vps39	CTTCTTGTTGGAACCAAGCAAGG	GCTTTCAGGTGAGGCTACATCT	qRT-PCR
vps41	CCCAAACTGAAGTATGAAAGGCT	CCAAAAACTTGTCATGGACCGT	qRT-PCR
Atg14	GAGGGCCTTTACGTGGCTG	AATAGACGAAATCACCGCTCTG	qRT-PCR
TFEB	CCTGCCGACCTGACTCAGA	CTCAATTAGGTTGTGATTGTCTTTCTTC	qRT-PCR
TFE3	CCTGAAGGCATCTGTGGATT	TGTAGGTCCAGAAGGGCATC	qRT-PCR
eIF2alpha (*fTg*)	GCTGGTTGTTGTGCTGTCTC	CCACCTCAGGAAATTTGTGTT	qRT-PCR
XBP1 total	CCTGAGCCCGGAGGAGAA	CTGCACCTGCTGCGGAC	qRT-PCR
XBP1 splicing	GAGTCCGCAGCAGGTG	AGGCTTGGTGTATACATGG	qRT-PCR
ATF4	ATGGCCGGCTATGGATGAT	CGAAGTCAAACTCTTTCAGATCCATT	qRT-PCR
Chop	ATGGCAGCTGAGTCATTGCCTTTC	AGAAGCAGGGTCAAGAGTGGTGAA	qRT-PCR
Bip	TCATCGGACGCACTTGGA	CAACCACCTTGAATGGCAAGA	qRT-PCR
Beclin1	ATGGAGGGGTCTAAGGCGTC	TGGGCTGTGGTAAGTAATGGA	qRT-PCR
Uvrag	CAAGCTGACAGAAAAGGAGCGAG	GGAAGAGTTTGCCTCAAGTCTGG	qRT-PCR
Hexb	CTGGTGTCGCTAGTGTCGC	CAGGGCCATGATGTCTCTTGT	qRT-PCR
Glb1	AAATGGCTGGCAGTCCTTCTG	ACCTGCACGGTTATGATCGGT	qRT-PCR
Tpp1	CCCCTCATGTGGATTTTGTGG	TGGTTCTGGACGTTGTCTTGG	qRT-PCR
β-actin	GATCTGGCACCACACACCTTCT	GGGGTGTTGAAGGTCTCAAA	qRT-PCR

Results

eIF2α phosphorylation contributes to the activation of all three UPR pathways.

To elucidate the physiological role of eIF2α phosphorylation in ER stress-mediated autophagy, I generated ***A/A;fTg/0;Cre^{Hep}/0 (A/A^{Hep}) mice*** by introducing a transgene (*fTg*) encoding constitutively expressed *Cont. eIF2*α flanked by *LoxP* sites into a non-phosphorylable *eIF2*α *S51A* knock-in background. This transgene rescued the otherwise neonatal lethal *eIF2*α *S51A* homozygous mutant. Then, homozygous (*A/A*) or heterozygous (*S/A*) animals carrying the transgene were bred with mice expressing CRE recombinase under the control of an albumin promoter to delete the transgene in hepatocytes [55].

I validated the conditional *eIF2α S51A* mouse model by using a Western blot analysis. To determine whether eIF2α phosphorylation was sufficiently repressed in hepatocyte-specific eIF2α phosphorylation-deficient mice, mice were intraperitoneally injected with tunicamycin (Tm), an inhibitor of N-linked glycosylation, to induce ER stress. Elevated PERK phosphorylation was detected in the liver lysates of both the *Control* (*Cont., S/A-fTg*) and *A/A^{Hep}* mice. Phosphorylation of eIF2α and its downstream factor CHOP were upregulated in the liver lysates of the *Cont.* mice injected with Tm, whereas no phosphorylated eIF2α (p-eIF2α) was detected in the liver lysates of Tm-challenged *A/A^{Hep}* mice, but EGFP was highly expressed due to deletion of the *floxed eIF2α* region of the transgene which activates *Egfp* expression (Fig. 1A). These results demonstrate that the *Cre-LoxP* system efficiently removed the *floxed Cont.* eIF2α transgene (*fTg*) from the hepatocytes of *A/A^{Hep}* mice. Furthermore, eIF2α phosphorylation deficiency greatly reduced the nuclear accumulation of XBP1s (spliced XBP1), although neither IRE1α activation (Fig. 1B) nor IRE1α-dependent *Xbp1* mRNA splicing changed significantly (Fig. 1B). In addition, activation of ATF6α, an ER stress sensor, was determined by monitoring the S1P and S2P protease-dependent cleavage fragment (ATF6αΔC) [23]. The proteolytic cleavage fragment (ATF6αΔc) of ATF6α was not observed in

the *A/A*^{Hep} liver lysates under ER stress (Fig.1D). Therefore, expression levels of its downstream target genes BiP and GRP94 were significantly reduced in the liver lysates of *A/A*^{Hep} mice compared with those of the *Cont.* mice under ER stress conditions. In agreement with the Western blot analyses, quantitative mRNA analyses revealed that the expression level of eIF2α *fTg* mRNA was significantly reduced by deletion of the transgene (*fTg*) in *A/A*^{Hep} mice. In addition, many UPR genes including *Chop*, *Bip*, *total Xbp1* and *spliced Xbp1*, were significantly decreased in *A/A*^{Hep} mice compared with *Cont.* mice (Fig.1E). Taken together, these results suggest that eIF2α phosphorylation deficiency impairs the activation of all three UPR pathways.

eIF2α phosphorylation is required for proper remodeling of the ER in response to ER stress.

An ER size increase is understood to be important in overcoming ER stress [56] through an expansion of the ER membrane [57]. Several reports suggest that an active N-terminal ATF6α fragment and XBP1s can enhance the capacity of ER biogenesis through lipid biosynthesis, which drives the expansion of the ER membrane [58, 59], [60-62]. To assess ER structure changes during ER stress, I performed an ultrastructural analysis by using transmission electron microscopy (TEM). I observed that the ER of both *Cont.* and *A/A*^{Hep} mice had a tubular structure in hepatocytes under normal conditions (Fig. 2A). However, during ER stress condition (Tm challenge), the ER cisternae were enlarged or distended in the hepatocytes of *Cont.* mice (Fig. 2A). By contrast, the eIF2α phosphorylation deficient hepatocytes displayed an abnormal ER morphology with condensed ER cisternae and electron-dense materials, possibly representing protein aggregates, but no enlargement or distension in the tubular ER structure (Fig. 2B). These results demonstrate that ER stress-mediated structural changes are impaired by the absence of eIF2α phosphorylation. It is possible that eIF2α phosphorylation is required for proper ER remodeling to mitigate ER stress.

eIF2α phosphorylation is required to maintain mitochondrial dynamics and membrane potential under ER stress.

Interactions between mitochondria and the ER play a role in the cellular adaptation to stress [63]. To mitigate the harmful effects of cellular stress, adaptive mechanisms include mitochondrial dynamics that determine the fate of mitochondria [64]. In mitochondrial fusion, mitochondrial elongation increases ATP synthesis to meet cellular energy needs and protect mitochondria from autophagic degradation [65]. In addition, a recent report suggests that the PERK-eIF2α axis promotes stress-induced mitochondrial hyperfusion to protect mitochondria during ER stress [66]. Hyperfusion protects mitochondria from pathologic fragmentation and increases metabolism to facilitate recovery from acute ER stress. On the contrary, mitochondrial fission divides dysfunctional mitochondria and is accompanied by extensive mitochondrial fragmentation and crista remodeling [67]. Therefore, to evaluate the contribution of eIF2α phosphorylation to the maintenance of mitochondrial dynamics in response to cellular stress, I monitored mitochondrial morphology changes by TEM and fluorescence microscopy. Interestingly, the hepatocytes of eIF2α phosphorylation-deficient mice were characterized by abnormally large and swollen mitochondrial morphology with disrupted cristae, compared with those of the *Cont.* mice (Fig. 3A). Next, to investigate mitochondrial dynamics, primary hepatocytes isolated from *Cont.* and *A/A*^{Hep} mice were stained with the Mitotracker Red fluorescent probe, which is widely used to stain viable mitochondria. Because mitochondrial morphology is determined by a dynamic balance between fusion and fission, the mitochondrial morphology of hepatocytes before Tm treatment did not differ much between the *Cont.* and *A/A*^{Hep} mice. ER stress promoted mitochondrial fusion in the hepatocytes of *Cont.* mice (Fig. 3B). However, the eIF2α phosphorylation-deficient hepatocytes under ER stress displayed abnormal mitochondrial fragmentation, possibly by increased fission and mitochondrial swelling, which produced a loss of mitochondrial mass and mitochondrial dysfunction (Fig. 3B). These results suggest that eIF2α phosphorylation is required to maintain mitochondrial

dynamics under ER stress.

The mitochondrial membrane potential (MMP) was evaluated using JC-1, a cationic MMP probe that accumulates in energized mitochondria. The Tm-treated *A/A*^{Hep} hepatocytes displayed greatly reduced red J-aggregate fluorescence and significantly increased cytoplasmic green monomer fluorescence compared with the Tm-treated *Cont.* hepatocytes for 24 and 36 h (Fig.3C), suggesting that eIF2α phosphorylation is essential to preserve MMP during ER stress.

eIF2α phosphorylation deficiency increases autophagosome formation in the liver in response to ER stress.

When cellular ER stress is excessive or sustained, it triggers autophagy as a degradative process to reduce the accumulation of misfolded proteins [68]. In addition, previous studies suggest that the ER is an important source of autophagosome membrane [69, 70] and that mitochondrial dysfunction is related to autophagy [71]. In Figs. 1-3, I show that eIF2α phosphorylation is important to maintain both ER and mitochondrial functions under ER stress conditions. Therefore, I deemed it necessary to investigate the roles of eIF2α phosphorylation in ER stress-induced autophagy. First, I examined expression changes in autophagy-related genes (Fig. 4A) and proteins (Fig. 4B) during ER stress. In the livers of *Cont.* mice, the mRNA levels of the pre-autophagosome markers Atg5 and Atg12 and the cargo receptors P62/Sqstm1 and Nbr1 were significantly induced at early time points (6 and 12 h) but gradually decreased over time (24 and 36 h) under ER stress. The level of LC3B transcripts remained persistent throughout ER stress in the livers of the *Cont.* mice (Fig. 4A). Meanwhile, the expression levels of most genes declined sharply at several time points after Tm treatment in the livers of *A/A*^{Hep} mice compared with *Cont.* mice (Fig. 4A). Surprisingly however, despite the decreased expression of those genes, autophagosome-associated proteins such as the ATG5-ATG12 conjugates, LC3B and P62 were excessively increased at multiple time points (6, 12, 24, and 36 h) after Tm treatment in the liver lysates of *A/A*^{Hep} mice (Fig. 4B). As a cargo

adaptor, P62 is crucial to the recruitment of ubiquitinated proteins into autophagosomes [72]. Because inhibition of the autophagy pathway can cause p62 accumulation, I demonstrated that ubiquitinated proteins accumulated inordinately at multiple time points (12, 24, and 36 h) under ER stress in *A/A*^{Hep} mice compared with *Cont.* mice, suggesting dysregulation of the autophagy pathway in the livers of *A/A*^{Hep} mice during ER stress. Moreover, liver sections of the *A/A*^{Hep} mice exhibited a higher accumulation of LC3B, P62, and ubiquitinated proteins 36 h after Tm treatment (Fig. 4C) than I found in the *Cont.* mice (Fig. 4C, D). Next, to monitor autophagic vacuole formation induced by ER stress, LC3-positive puncta were visualized in liver sections from *Cont.* and *A/A*^{Hep} mice infected by RFP-LC3B expressing recombinant adenoviruses (Fig 4E). Compared with sections from the *Cont.* mice, *A/A*^{Hep} liver sections displayed markedly increased RFP-LC3-positive puncta in a time-dependent manner under ER stress (Fig. 4E). Because cargo recognition is critical to the formation of the autophagosome, I examined the co-localization of RFP-LC3B and P62 and found it to be significantly higher in *A/A*^{Hep} mice than in *Cont.* mice (Fig. 4F). Taken together, these findings suggest that eIF2α phosphorylation deficiency causes autophagosome accumulation, which might be induced by dysregulation of autophagic pathway during ER stress.

eIF2α phosphorylation deficiency results in the accumulation of autophagic vesicles in the liver in response to ER stress.

To verify the accumulation of autophagic puncta in *A/A*^{Hep} hepatocytes under ER stress (Fig. 4D-F), a TEM analysis was applied to liver sections. In the liver sections of *A/A*^{Hep} mice, a vast number of autophagic compartments was clustered in certain intracellular areas in response to prolonged ER stress (dotted lines in Figs. 3A, 5A). The high magnification observation reveals many double membranes but aberrantly small autophagic vesicles (red arrow heads) in the Tm-treated *A/A*^{Hep} hepatocytes at 24 h (Fig. 5B). In addition, the number of autolysosomes in *A/A*^{Hep} mice was lower than that in the *Cont.* mice under Tm treatment. Therefore, eIF2α phosphorylation deficiency could block basal autophagy after autophagosome formation but before lysosomal degradation, thus leading to the accumulation of small autophagic vacuoles under ER stress.

eIF2α phosphorylation deficiency impairs the fusion of autophagosomes with lysosomes in the liver in response to ER stress.

Fusion of autophagosomes with lysosomes, a part of autophagy flux, is critical to functional autophagy. To confirm its occurrence, I microscopically examined the co-localization of RFP-LC3B and lysosomal proteins (Lamp1, Cathepsin B, and Cathepsin D) in the livers of RFP-LC3B-transduced mice under ER stress conditions. Although RFP-LC3-positive puncta increased, the liver sections of *A/A*^{Hep} mice showed that co-localization of RFP-LC3B and LAMP1, a lysosomal membrane protein, was significantly reduced in a time-dependent manner under ER stress (Fig. 6A). Similarly, I confirmed that RFP-LC3B did not co-localize with Cathepsin B (Fig. 6B) or Cathepsin D (Fig. 6C), lysosomal enzymes that are required to degrade the autophagosomal contents, in *A/A*^{Hep} mice. I established these results by calculating Pearson's correlation coefficients (Fig. 6A, B, C).

To assess autophagic flux in vivo, I applied pharmacological research by using

leupeptin, an inhibitor of lysosomal cysteine proteinases (Fig. 6D) [73]. The administration of leupeptin caused LC3B-II accumulation in the livers of mice with both genotypes both before Tm treatment and 6 h after Tm treatment (Fig. 6D). Thus, autophagy flux was normally maintained in an eIF2α phosphorylation-independent manner until early into the time of ER stress. However, although Tm treatment for 24 h alone caused a strong increase in L3B-II, no further enhancement was observed upon leupeptin administration in the livers of *A/A^{Hep}* mice, whereas the livers of *Cont.* mice maintained the capability for leupeptin-mediated LC3B-II accumulation until 24 h after Tm treatment. Taken together, these results confirm that eIF2α phosphorylation deficiency disrupts autophagy flux in response to ER stress.

eIF2α phosphorylation deficiency impairs the fusion between autophagosomes and lysosomes in primary hepatocytes in response to ER stress.

I also investigated autophagosome formation, the fusion of autophagosomes with lysosomes, and autophagy flux by using primary hepatocytes isolated from *Cont.* and *A/A^{Hep}* mice during ER stress. An immunofluorescence analysis revealed a higher accumulation and co-localization of both LC3B and P62 in Tm-treated *A/A^{Hep}* hepatocytes (Fig. 7A), similar to the results of Tm-treated *A/A^{Hep}* liver sections (Fig. 4C~4F), suggesting that eIF2α phosphorylation is not a critical factor in inducing autophagosome formation upon ER stress. Localization analyses of LC3B and LAMP1 and p62 and LAMP1 showed that autophagosome markers (LC3B and P62) did not co-localize with the lysosomal marker LAMP1 in Tm-treated *A/A^{Hep}* hepatocytes (Fig. 7B, C), whereas they co-localized in Tm-treated *Cont.* hepatocytes, indicating that eIF2α phosphorylation is important for the fusion of autophagosomes with lysosomes during ER stress. In addition, the co-localization of LAMP1 and Cathepsin D was partially reduced in Tm-treated *A/A^{Hep}* hepatocytes compared with Tm-treated *Cont.* hepatocytes, demonstrating that transportation of the lysosomal enzyme to the lysosomal vesicle might be impaired (Fig. 7D).

Next, to assess autophagic flux, I used bafilomycin. a lysosomal V-ATPase inhibitor,

to block fusion between the autophagosome and the lysosome during autophagy. Tm treatment caused an increase in LC3-II levels that was further enhanced by bafilomycin treatment in *Cont.* hepatocytes. In contrast, even though Tm treatment alone caused a strong increase in LC3-II levels in *A/A*^{Hep} hepatocytes, no further enhancement was observed upon the addition of bafilomycin, confirming that autophagic flux is indeed blocked in eIF2α phosphorylation-deficient cells during ER stress (Fig. 7E, F). These observations suggest that eIF2α phosphorylation deficiency diminished autophagic degradation by causing a defect in autophagosome-lysosome fusion in response to ER stress.

Wild type eIF2α overexpression increases autolysosome formation in eIF2α phosphorylation-deficient cells in response to ER stress.

Next, I examined whether autophagosome-lysosome fusion defects can be rescued by transient overexpression of wild type eIF2α in *A/A*^{Hep} cells. I infected *A/A*^{Hep} primary hepatocytes with Flag tagged wild type eIF2α expressing adenoviruses (*Ad-Flag-eIF2α*). Overexpression of wild type eIF2α drastically reduced the expression levels of both LC3B-I/II forms, regardless of Tm treatment, and prevented the accumulation of P62 in the Tm treatment condition, indicating diminished autophagosome accumulation in response to ER stress (Fig. 8A, B). To microscopically observe the beneficial effect of wild type eIF2α overexpression in eIF2α phosphorylation-deficient cells, co-localization of the autophagosome marker LC3B and lysosome marker LAMP1 was examined by using confocal microscopy. The results indicate that the co-localization of LC3B and LAMP1 was markedly enhanced by the overexpression of wild type eIF2α in both *A/A*^{Hep} primary hepatocytes and *A/A* immortalized hepatocytes whereas it was severely defective in *Ad-Vec*-infected eIF2α phosphorylation-deficient cells (Fig. 14C, D). Collectively, these results suggest that eIF2α phosphorylation plays an essential role in maintaining autophagy flux in response to ER stress.

eIF2α phosphorylation deficiency leads to dysregulated expression of autophagy related genes in the liver upon ER stress.

To assess whether the observed autophagic flux defect in eIF2α phosphorylation-deficient hepatocytes is related to the dysregulated gene expression of lysosomal genes or autophagosome-lysosome fusion-related genes during ER stress, I measured the mRNA and protein levels of lysosomal membrane proteins (*Mcoln1*, *Lamp-1*, *Lamp-2a*, *Lamp-2b*, *Lamp-2c*, *Limp-1*, and *Limp-2*) [74] and cathepsins (*CtsB*, *CtsD*, *CtsF*, *CtsH*, *CtsK*, *CtsL*, *CtsO*, *CtsS*, and *CtsZ*) [75] for lysosomal genes (Fig. 9A, C) and components (*Stx8*, *Stx17*, *Vit1b*, *Vamp3*, *Vamp7*, *Vamp8*, *SNAP29*) of SNARE complexes, a component (*Vps8*) of CORVET (class C core vacuole/endosome tethering), and components (*Vps11*, *Vps16*, *Vps18*, *Vps33a*, and *Vps39*) of HOPS tethering complex for autophagosome-lysosome fusion (Fig. 9B) [42, 76]. First, without ER stress *A/A^{Hep}* mice displayed significantly decreased expression of a lysosomal membrane protein (*Mcoln1*), several cathepsins (*CtsF*, *CtsH*, *CtsO*, and *CtsZ*), and autophagosome-lysosome fusion related genes (*DTCN1*, *Rab7*, *Stx8*, *Stx17*, *Vit1b*, *Vamp3*, *Vamp8*, *SNAP29*, *Vps18, Vps33a*, and *Atg14*) (Fig. 9A, B) compared with the *Cont.* mice, suggesting that eIF2α phosphorylation in hepatocytes is required for optimal expression of a subset of lysosomal genes and autophagosome-lysosome fusion related genes. Second, upon ER stress induction, the transcript levels of all the tested genes except *Limp-1*, *Vps16*, and *Vps 18* were significantly reduced in the livers of *A/A^{Hep}* mice compared with the levels in the *Cont.* mice, although ER stress reduced the expression levels of several lysosomal genes and autophagosome-lysosome fusion-related genes in the livers of *Cont.* mice (Fig. 9A, B). In addition, a Western blot analysis of cathepsin proteins revealed decreased levels of the intermediate single-chains and mature double-chains of cathepsin B and D enzymes 36 h after Tm treatment in the livers of *A/A^{Hep}* mice compared with the levels in the *Cont.* mice, although cathepsin L did not differ significantly between the genotypes (Fig. 9C). Collectively, these gene expression studies suggest that eIF2α phosphorylation is required to maintain the

expression of multiple lysosomal genes and autophagosome-lysosome fusion related genes during ER stress.

Several recent reports [45, 77, 78] suggest that TFEB and TFE3 are master transcriptional regulators of genes involved in lysosomal biogenesis and autophagy. Therefore, I checked the possibility that the expression levels of TFEB and TFE3 could be related to the dysregulated expression of autophagy-related genes in the livers of *A/A^{Hep}* mice under ER stress. However, Western blot results indicate that the protein amounts of TFEB and TFE3 increased in the liver lysates of both *A/A^{Hep}* and *Cont.* mice under ER stress conditions (Fig. 9C), although the levels of both the *Tfeb* and *Tfe3* transcripts were downregulated in the livers of *A/A^{Hep}* mice compared with *Cont.* mice upon ER stress (Fig. 9D), suggesting that expression changes in the TFEB and TFE3 transcription factors are not responsible for the dysregulated expression of genes involved in autophagy in the liver upon ER stress.

eIF2α phosphorylation deficiency leads to dysregulated expression of autophagy related genes in primary hepatocytes upon ER stress.

Next, I tested whether *in vivo* observation of dysregulated gene expression in the livers of *A/A^{Hep}* mice could be reproduced in primary hepatocytes isolated from *A/A^{Hep}* mice during ER stress. As I expected, the transcript and protein levels of UPR genes, including *eIF2α fTg, total xbp1*, *atf4*, *chop, Grp94*, and *BiP,* were significantly downregulated in *A/A^{Hep}* primary hepatocytes compared with *Cont.* primary hepatocytes after Tm treatment (Fig. 10A, B). In the *Cont.* primary hepatocytes, Tm treatment significantly induced the transcription of autophagosome formation genes (*Beclin1*, *Uvrag*, *Atg5*, *Atg12*, *Lc3b*, and *p62*), lysosomal genes (*Lamp-1, Lamp-2b, Mcoln1*, *CtsD, CtsL*, *Hexb*, *Glb1*, and *Tpp1*), and fusion related genes (*Rab7*, *Stx17*, *SNAP29*, *Vps8*, *Vps33a*, *Vps41*, *Vamp8*, and *Atg14*) upon ER stress (Fig. 10C). However, upon ER stress, the transcript levels of all the tested genes except *Lc3b*, *p62*, *Lamp2a*, *Rap7*, and *SNAP29* were significantly reduced in *A/A^{Hep}* primary hepatocytes compared with the levels in *Cont.* primary hepatocytes (Fig. 10C). Furthermore, eIF2α

phosphorylation deficiency downregulated transcript levels of *Tfeb* and *Tfe3*, which modulate autophagy and lysosomal biogenesis in response to ER stress (Fig. 10C). These results indicate that the expression of autophagosome formation genes and lysosome biogenesis and fusion-related genes apparently requires eIF2α phosphorylation in primary hepatocytes during ER stress.

Consistent with the results from the mouse model, eIF2α phosphorylation deficiency in primary hepatocytes led to an accumulation of LC3B and P62 expression under ER stress, compared with *Cont.* hepatocytes. Among the lysosome-related proteins, Vamp8 was especially decreased in A/A^{Hep} primary hepatocytes upon ER stress, although other proteins (LAMP1, LAMP2, and STX17) were not changed (Fig. 10D). In addition, A/A^{Hep} primary hepatocytes had reduced cleaved forms, such as intermediate single-chain and mature double-chain forms of cathepsins B, D, and L, upon ER stress, suggesting that eIF2α phosphorylation contributes to the maturation of cathepsin enzymes in lysosomes in response to ER stress (Fig. 10E). Taken together, these results suggest that eIF2α phosphorylation deficiency impairs lysosomal function and could block autophagic clearance.

eIF2α phosphorylation deficiency disrupts lysosome positioning and lysosome functionality which can affect autophagic flux upon ER stress.

To discern whether lysosomal dysfunction can contribute to autophagy flux defects in A/A^{Hep} hepatocytes, I observed the localization of lysosome proteins and assessed lysosome functionality. Consistent with the results shown in Figs 9A, 9C, 10C, and 10E, the immunofluorescence analyses revealed that ER stress decreased the expression of LAMP1 and cathepsins B and D in both genotypes (Figs. 11A-D). These results demonstrate that ER stress can downregulate the expression of lysosomal proteins in an eIF2α phosphorylation-independent manner. Interestingly, I observed that LAMP1-positive puncta were localized to the perinuclear region in the hepatocytes of *Cont.* mice under ER stress, whereas in the eIF2α phosphorylation-deficient mice, the LAMP1 positive puncta were distributed to the peripheral

plasma membrane (Fig. 11A). In addition, the signal intensities of lysosomal cathepsin B-, D-, L-positive puncta decreased more rapidly upon ER stress in *A/A*^{Hep} mice than in *Cont.* mice (Figs. 11B-D), suggesting that eIF2α phosphorylation deficiency disrupts proper lysosomal positioning and reduces the expression of lysosomal enzymes during ER stress.

Lysosomes move toward the perinuclear region, where autophagosome-lysosome fusion occurs upon activation of the autophagy process [79]. To monitor changes in lysosome localization and acidification during ER stress, I used LysoTracker-Red-Red, a fluorescent dye that labels acidic organelles, in primary hepatocytes isolated from *Cont.* and *A/A*^{Hep} mice (Fig. 11E). ER stress significantly induced time-dependent perinuclear clustering of lysosomes in *Cont.* hepatocytes. However, in *A/A*^{Hep} primary hepatocytes, the fluorescence intensity of LysoTracker-Red-Red decreased rapidly as the labeled lysosomes moved toward the adjacent plasma membrane, unlike in the *Cont.* hepatocytes under ER stress (Fig. 11E). These results are congruent with the data in Fig. 10A showing mis-localization of LAMP1 positive puncta during ER stress

Next, to visualize cathepsin B and L activity, Magic Red Cathepsin assay kits that label pH-sensitive lysosomal protease were used (Figs. 11F, G). I found that the fluorescence intensities of cathepsins B and L were significantly attenuated in *A/A*^{Hep} primary hepatocytes compared with *Cont.* primary hepatocytes under ER stress conditions. Taken together, these results indicate that eIF2α phosphorylation deficiency disrupts both lysosome positioning and lysosome functionality which can affect autophagic flux upon ER stress.

eIF2α phosphorylation is responsible for the assembly of SNARE complexes for autophagosome-lysosome fusion in response to ER stress.

The recruitment of the SNARE protein STX17 to the autophagosome is believed to play an essential role in autophagosome-lysosome formation [80]. To elucidate the effect of eIF2α phosphorylation in autophagosome-lysosome fusion, I examined the co-localization of STX 17

and LC3B in an autophagosome induced by ER stress (Fig. 12A). In the absence of ER stress, Flag-STX17 localized at tubular structures, believed to be the ER [42], and did not co-localize with the autophagosomal marker LC3 in either *S/S* or *A/A* immortalized hepatocytes. Upon ER stress, however, many LC3 puncta co-localized with Flag-STX17 in *S/S* cells, which also formed puncta, whereas obvious co-localization was not observed in *A/A* cells (Fig. 12A). Co-localization intensity spatial profiles support those observations (Fig. 12A), suggesting that eIF2α phosphorylation is required to recruit STX17 into autophagosomes during ER stress.

Stx17 is required for fusion between the autophagosome and endosome/lysosome [81]. To confirm the assembly of components for membrane fusion between the autophagosome and lysosomes, I co-immunoprecipitated the endosomal/lysosomal SNARE Vamp7 with Flag-STX17 (Fig. 12B). The association of Flag-STX17 with Vamp7 on lysosomal membranes was increased in *S/S* cells, whereas in *A/A* cells it was significantly reduced 16 h after Tm treatment. These results suggest that eIF2α phosphorylation is required for the recruitment of STX17 to the autophagosome and the assembly of SNARE complexes for autophagosome-lysosome fusion in response to ER stress.

eIF2α phosphorylation is responsible for the nuclear translocation of the autophagy master regulators TFE3/TFEB in response to ER stress.

In Figs 4A, 4B, 9A-D, 10C-E, the gene expression analyses of livers and primary hepatocytes indicate that eIF2α phosphorylation deficiency led to dysregulated expression of TFEB- and TFE3-dependent genes, whereas TFEB and TFE3 protein levels were increased in eIF2α phosphorylation-deficient cells in response to ER stress. Upon the induction of autophagy, TFEB and TFE3 are translocated from the cytoplasm to the nucleus to induce the transcription of target genes [82]. Therefore, I checked whether TFEB and TFE3 were translocated to the nuclei of eIF2α phosphorylation-deficient cells upon ER stress. To assess the nuclear translocation of endogenous TFE3, I performed immunocytochemistry in primary hepatocytes isolated from *Cont.* and *A/A*^{Hep} mice under ER stress (Fig. 13A). In addition, due to difficulty detecting endogenous TFEB with commercial antibodies, I used Flag-tagged TFEB-expressing adenovirus in primary hepatocytes (Fig. 13B). The results show that ER stress efficiently induced the translocation of both TFE3 and TFEB-Flag to the nucleus in *Cont.* primary hepatocytes, whereas their nuclear translocation was significantly blocked in *A/A*^{Hep} primary hepatocytes upon ER stress (Fig. 13A, B). Although both starvation and ER stress have been known to induce autophagy [83], I observed that TFEB almost translocated to the nucleus in *A/A*^{Hep} primary hepatocytes upon amino acid deprivation, although the efficiency of TFEB nuclear translocation was lower than that in *Cont.* primary hepatocytes (Fig. 13B). Collectively, these results suggest that eIF2α phosphorylation deficiency could result in decreased nuclear localization of TFEB and TFE3, producing dysregulated expression of TFEB- and TFE3-dependent genes in response to ER stress.

TFEB overexpression restores lysosome functionality and mitochondrial dynamics in eIF2α phosphorylation-deficient primary hepatocytes upon ER stress.

Because the dysregulation of TFEB nuclear translocation contributes to autophagic failure and mitochondrial dysfunction [84], I next tried to restore the defects of eIF2α phosphorylation-deficient primary hepatocytes observed in these results through TFEB overexpression. In *A/A*^{Hep} primary hepatocytes, adenovirus-mediated TFEB-Flag overexpression significantly and preferentially increased the expression of a subset of its target genes: *Lamp-2a*, *Lamp-2b*, *Cts L*, *Glb-1*, and *Pgc-1* (Fig. 14A) [74, 75].

Next, to investigate the potential recovery effect of TFEB in lysosomes, I analyzed lysosomal positioning and functional activity by using LysoTracker-Red. Those results indicate that TFEB overexpression promoted lysosomal acidification and restored the perinuclear clustering of lysosomes in *A/A*^{Hep} primary hepatocytes during ER stress (Fig. 14B). Furthermore, TFEB overexpression effectively alleviated mitochondrial fragmentation, indicating that TFEB rescued mitochondrial dynamic imbalance. These observations suggest that TFEB overexpression could restore the lysosomal and mitochondrial defects of *A/A*^{Hep} primary hepatocytes during ER stress.

TFEB overexpression ameliorates the impairment of the autophagy-lysosome pathway in eIF2α phosphorylation-deficient primary hepatocytes upon ER stress.

Because I observed that TFEB overexpression positively influenced the expression of autophagy-related genes, lysosome functionality, and mitochondrial dynamics, I next checked whether TFEB overexpression could restore the failures of autophagosome-lysosome fusion and autophagic flux in *A/A*^{Hep} primary hepatocytes during ER stress.

As shown by the results in Figs 4D, 4F, and 7A, *Ad-Vec*-infected *A/A^{Hep}* primary hepatocytes displayed increased LC3 and p62 correlation coefficients compared with *Ad-Vec* infected *Cont.* cells, suggesting an accumulation of LC3B and P62 double-positive autophagic puncta under Tm-treated conditions. TFEB overexpression significantly reduced the puncta accumulation to a level similar to that of the *Ad-Vec*-infected *Cont.* cells upon ER stress, indicating that TFEB overexpression can prevent the aberrant accumulation of autophagosomes caused by the impairment of the autophagy-lysosome pathway in eIF2α phosphorylation-deficient primary hepatocytes upon ER stress (Fig. 15A). Next, I examined whether TFEB overexpression can restore the failures of autophagosome-lysosome fusion in *A/A^{Hep}* primary hepatocytes during ER stress. I observed that TFEB overexpression significantly increased the co-localization rate of LC3B and LAMP2 to a level similar to that of *Ad-Vec*-infected *Cont.* cells upon ER stress, confirming that autophagosome-lysosome fusion failure can be prevented (Fig. 15B). Furthermore, TFEB overexpression enhanced the co-localization rate of LAMP2 and Cathepsin B in *A/A^{Hep}* primary hepatocytes during ER stress (Fig. 15C). Likewise, I found that TFEB overexpression prevented autophagy-lysosome fusion failure in *A/A* immortalized hepatocyte cell lines (Fig. 15D). Together, these observations suggest that TFEB overexpression, possibly through increased expression of its target genes (Fig. 14A), restores lysosome function and then promotes autophagosome-lysosome fusion in eIF2α phosphorylation deficient cells during ER stress.

Because impaired autophagosome-lysosome fusion can be restored by TFEB overexpression in eIF2α phosphorylation deficient cells, I envisaged TFEB overexpression as a relevant strategy to ameliorate the autophagy flux blockade in *A/A^{Hep}* primary hepatocytes. As expected, the autophagic flux assay using bafilomycin A1 (Baf. A1) confirmed that the Baf. A1-mediated increase in the LC3B-II and P62 steady state levels was observed in *Ad-TFEB-Flag*-infected *A/A^{Hep}* primary hepatocytes, whereas no further enhancement in their protein levels was observed upon the addition of Baf. A1 to *Ad-Vec*-infected *A/A^{Hep}* primary

hepatocytes during ER stress, indicating that TFEB overexpression, which can increase the expression of autophagy-related and lysosomal genes, promotes lysosomal clearance of autophagic cargoes (Fig. 15E, F).

Figures

Figure 1.

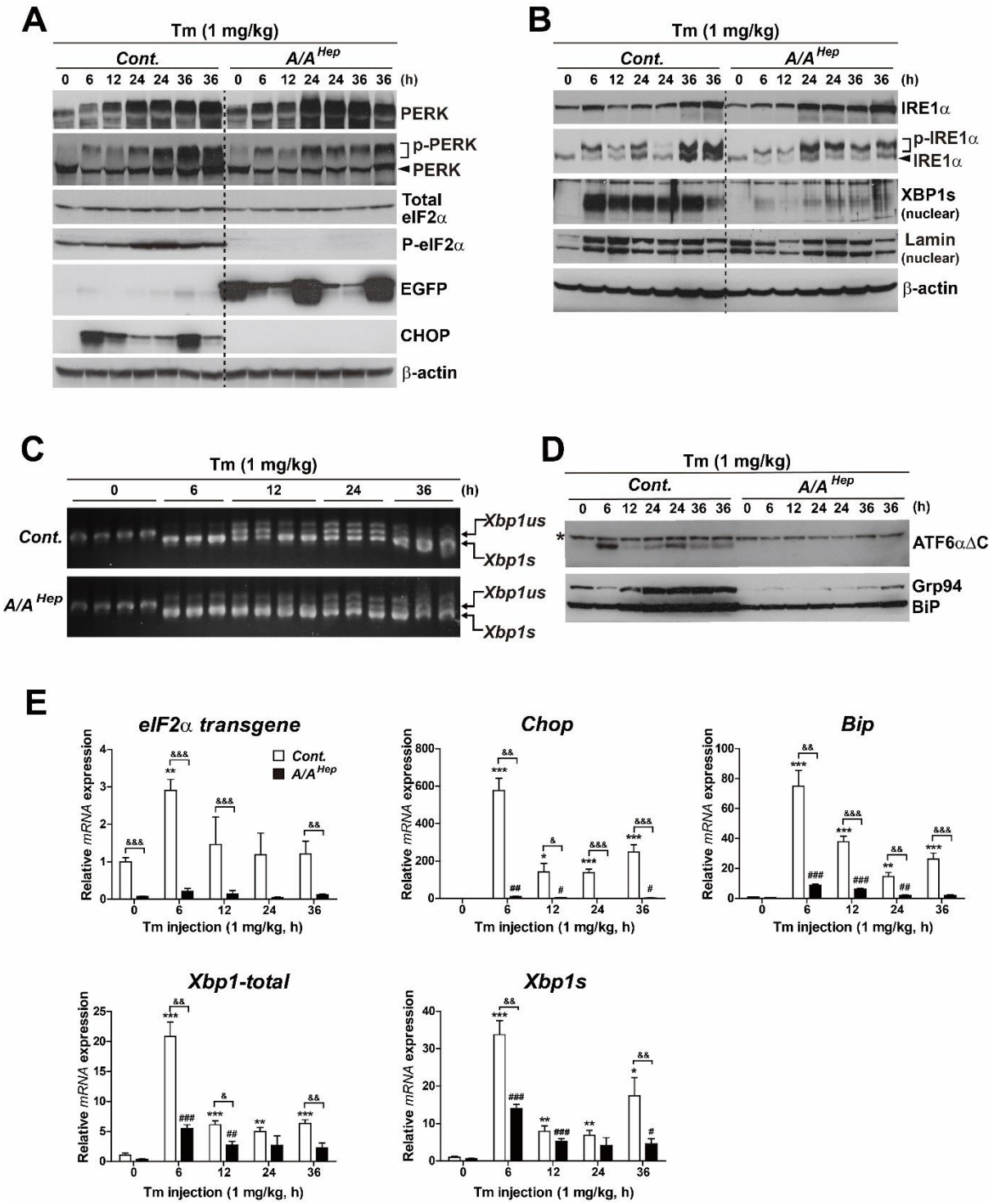

Figure 1. eIF2α phosphorylation contributes to the activation of all three UPR pathways.

(A, B). Western blot analyses of proteins of (A) PERK/eIF2α and (B) IRE1α/XBP1 pathways were performed in liver lysates from *Control* (*Cont.*) and *A/A*^{Hep} mice treated with tunicamycin (Tm,1 mg/kg) for indicated times. β-actin was probed to demonstrate equal loading.

(C). Unspliced *Xbp1* (*Xbp1us*) and spliced *Xbp1* (*Xbp1s*) mRNA levels were detected by RT-PCR in liver lysates from *Control* (*Cont.*) and *A/A*^{Hep} mice treated with tunicamycin (Tm,1 mg/kg) for indicated times.

(D). Western blot analyses of ATF6α, Grp94 and BiP were performed in liver lysates from *Control* (*Cont.*) and *A/A*^{Hep} mice treated with tunicamycin (Tm,1 mg/kg) for indicated times. (* : non-specific band).

(E) Expression levels of UPR related genes induced by ER stress were measured by quantitative real-time PCR in liver lysates from *Control* (*Cont.*) and *A/A*^{Hep} mice treated with tunicamycin (Tm,1 mg/kg) for indicated times.

All data are mean ± SEM (n=3 mice per group); *p < 0.05, **p < 0.01 and ***p < 0.001; 0 vs each time points in the control group, $^{\#}$p < 0.05, $^{\#\#}$p < 0.01 and $^{\#\#\#}$p < 0.001; 0 vs each time points in the *A/A*^{Hep} group, $^{\&}$p < 0.05, $^{\&\&}$p < 0.01 and $^{\&\&\&}$p < 0.001; *Control* (*Cont.*) vs *A/A*^{Hep} mice at each time points.

Figure 2.

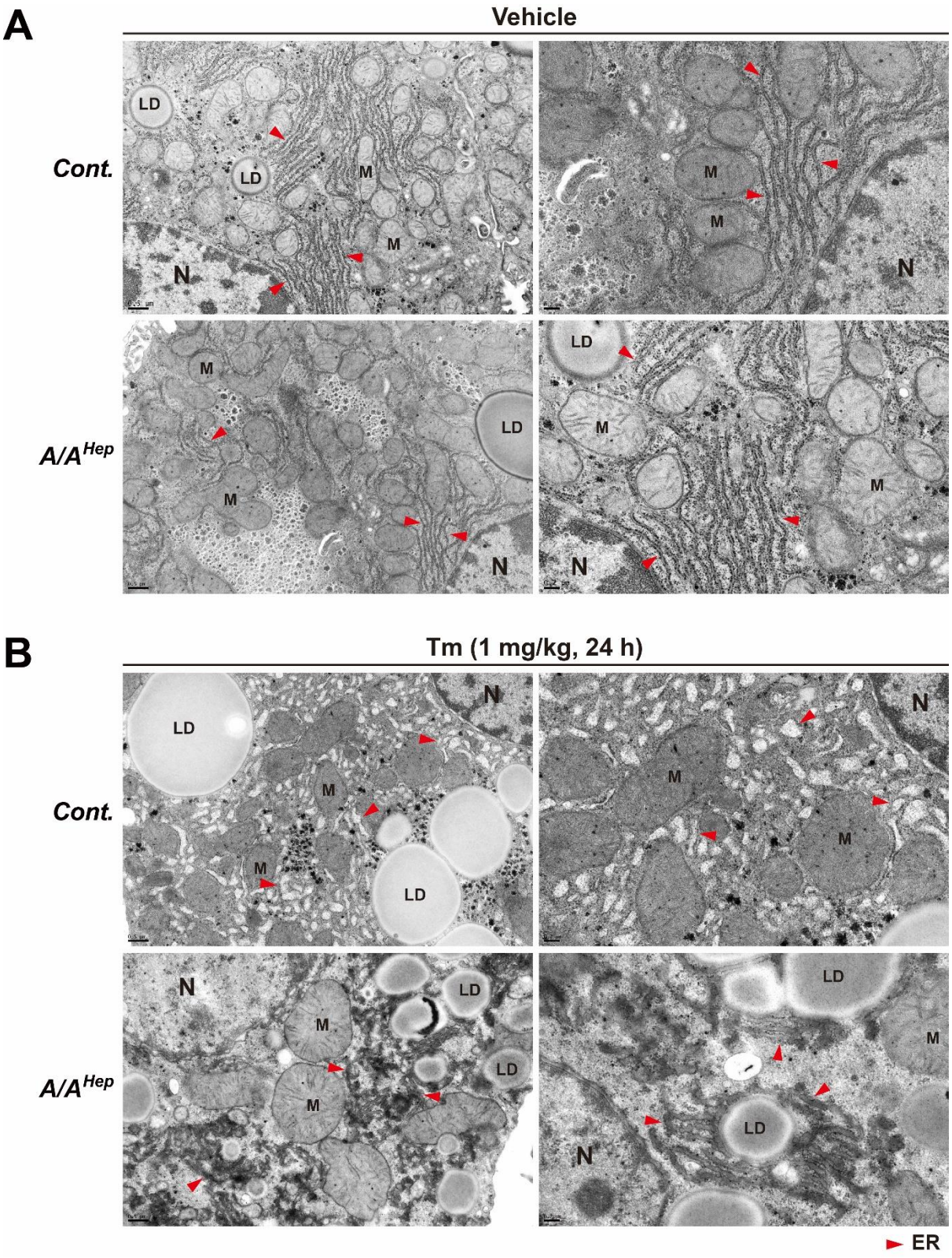

Figure 2. eIF2α phosphorylation is required for proper remodeling of the ER in response to ER stress.

(A, B) Transmission electron microscopy (TEM) analyses of ER structures were performed in liver sections from *Control* (*Cont.*) and *A/A*^{Hep} mice treated with (A) vehicle or (B) tunicamycin (1 mg/kg) for 24 h. Red arrowheads indicate ER structures. Scale bars in left panels: 0.5 μm and Scale bars in right panels: 0.2 μm.

Figure 3.

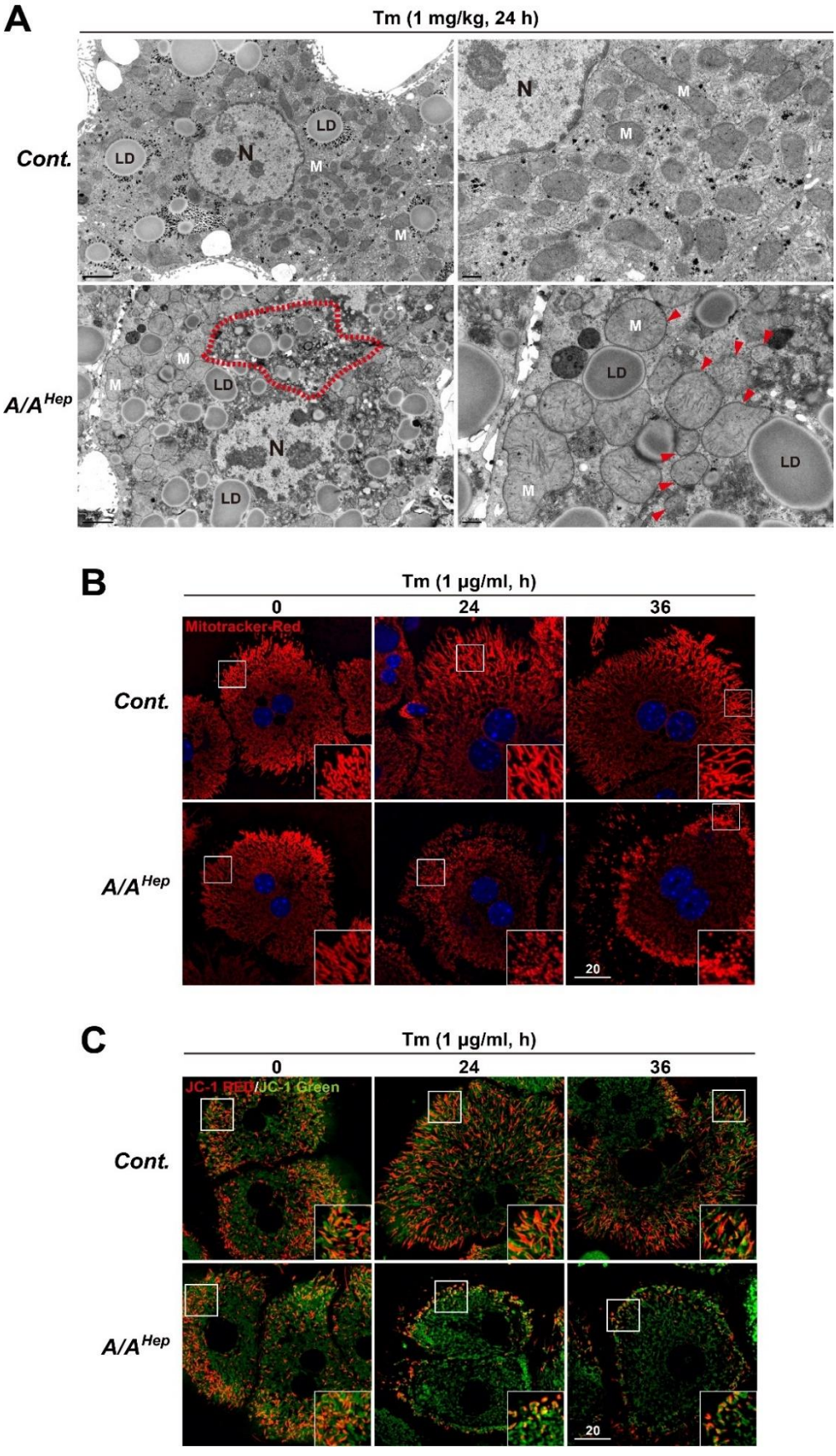
A
Tm (1 mg/kg, 24 h)
Cont.
A/A Hep
LD
N
M
B
Tm (1 μg/ml, h)
0
24
36
Mitotracker-Red
Cont.
A/A Hep
20
C
Tm (1 μg/ml, h)
0
24
36
JC-1 RED/JC-1 Green
Cont.
A/A Hep
20

Figure 3. eIF2α phosphorylation is required to maintain mitochondrial dynamics and membrane potential under ER stress.

(A) Transmission electron microscopy (TEM) analyses of mitochondrial structures were performed in liver sections from *Control* (*Cont.*) and *A/A*^{Hep} mice treated with tunicamycin for 24 h. Red dotted line represents accumulated autophagic vesicles. Red arrowheads indicate mitochondria. Mitochondria of *A/A*^{Hep} mice were larger than them of the *control* mice. M: Mitochondria, LD: Lipid droplet and N: nucleus. Scale bars in left panels: 0.5 μm and Scale bars in right panels: 0.2 μm.

(B) Change of mitochondrial morphology was observed in the *Cont.* and *A/A*^{Hep} primary hepatocytes treated with tunicamycin (Tm,1 μg/ml) for indicated times. The cells were labeled with 50 nM Mitotracker-Red CMXRos and 4 μg/ml Hoechst 33258 for 30 min. Insets show magnified views of the area outlined in the white boxes. Scale bars: 20 μm.

(C) Change of mitochondrial membrane potential was observed in the *Cont.* and *A/A*^{Hep} primary hepatocytes treated with tunicamycin (Tm,1 μg/ml) for indicated times. The cells were labeled with 2.5 μM JC-1 for 30 min. Insets show magnified views of the area outlined in the white boxes. Scale bars: 20 μm.

Figure 4.

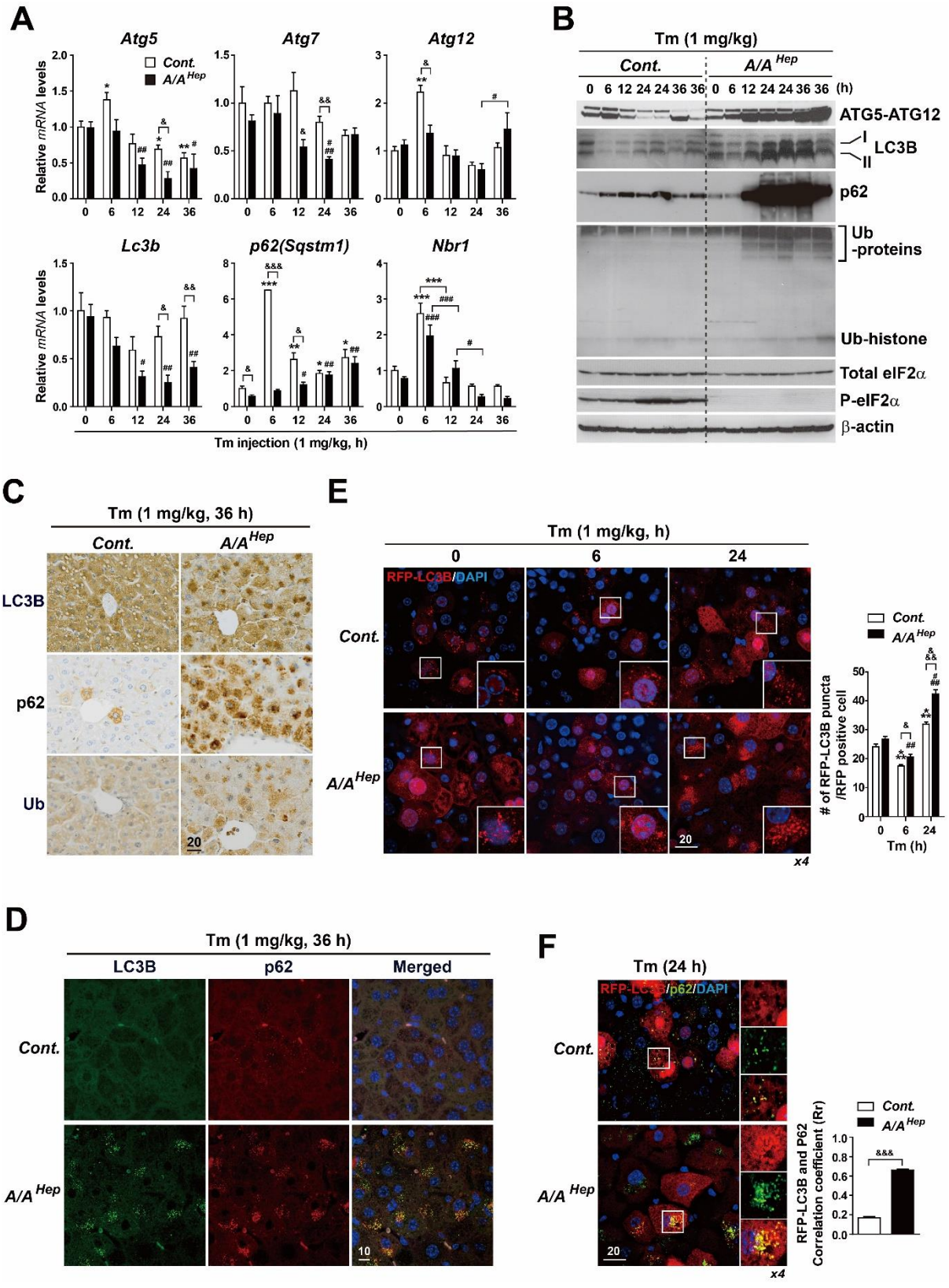
A
Atg5
Atg7
Atg12
Cont.
A/A Hep
Relative mRNA levels
Lc3b
p62(Sqstm1)
Nbr1
Tm injection (1 mg/kg, h)
B
Tm (1 mg/kg)
Cont.
A/A Hep
0 6 12 24 24 36 36 0 6 12 24 24 36 36 (h)
ATG5-ATG12
I
II
LC3B
p62
Ub -proteins
Ub-histone
Total eIF2α
P-eIF2α
β-actin
C
Tm (1 mg/kg, 36 h)
Cont.
A/A Hep
LC3B
p62
Ub
20
D
Tm (1 mg/kg, 36 h)
LC3B
p62
Merged
Cont.
A/A Hep
10
E
Tm (1 mg/kg, h)
0
6
24
RFP-LC3B/DAPI
Cont.
A/A Hep
20
x4
Cont.
A/A Hep
# of RFP-LC3B puncta /RFP positive cell
Tm (h)
F
Tm (24 h)
RFP-LC3B/p62/DAPI
Cont.
A/A Hep
20
x4
Cont.
A/A Hep
RFP-LC3B and P62 Correlation coefficient (Rr)

Figure 4. eIF2α phosphorylation deficiency increases autophagosome formation in the liver in response to ER stress.

(A) Expression profiles of autophagy related genes in response to ER stress. Quantitative real-time PCR was performed by using total RNAs from liver tissues of the *Control* (*Cont.*) and *A/A^{Hep}* mice treated with tunicamycin (Tm,1 mg/kg) for indicated times. (n=3 independent experiments at each time point per group).
(B). Western blot analyses of ATG5-ATG12 complex, LC3B, P62 and ubiquitinated protein (Ub) were performed in liver lysates from *Control* (*Cont.*) and *A/A^{Hep}* mice treated with tunicamycin (Tm,1 mg/kg) for indicated times. β-actin was probed to demonstrate equal loading.
(C) Immunohistochemistry of LC3B, P62 and Ubiquitinated protein (Ub) expression was performed in liver sections of the *Control* and *A/A^{Hep}* mice treated with tunicamycin (Tm,1 mg/kg) for 36 h. Scale bars: 20 μm.
(D) Immunofluorescence analyses of autophagosome marker proteins LC3B and P62 were performed in liver sections of the *Control* and *A/A^{Hep}* mice treated with tunicamycin (Tm,1 mg/kg) for 36 h. Scale bars: 10 μm.
(E) Observation of RFP-LC3B puncta in liver sections. RFP-LC3B expressing adenovirus (2.0 x10^9 IFU/100μl per mouse) was administered by tail-vein injection. The left panels show confocal microscopy images of RFP-LC3B in liver vibratome sections from *Control* (*Cont.*) and *A/A^{Hep}* mice treated with tunicamycin (Tm,1 mg/kg) for indicated times. Quantification of RFP-LC3B puncta is shown in the graphs. Insets show magnified views of the area outlined in the white boxes. Scale bars: 20 μm.
(F) Observation of RFP-LC3B and P62 colocalization in liver sections. RFP-LC3B expressing adenovirus (2.0 x10^9 IFU/100 μl per mouse) was administered by tail-vein injection. RFP-LC3B fluorescence (Red) and P62 immunofluorescence (Green) were observed in liver vibratome sections from *Control* (*Cont.*) and *A/A^{Hep}* mice treated with tunicamycin (Tm,1 mg/kg) for 24 h. Panels on the right are high magnifications of the boxed regions. Co-localization of RFP-LC3B and P62 was analyzed by pearson correlation coefficients (Rr) by using FV10-ASW software (Olympus). Scale bars: 20 μm.

All data are mean ± SEM (n=3 mice per group); *p < 0.05, **p < 0.01 and ***p < 0.001; 0 vs each time point in the control group, $^{\#}$p < 0.05, $^{\#\#}$p < 0.01 and $^{\#\#\#}$p < 0.001; 0 vs each time points in the *A/A^{Hep}* group, $^{\&}$p < 0.05, $^{\&\&}$p < 0.01 and $^{\&\&\&}$p < 0.001; *Control* (*Cont.*) vs *A/A^{Hep}* mice at each time point.

Figure 5.

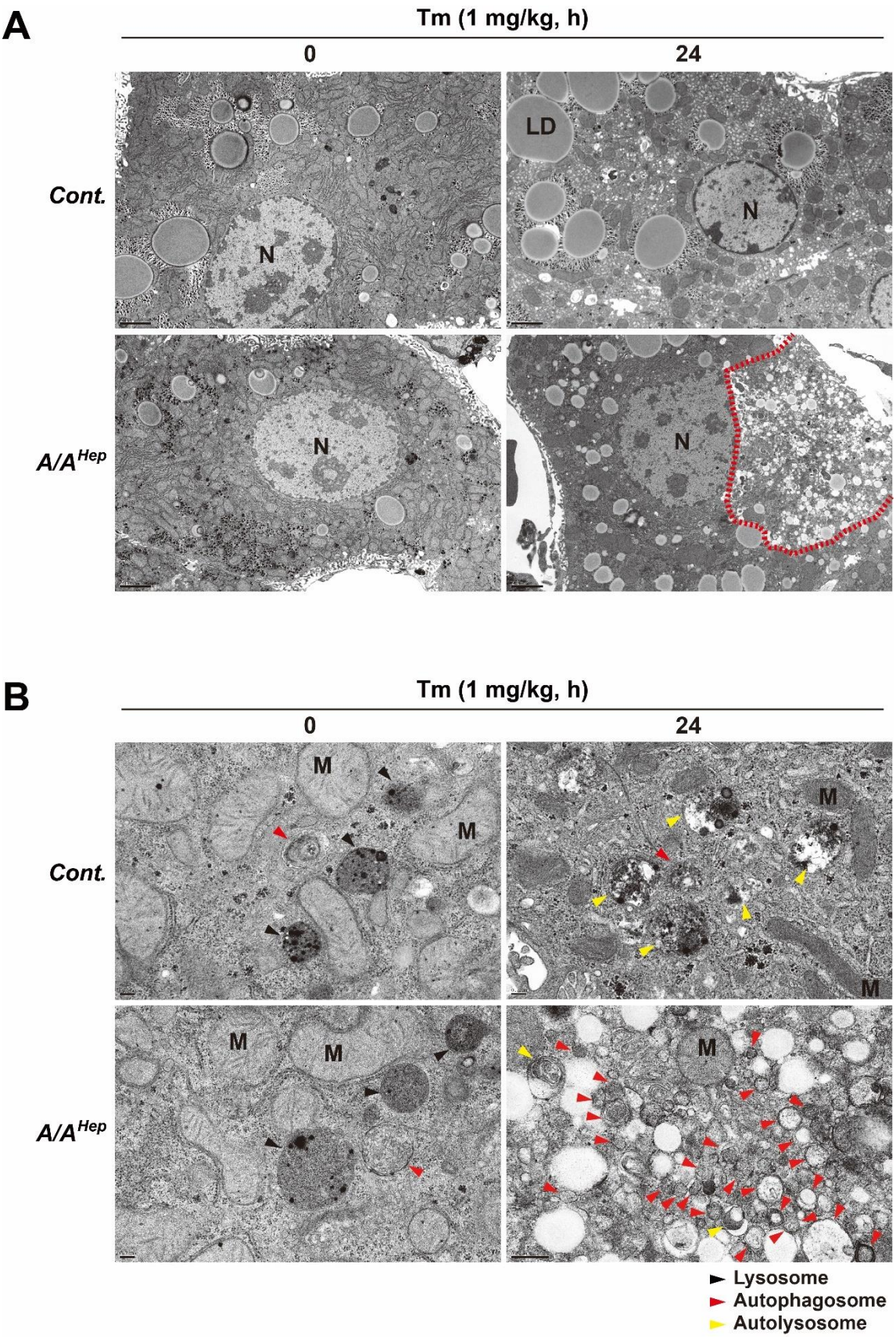
A
Tm (1 mg/kg, h)
0
24
Cont.
A/A Hep
LD
N
B
Tm (1 mg/kg, h)
0
24
Cont.
A/A Hep
M
Lysosome
Autophagosome
Autolysosome

Figure 5. eIF2α phosphorylation deficiency results in the accumulation of autophagic vesicles in the liver in response to ER stress.

(A, B) Transmission electron microscopy analyses of autophagic vesicles were performed in liver sections of the *Control* and *A/A*^{Hep} mice treated with tunicamycin (Tm,1 mg/kg) for 24 h. Red dotted line represents accumulated autophagic vesicles. Red arrow heads indicate double membrane-autophagosome (AP). Black arrow heads indicate lysosome, red arrow heads indicate autophagosome and yellow arrow heads indicate autolysosome. Scale bars in Figure A: 2 μm and Scale bars in Figure B: 0.2 μm.

Figure 6.

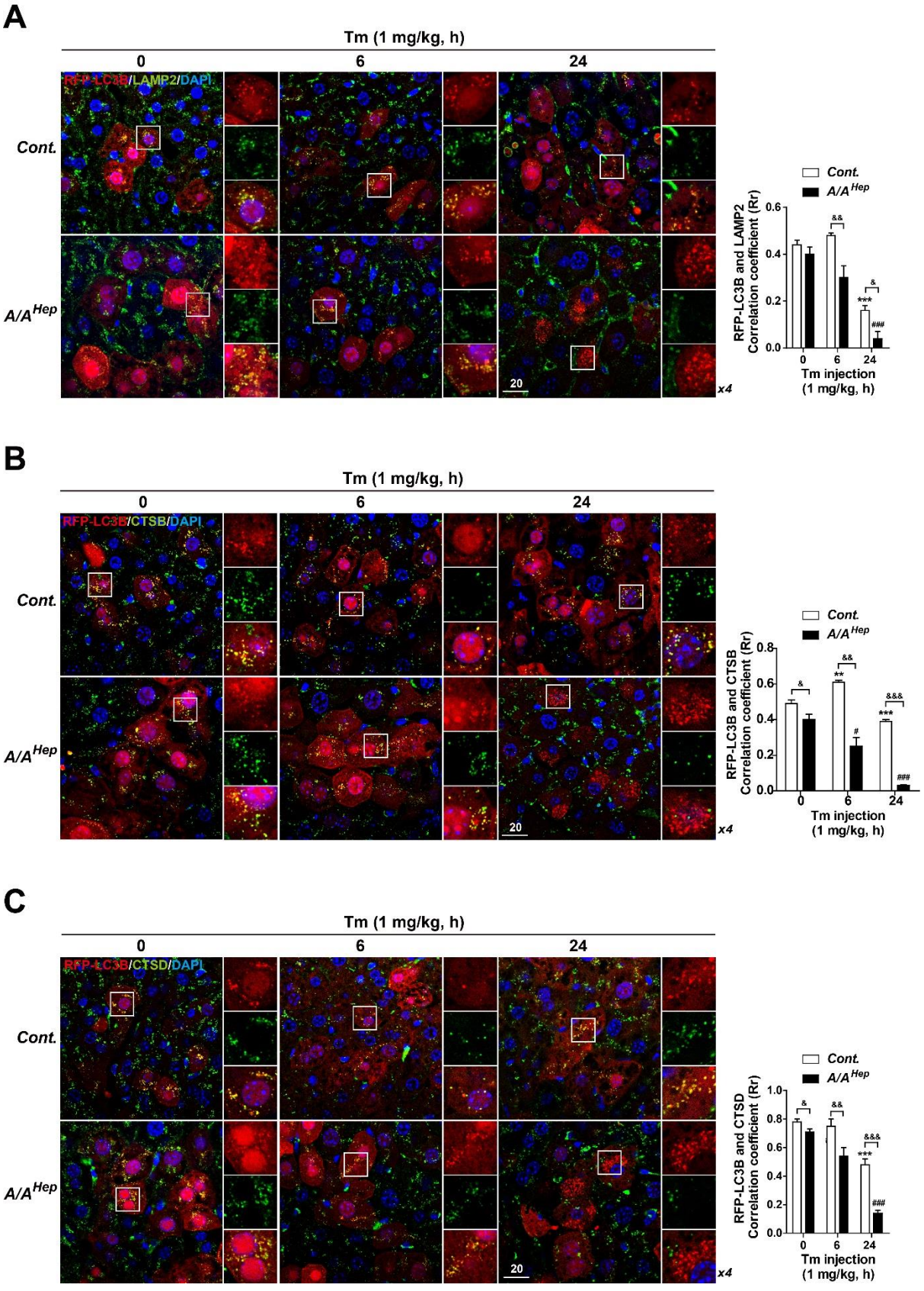
A
Tm (1 mg/kg, h)
0
6
24
RFP-LC3B/LAMP2/DAPI
Cont.
A/A Hep
20
x4
Cont.
A/A Hep
RFP-LC3B and LAMP2 Correlation coefficient (Rr)
0.6
0.4
0.2
0.0
&&
&
***
###
0
6
24
Tm injection (1 mg/kg, h)
B
Tm (1 mg/kg, h)
0
6
24
RFP-LC3B/CTSB/DAPI
Cont.
A/A Hep
20
x4
Cont.
A/A Hep
RFP-LC3B and CTSB Correlation coefficient (Rr)
0.8
0.6
0.4
0.2
0.0
&
&&
**
#
&&&
***
###
0
6
24
Tm injection (1 mg/kg, h)
C
Tm (1 mg/kg, h)
0
6
24
RFP-LC3B/CTSD/DAPI
Cont.
A/A Hep
20
x4
Cont.
A/A Hep
RFP-LC3B and CTSD Correlation coefficient (Rr)
1.0
0.8
0.6
0.4
0.2
0.0
&
&&
&&&
***
###
0
6
24
Tm injection (1 mg/kg, h)

D

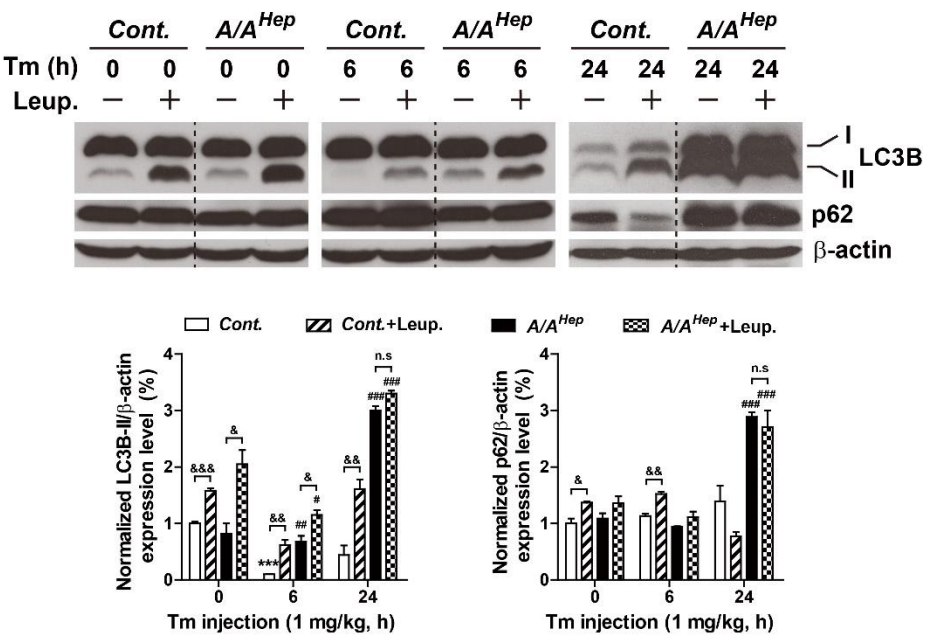
Cont.
A/A^Hep
Cont.
A/A^Hep
Cont.
A/A^Hep
Tm (h) 0 0 0 0 6 6 6 6 24 24 24 24
Leup. − + − + − + − + − + − +
I
II
LC3B
p62
β-actin
Cont.
Cont.+Leup.
A/A^Hep
A/A^Hep+Leup.
Normalized LC3B-II/β-actin expression level (%)
Tm injection (1 mg/kg, h)
Normalized p62/β-actin expression level (%)
Tm injection (1 mg/kg, h)

Figure 6. eIF2α phosphorylation deficiency impairs the fusion of autophagosomes with lysosomes in the liver in response to ER stress.

(A-C). To observe co-localization between autophagosome marker and lysosome marker, RFP-LC3B-expressing adenovirus (2.0 x10^9 IFU/100 μl per mouse) was administered by tail-vein injection (n = 3 per group). Immunofluorescence analyses were performed in the liver vibratome sections of the *Control* (*Cont.*) and *A/A^{Hep}* mice treated with tunicamycin (Tm, 1 mg/kg) for indicated times. Liver sections infected by RFP-LC3B-expressing adenovirus were stained with anti-LAMP2 (A), Cathepsin B (B), or Cathepsin D (C) antibodies. RFP-LC3B fluorescence (Red) and LAMP2 (A), Cathepsin B (B), or Cathepsin D (C) immunofluorescence (Green) were observed. Small panels on the right of each panel are high magnifications of the boxed regions. Co-localization of RFP-LC3B and LAMP2 (A), Cathepsin B (B), or Cathepsin D (C) were analyzed by Pearson correlation coefficients (Rr) by using FV10-ASW software (Olympus). Scale bars: 20 μm.

(D) Western blot analyses of LC3B and P62 were performed in the liver lysates of the *Control* and *A/A^{Hep}* mice treated with tunicamycin (Tm,1 mg/kg) for indicated times. For leupeptin (Leup.) administration, leupeptin was injected intraperitoneally at a dose of 35 mg/kg prior to 1 h of euthanasia in the *Control* and *A/A^{Hep}* mice (n = 3 per group). Band intensity was quantified and analyzed with ImageJ software after normalizing the expression levels of protein to β-actin.

All data are mean ± SEM (n=3 mice per group); *p < 0.05, **p < 0.01 and ***p < 0.001; 0 vs each time point in the control group, $^{\#}$p < 0.05, $^{\#\#}$p < 0.01 and $^{\#\#\#}$p < 0.001; 0 vs each time point in the *A/A^{Hep}* group, $^{\&}$p < 0.05, $^{\&\&}$p < 0.01 and $^{\&\&\&}$p < 0.001; *Control* (*Cont.*) vs *A/A^{Hep}* mice, *Control* (*Cont.*) vs leupeptin-injected *Control* (*Cont.*) mice, or *A/A^{Hep}* vs leupeptin-injected *A/A^{Hep}* mice at each time point.

Figure 7.

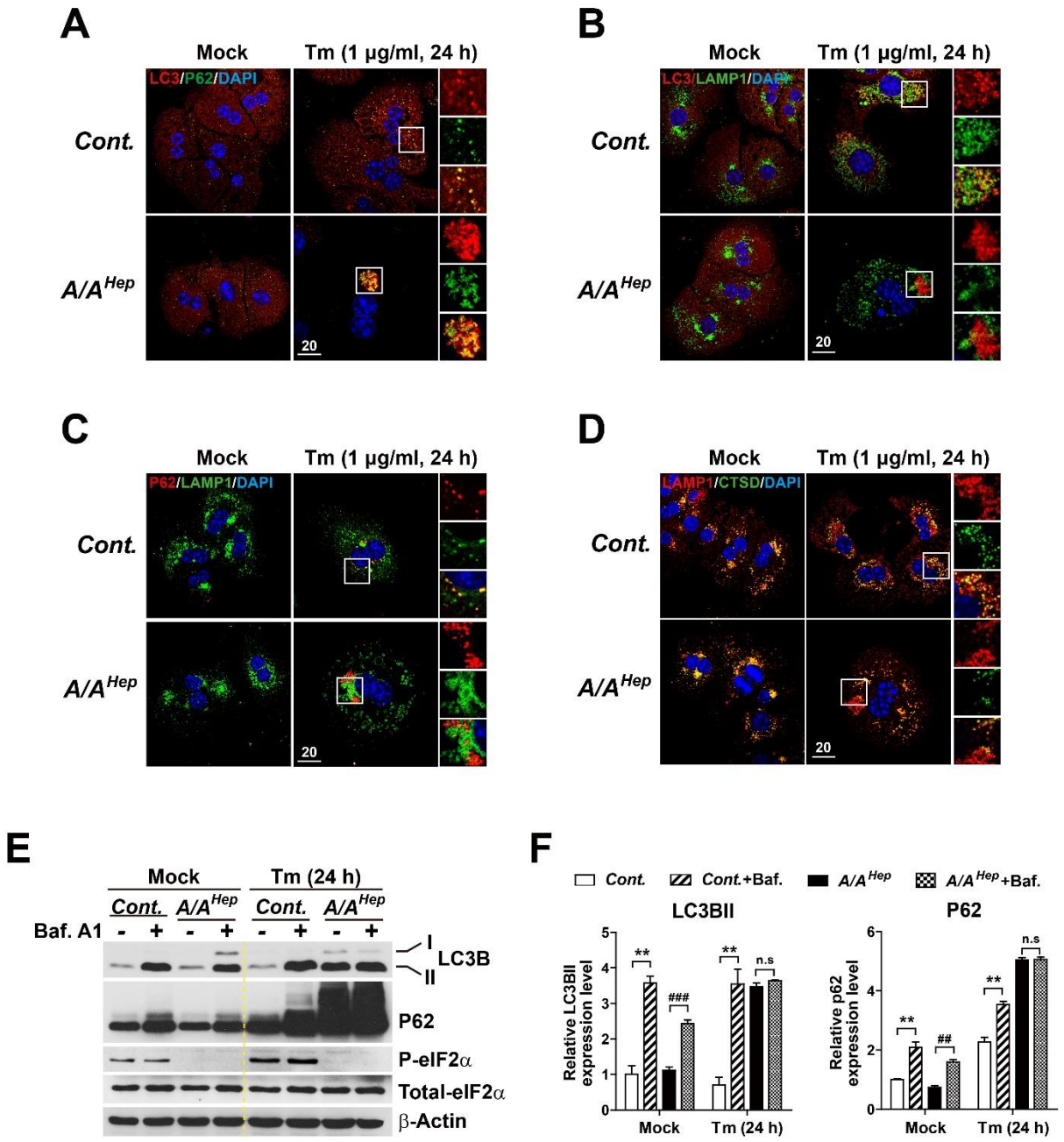
A
Mock
Tm (1 μg/ml, 24 h)
LC3/P62/DAPI
Cont.
A/A^Hep
20
B
Mock
Tm (1 μg/ml, 24 h)
LC3/LAMP1/DAPI
Cont.
A/A^Hep
20
C
Mock
Tm (1 μg/ml, 24 h)
P62/LAMP1/DAPI
Cont.
A/A^Hep
20
D
Mock
Tm (1 μg/ml, 24 h)
LAMP1/CTSD/DAPI
Cont.
A/A^Hep
20
E
Mock
Tm (24 h)
Cont.
A/A^Hep
Cont.
A/A^Hep
Baf. A1
- + - + - + - +
I
II
LC3B
P62
P-eIF2α
Total-eIF2α
β-Actin
F
Cont.
Cont.+Baf.
A/A^Hep
A/A^Hep+Baf.
LC3BII
P62
Relative LC3BII expression level
Relative p62 expression level
**
###
n.s
##
Mock
Tm (24 h)

Figure 7. eIF2α phosphorylation deficiency impairs the fusion between autophagosome and lysosomes in primary hepatocytes in response to ER stress.

(A-D). Immunofluorescence analyses of (A) LC3B (Red) and P62 (Green), (B) LC3B (Red) and LAMP1 (Green), (C) P62 (Red) and LAMP1 (Green), or (D) LAMP1 (Red) and Cathepsin D(CTSD) (Green) were performed in the *Control* and *A/A*^{Hep} primary hepatocytes treated with mock or tunicamycin (Tm,1 μg/ml) for indicated times. Small panels on the right of each panel are high magnifications of the white boxed regions. Scale bars: 20 μm.

(E, F). Western blot analyses of LC3B, P62, total eIF2α, and phospho-eIF2α were performed in the *Control* and *A/A*^{Hep} primary hepatocytes treated with mock or tunicamycin (Tm,1 μg/ml) for 24 h. The cells were treated with or without bafilomycin A1 (Baf.A1, 200 nM) for 3 h prior to harvest. (n=3 independent experiments at each time point per group). Band intensity was quantified and analysed with ImageJ software after normalizing the expression levels of protein to β-actin.

All data are mean ± SEM (n=3 mice per group); **p < 0.01; *Control* (*Cont.*) vs bafilomycin A1-treated *Control* (*Cont.*) cells at each condition and $^{\#\#}$p < 0.01 and $^{\#\#\#}$p < 0.001; *A/A*^{Hep} vs bafilomycin A1-treated *A/A*^{Hep} cells at each condition.

Figure 8.

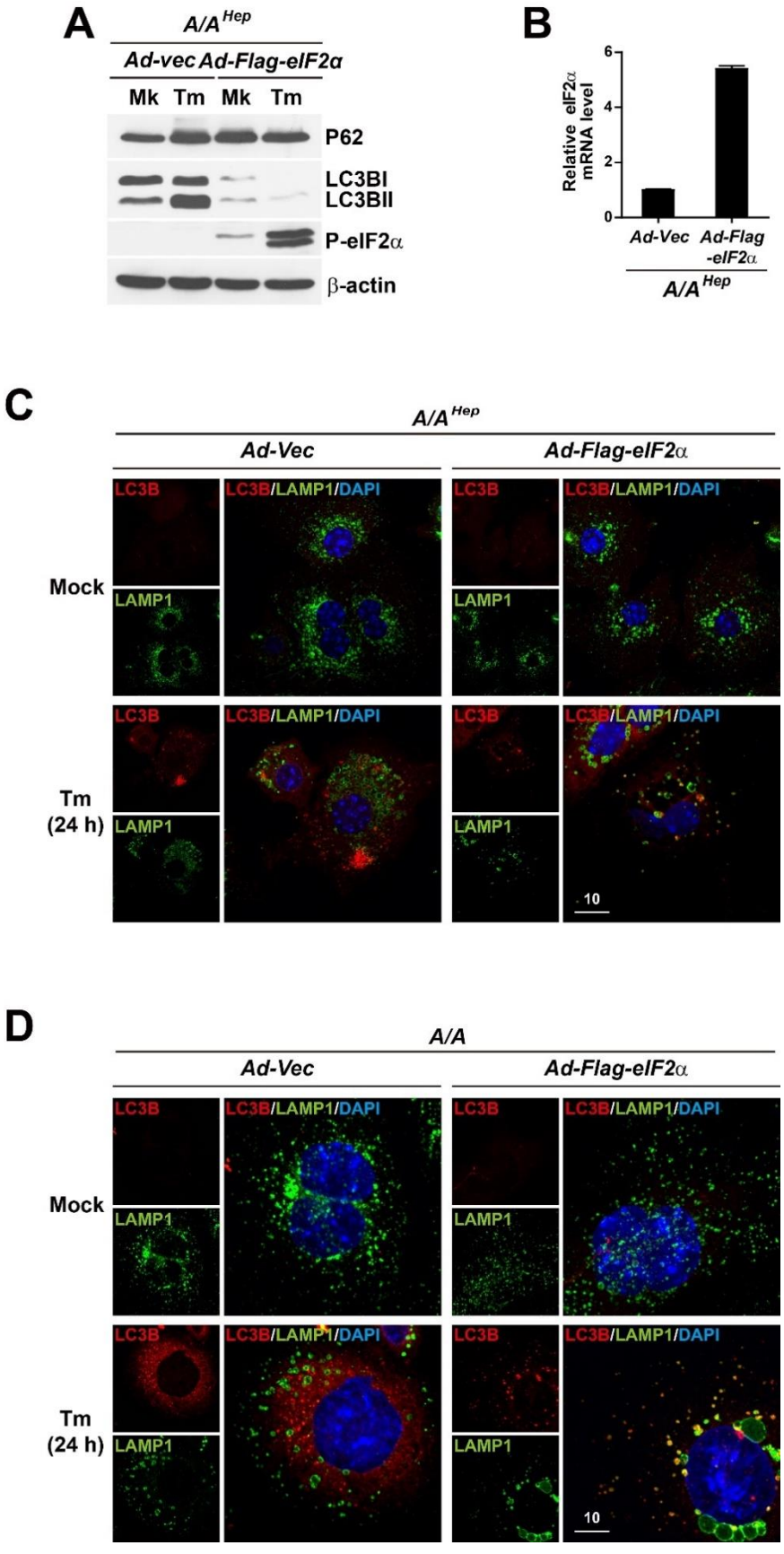
A
A/A Hep
Ad-vec Ad-Flag-eIF2α
Mk Tm Mk Tm
P62
LC3BI
LC3BII
P-eIF2α
β-actin
B
Relative eIF2α mRNA level
6
4
2
0
Ad-Vec
Ad-Flag -eIF2α
A/A Hep
C
A/A Hep
Ad-Vec
Ad-Flag-eIF2α
Mock
Tm (24 h)
LC3B
LC3B/LAMP1/DAPI
LAMP1
10
D
A/A
Ad-Vec
Ad-Flag-eIF2α
Mock
Tm (24 h)
LC3B
LC3B/LAMP1/DAPI
LAMP1
10

Figure 8. Wild type eIF2α overexpression increases autolysosome formation in eIF2α phosphorylation-deficient cells in response to ER stress.

(A-C) Primary hepatocytes isolated from *A/A*^{Hep} mice were infected with recombinant adenovirus expressing wild type mouse Flag-eIF2α (*Ad-Flag-eIF2α*) or empty (*Ad-Vec*) for 24 h and then treated with mock (Mk) or tunicamycin (Tm, 1 μg/ml) for 24 h.

(A) Western blot analyses of LC3B, P62, P-eIF2α and β-actin were performed in lysates of the primary hepatocytes treated with mock or tunicamycin (Tm,1 μg/ml) for 24 h.

(B) To measure mRNA levels of total eIF2α, quantitative real-time PCR was performed by using total RNAs of the primary hepatocytes treated with mock or tunicamycin (Tm,1 μg/ml) for 24 h (n=3 independent experiments at each condition).

(C) Immunofluorescence analyses of LC3B and LAMP1 were performed in primary hepatocytes treated with mock or tunicamycin (Tm,1 μg/ml) for 24 h. In each condition, left two small panels are for LC3B (Red channel) and LAMP1 (Green channel) staining images. Right big panel is for LC3B/LAMP1/DAPI merged image. Scale bars: 20 μm.

(D) *A/A* hepatocytes were infected with recombinant adenovirus expressing wild type mouse Flag-eIF2α (*Ad-Flag-eIF2α*) or empty (*Ad-Vec*) for 24 h and then treated with tunicamycin (Tm, 1 μg/ml) for 24 h. Immunofluorescence analyses of LC3B (Red channel) and LAMP1 (Green channel) were performed in primary hepatocytes treated with mock or tunicamycin. In each condition, left two small panels are for LC3B (Red channel) and LAMP1 (Green channel) staining images. Right big panel is for LC3B/LAMP1/DAPI merged image. Scale bars: 20 μm.

Figure 9.

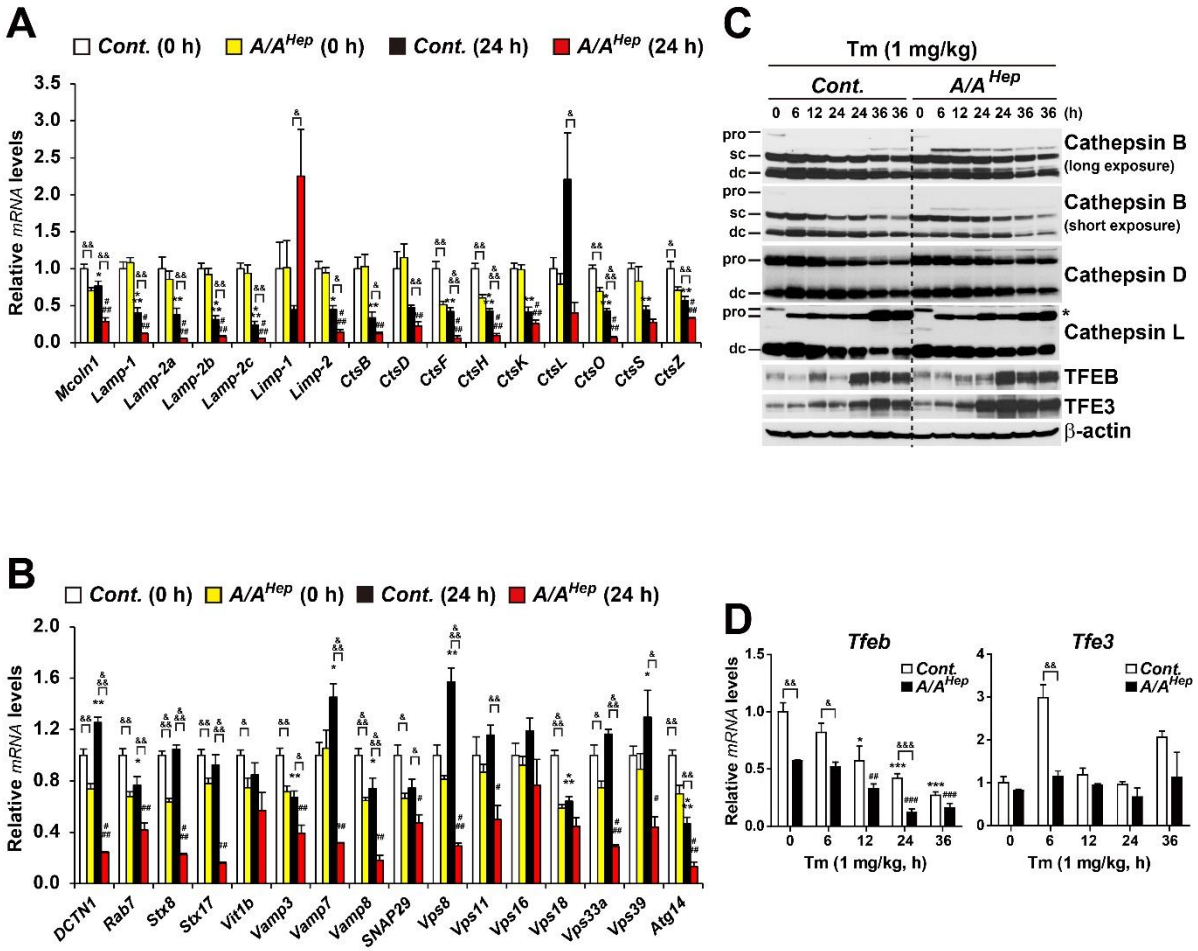
A
Cont. (0 h)
A/A^Hep (0 h)
Cont. (24 h)
A/A^Hep (24 h)
Relative mRNA levels
Mcoln1
Lamp-1
Lamp-2a
Lamp-2b
Lamp-2c
Limp-1
Limp-2
CtsB
CtsD
CtsF
CtsH
CtsK
CtsL
CtsO
CtsS
CtsZ
B
DCTN1
Rab7
Stx8
Stx17
Vit1b
Vamp3
Vamp7
Vamp8
SNAP29
Vps8
Vps11
Vps16
Vps18
Vps33a
Vps39
Atg14
C
Tm (1 mg/kg)
Cont.
A/A Hep
0 6 12 24 24 36 0 6 12 24 24 36 36 (h)
Cathepsin B
(long exposure)
Cathepsin B
(short exposure)
Cathepsin D
Cathepsin L
TFEB
TFE3
β-actin
D
Tfeb
Tfe3
Tm (1 mg/kg, h)

Figure 9. eIF2α phosphorylation deficiency leads to dysregulated expression of autophagy-related genes in the liver upon ER stress.

(A, B) Expression profiles of lysosomal genes (A) and autophagosome-lysosomal fusion related genes (B) in response to ER stress. Quantitative real-time PCR was performed by using total RNAs from liver tissues of the *Control* (*Cont.*) and *A/A*^{Hep} mice treated with tunicamycin (Tm,1 mg/kg) for 24 h. (n=3 independent experiments per group).
(C) Western blot analyses of lysosomal proteins Cathepsin B, D, and L and autophagy master transcription factors TFEB and TFE3 were performed in the liver lysates of the *Control* (*Cont.*) and *A/A*^{Hep} mice treated with tunicamycin (Tm,1 mg/kg) for indicated times.
(D) mRNA expression levels of TFEB and TFE3. Quantitative real-time PCR was performed by using total RNAs from liver tissues of the *Control* (*Cont.*) and *A/A*^{Hep} mice treated with tunicamycin (Tm,1 mg/kg) for indicated times. (n=3 independent experiments at each time point per group).
All data are mean ± SEM (n=3 mice per group); *p < 0.05, **p < 0.01 and ***p < 0.001; 0 h vs 24 h in the control group, $^{\#}$p < 0.05, $^{\#\#}$p < 0.01 and $^{\#\#\#}$p < 0.001; 0 h vs 24 h in the *A/A*^{Hep} group, $^{\&}$p < 0.05, $^{\&\&}$p < 0.01 and $^{\&\&\&}$p < 0.001; *Control* (*Cont.*) vs *A/A*^{Hep} mice at each time point.

Figure 10.

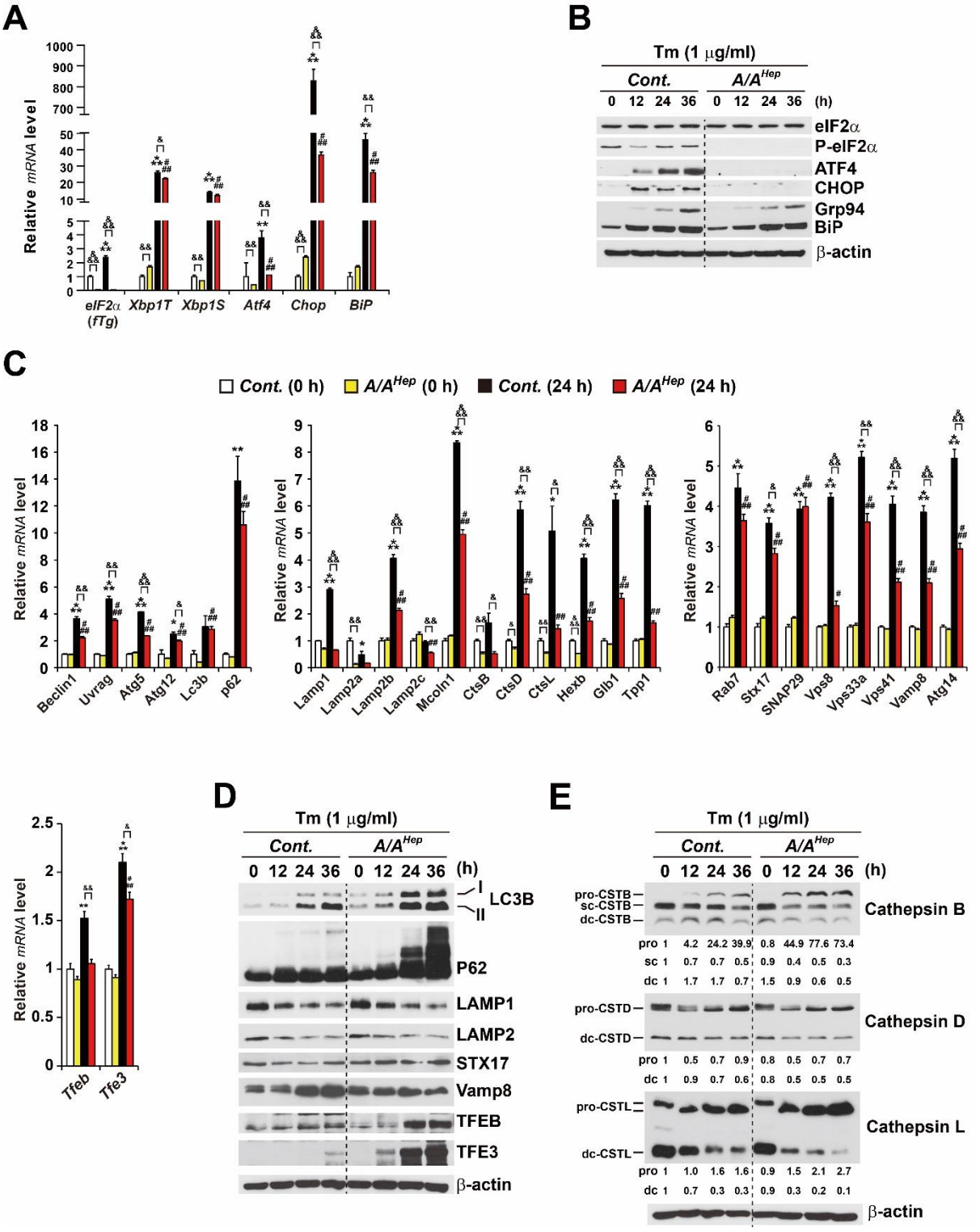
A
Relative mRNA level
eIF2α (fTg)
Xbp1T
Xbp1S
Atf4
Chop
BiP
B
Tm (1 μg/ml)
Cont.
A/A^Hep
0 12 24 36 0 12 24 36 (h)
eIF2α
P-eIF2α
ATF4
CHOP
Grp94
BiP
β-actin
C
Cont. (0 h)
A/A^Hep (0 h)
Cont. (24 h)
A/A^Hep (24 h)
Relative mRNA level
Beclin1
Uvrag
Atg5
Atg12
Lc3b
p62
Lamp1
Lamp2a
Lamp2b
Lamp2c
Mcoln1
CtsB
CtsD
CtsL
Hexb
Glb1
Tpp1
Rab7
Stx17
SNAP29
Vps8
Vps33a
Vps41
Vamp8
Atg14
Tfeb
Tfe3
D
Tm (1 μg/ml)
Cont.
A/A^Hep
0 12 24 36 0 12 24 36 (h)
LC3B
I
II
P62
LAMP1
LAMP2
STX17
Vamp8
TFEB
TFE3
β-actin
E
Tm (1 μg/ml)
Cont.
A/A^Hep
0 12 24 36 0 12 24 36 (h)
pro-CSTB
sc-CSTB
dc-CSTB
Cathepsin B
pro 1 4.2 24.2 39.9 0.8 44.9 77.6 73.4
sc 1 0.7 0.7 0.5 0.9 0.4 0.5 0.3
dc 1 1.7 1.7 0.7 1.5 0.9 0.6 0.5
pro-CSTD
dc-CSTD
Cathepsin D
pro 1 0.5 0.7 0.9 0.8 0.5 0.7 0.7
dc 1 0.9 0.7 0.6 0.8 0.5 0.5 0.5
pro-CSTL
dc-CSTL
Cathepsin L
pro 1 1.0 1.6 1.6 0.9 1.5 2.1 2.7
dc 1 0.7 0.3 0.3 0.9 0.3 0.2 0.1
β-actin

Figure 10. eIF2α phosphorylation deficiency leads to dysregulated expression of autophagy-related gene in primary hepatocytes upon ER stress.

(A) Expression profiles of UPR-related genes in response to ER stress. Quantitative real-time PCR was performed by using total RNAs of the *Control* (*Cont.*) and *A/A*^{Hep} primary hepatocytes treated with tunicamycin (Tm,1 mg/kg) for 24 h. (n=3 independent experiments per group).
(B) Western blot analyses of UPR-related proteins were performed in lysates of the *Control* (*Cont.*) and *A/A*^{Hep} primary hepatocytes treated with tunicamycin (Tm,1 mg/kg) for indicated times.
(C) Expression profiles of autophagosome, lysosome, and autophagosome-lysosomal fusion related genes in response to ER stress. Quantitative real-time PCR was performed by using total RNAs from liver tissues of the *Control* (*Cont.*) and *A/A*^{Hep} mice treated with tunicamycin (Tm,1 mg/kg) for 24 h. (n=3 independent experiments per group).
(D) Western blot analyses of autophagy-related proteins were performed in lysates of the *Control* (*Cont.*) and *A/A*^{Hep} primary hepatocytes treated with tunicamycin (Tm,1 mg/kg) for indicated times.
(E) Western blot analyses of lysosomal enzymes were performed in lysates of the *Control* (*Cont.*) and *A/A*^{Hep} primary hepatocytes treated with tunicamycin (Tm,1 mg/kg) for indicated times. Band intensity was quantified and analysed with ImageJ software after normalizing the expression levels of protein to β-actin.
All data are mean ± SEM (n=3 mice per group); *$p < 0.05$, **$p < 0.01$ and ***$p < 0.001$; 0 h vs 24 h in the control group, $^{\#}p < 0.05$, $^{\#\#}p < 0.01$ and $^{\#\#\#}p < 0.001$; 0 h vs 24 h in the *A/A*^{Hep} group, $^{\&}p < 0.05$, $^{\&\&}p < 0.01$ and $^{\&\&\&}p < 0.001$; *Control* (*Cont.*) vs *A/A*^{Hep} cells at each time point.

Figure 11.

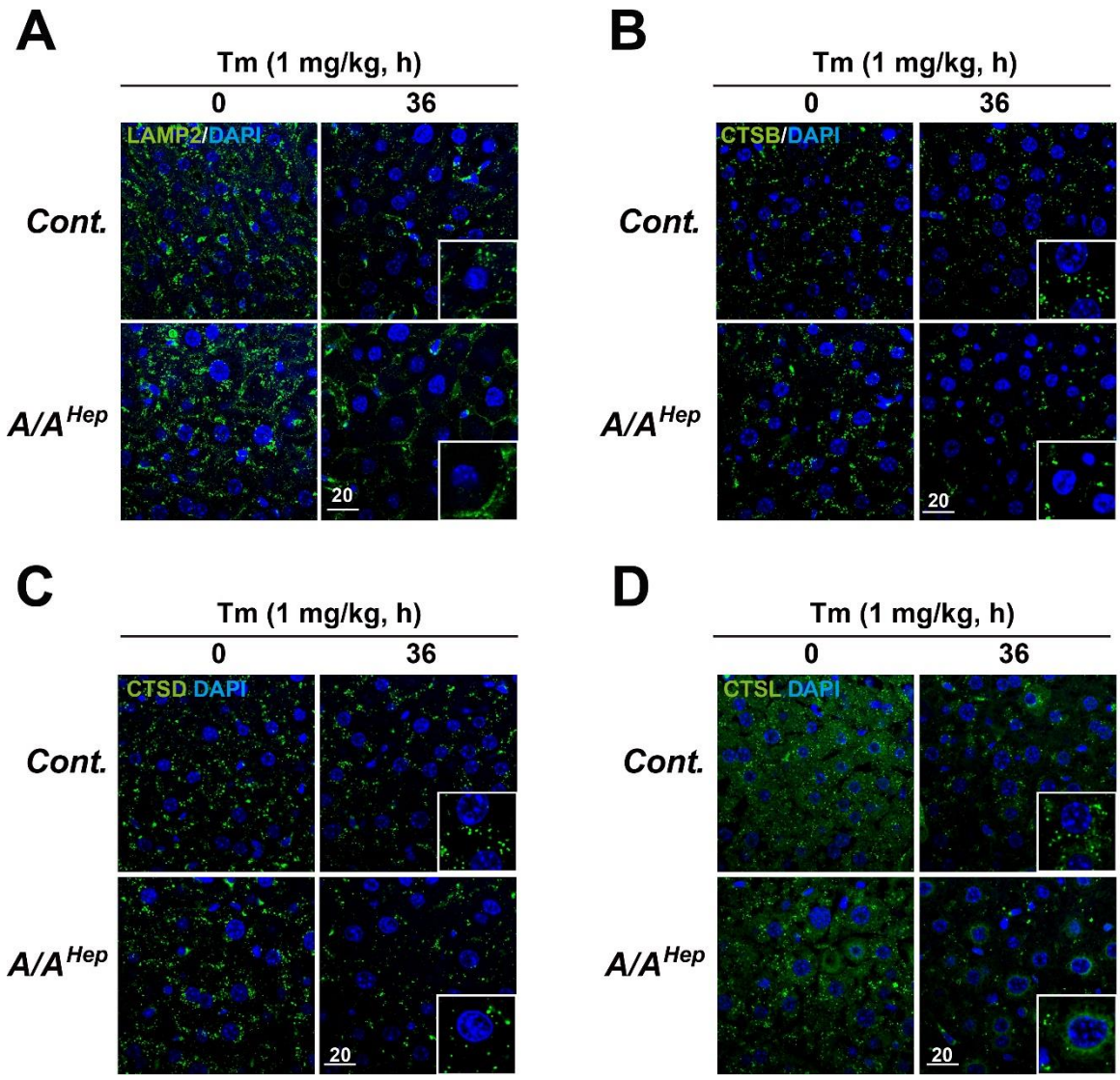
A
Tm (1 mg/kg, h)
0
36
LAMP2/DAPI
Cont.
A/A Hep
20
B
Tm (1 mg/kg, h)
0
36
CTSB/DAPI
Cont.
A/A Hep
20
C
Tm (1 mg/kg, h)
0
36
CTSD DAPI
Cont.
A/A Hep
20
D
Tm (1 mg/kg, h)
0
36
CTSL DAPI
Cont.
A/A Hep
20

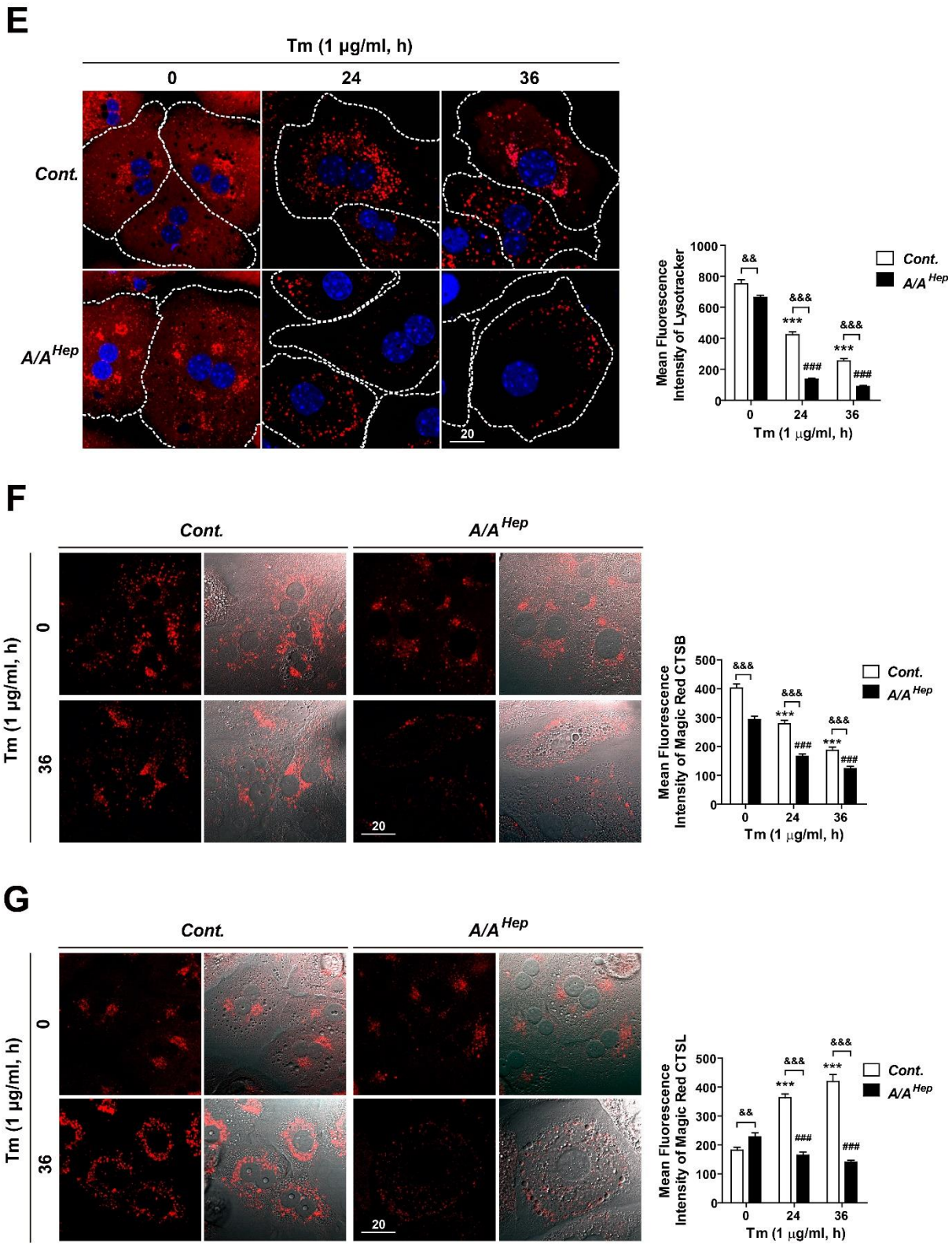
E
Tm (1 μg/ml, h)
0
24
36
Cont.
A/A Hep
20
Mean Fluorescence Intensity of Lysotracker
1000
800
600
400
200
0
&&
&&&
&&&
***
***
###
###
Cont.
A/A Hep
0
24
36
Tm (1 μg/ml, h)
F
Cont.
A/A Hep
Tm (1 μg/ml, h)
0
36
20
Mean Fluorescence Intensity of Magic Red CTSB
500
400
300
200
100
0
&&&
&&&
&&&
***
***
###
###
Cont.
A/A Hep
0
24
36
Tm (1 μg/ml, h)
G
Cont.
A/A Hep
Tm (1 μg/ml, h)
0
36
20
Mean Fluorescence Intensity of Magic Red CTSL
500
400
300
200
100
0
&&
&&&
&&&
***
***
###
###
Cont.
A/A Hep
0
24
36
Tm (1 μg/ml, h)

Figure 11. eIF2α phosphorylation deficiency disrupts lysosome positioning and lysosome functionality, which can affect autophagic flux upon ER stress.

(A-D). To observe localization of lysosomal proteins (A) LAMP2, (B) Cathepsin B (CTSB), (C) Cathepsin D (CTSD) and (D) Cathepsin L (CTSL), Immunofluorescence analyses were performed in the liver vibratome sections from *Control* and *A/A*^{Hep} mice injected with tunicamycin (Tm,1 mg/kg) for 36 h. Scale bars: 20 μm.

(E) The Tm (1 μg/ml)-treated *Control* and *A/A*^{Hep} primary hepatocytes were labeled with lysotracker (400 nM) to observe active lysosomes at indicated times. Mean fluorescence intensities (MFI) of lysotracker staining were measured with FV10-ASW image analysis software (Olympus) (n=50 at each time point per group). Scale bars: 20 μm.

(F, G) The Tm (1 μg/ml)-treated *Control* and *A/A*^{Hep} primary hepatocytes were labeled with Magic Red Cathepsin B assay (F) and Magic Red Cathepsin L assay (G) kits to monitor lysosomal enzyme activity at indicated times. Mean fluorescence intensities (MFI) of lysotracker staining were measured with FV10-ASW image analysis software (Olympus) (n=50 at each time point per group). Scale bars: 20 μm.

All data are mean ± SEM (n=3 mice per group); ***$p < 0.001$; 0 h vs 24 h in the control group, $^{###}p < 0.001$; 0 h vs 24 h in the *A/A*^{Hep} group, $^{\&\&}p < 0.01$ and $^{\&\&\&}p < 0.001$; *Control* (*Cont.*) vs *A/A*^{Hep} cells at each time point.

Figure 12.

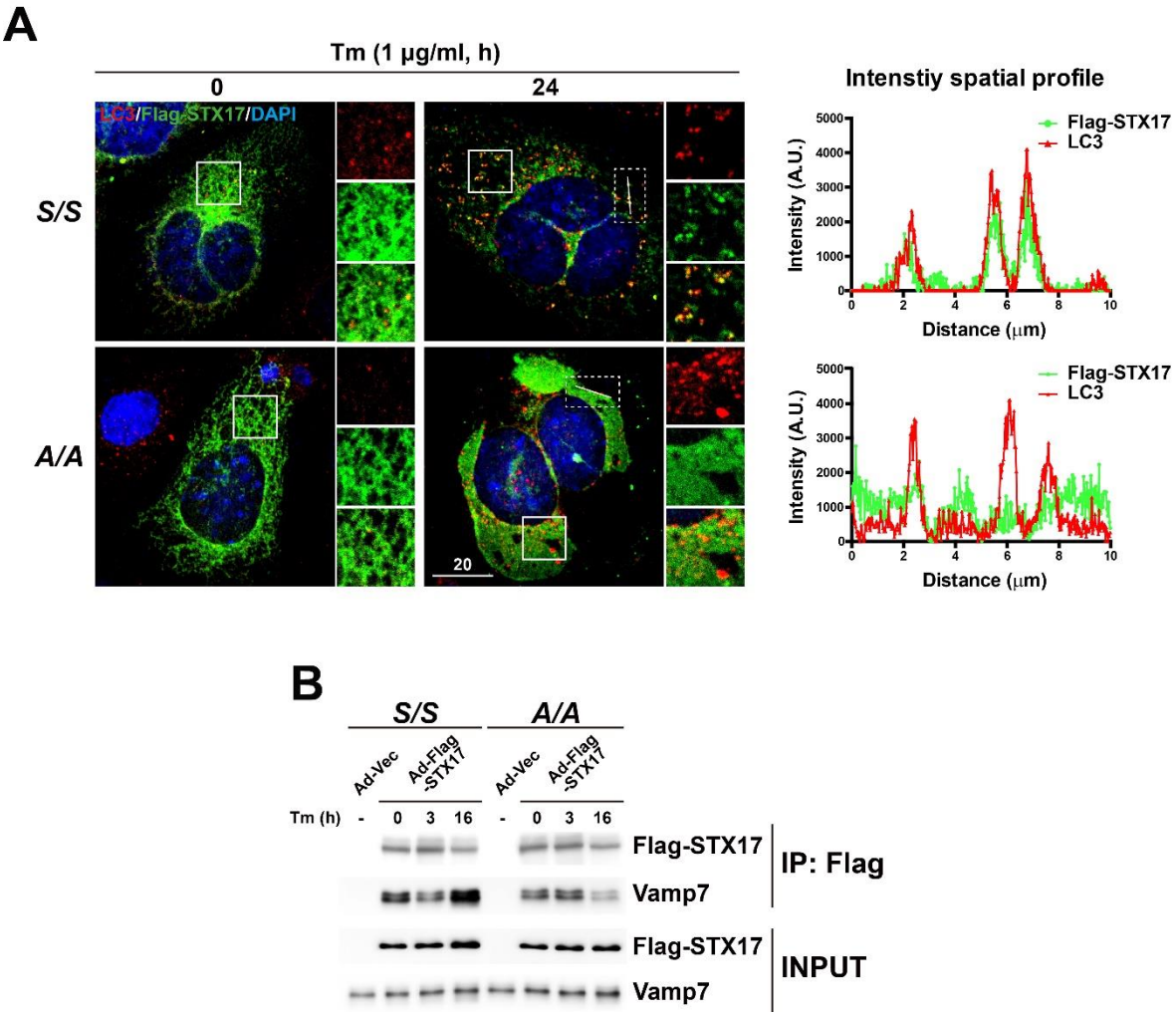

Figure 12. eIF2α phosphorylation is responsible for the recruitment of SNARE complexes for autophagosome-lysosome fusion in response to ER stress.

(A) Confocal microscopy analysis of co-localization between LC3B (red channel) and Flag-Syntaxin 17 (green channel) in the *S/S* (*Control)* and *A/A* hepatocyte cell lines treated with Tm (1 μg/ml) for 24 h. Small panels on the right of each panel are high magnifications of the white boxed regions. Scale bars: 20 μm. Intensity spatial profiles of the marked lines were obtained by FV10-ASW software (Olympus). Traces of fluorescence intensity spatial profiles indicate the intensity distribution of red and green channels through the white line in the dotted boxes.

(B) To verify interactions between Flag-STX17 and Vamp7, Co-immunoprecipitation analyses were performed with Flag-magnetic beads in cell extracts of Flag-STX17 expressing or empty adenovirus infected *S/S* (*Control)* and *A/A* hepatocytes treated with tunicamycin (Tm, 1 μg/ml) for indicated times. Immunoprecipitated proteins were analyzed by Western blotting.

Figure 13.

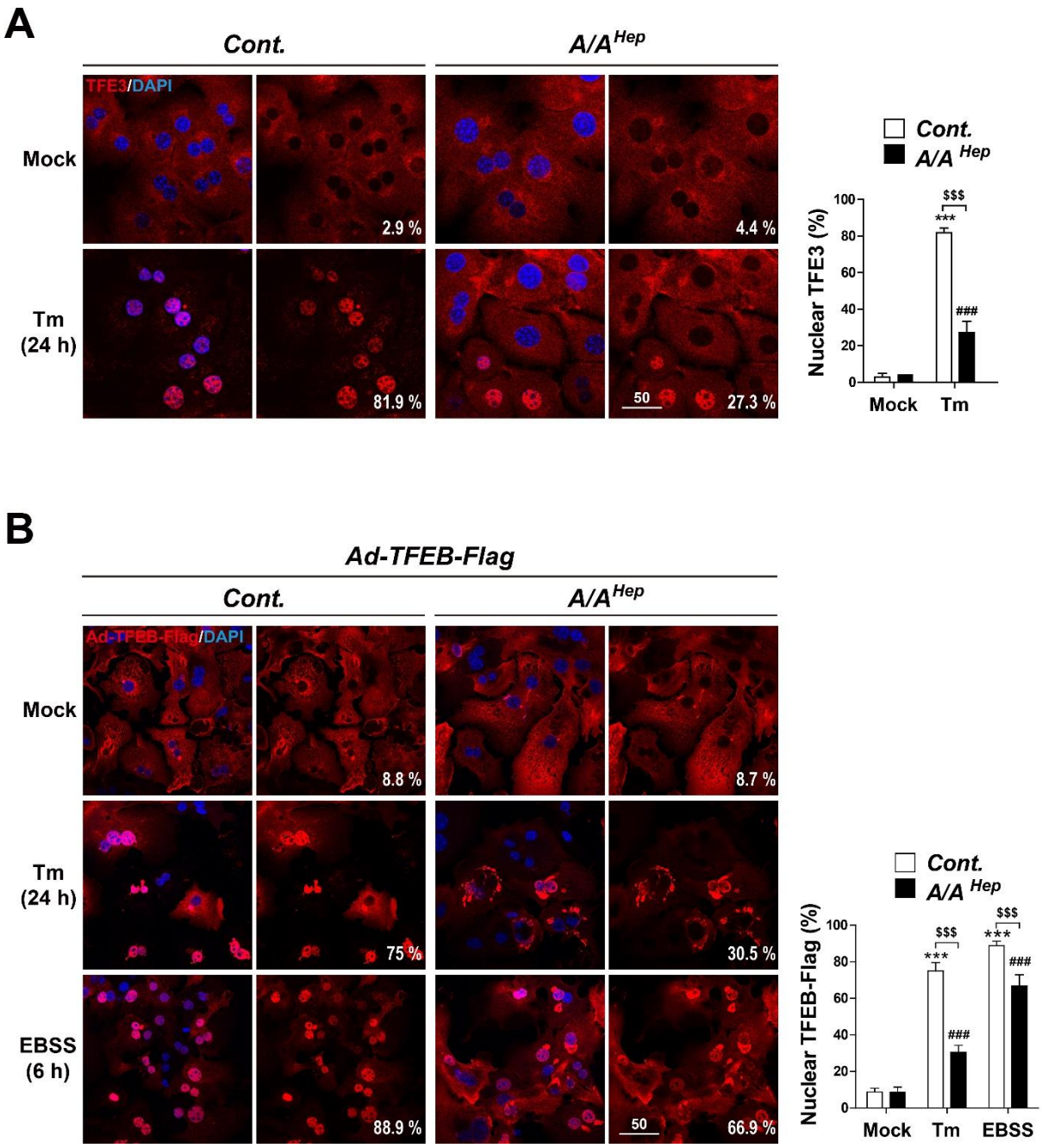
A
Cont.
A/A Hep
TFE3/DAPI
Mock
Tm
(24 h)
2.9 %
4.4 %
81.9 %
50
27.3 %
Cont.
A/A Hep
Nuclear TFE3 (%)
100
80
60
40
20
0
$$$
***
###
Mock
Tm
B
Ad-TFEB-Flag
Cont.
A/A Hep
Ad-TFEB-Flag/DAPI
Mock
Tm
(24 h)
EBSS
(6 h)
8.8 %
8.7 %
75 %
30.5 %
88.9 %
50
66.9 %
Cont.
A/A Hep
Nuclear TFEB-Flag (%)
100
80
60
40
20
0
$$$
***
###
$$$
***
###
Mock
Tm
EBSS

Figure 13. eIF2α phosphorylation is responsible for the nuclear translocation of the autophagy master regulators TFE3/TFEB in response to ER stress.

(A) Immunofluorescence analysis of TFE3 was performed in primary hepatocytes treated with tunicamycin (Tm, 1 μg/ml) for 24 h. Quantification of the number of cells with nuclear translocation. The percentages of nuclei positive for TFE3 staining were estimated by examining 100 cells. Scale bars: 20 μm.

(B) Immunofluorescence analyses of TFEB-Flag were performed by using anti-Flag antibody in TFEB-Flag expressing adenovirus (*Ad-TFEB-Flag*) infected *S/S*(*Control)* and *A/A* primary hepatocytes treated with tunicamycin (Tm, 1 μg/ml) or EBSS for indicated times. The percentages of nuclei positive for Flag staining were estimated by examining 100 cells.

All data are mean ± SEM (n=3 mice per group); ***p < 0.001; Mock vs treated cells in the control group, $^{###}$p < 0.001; Mock vs treated cells in the *A/A*^{Hep} group, $^{\&\&\&}$p < 0.001; *Control* (*Cont.*) vs *A/A*^{Hep} cells at each condition. Scale bars: 20 μm.

Figure 14.

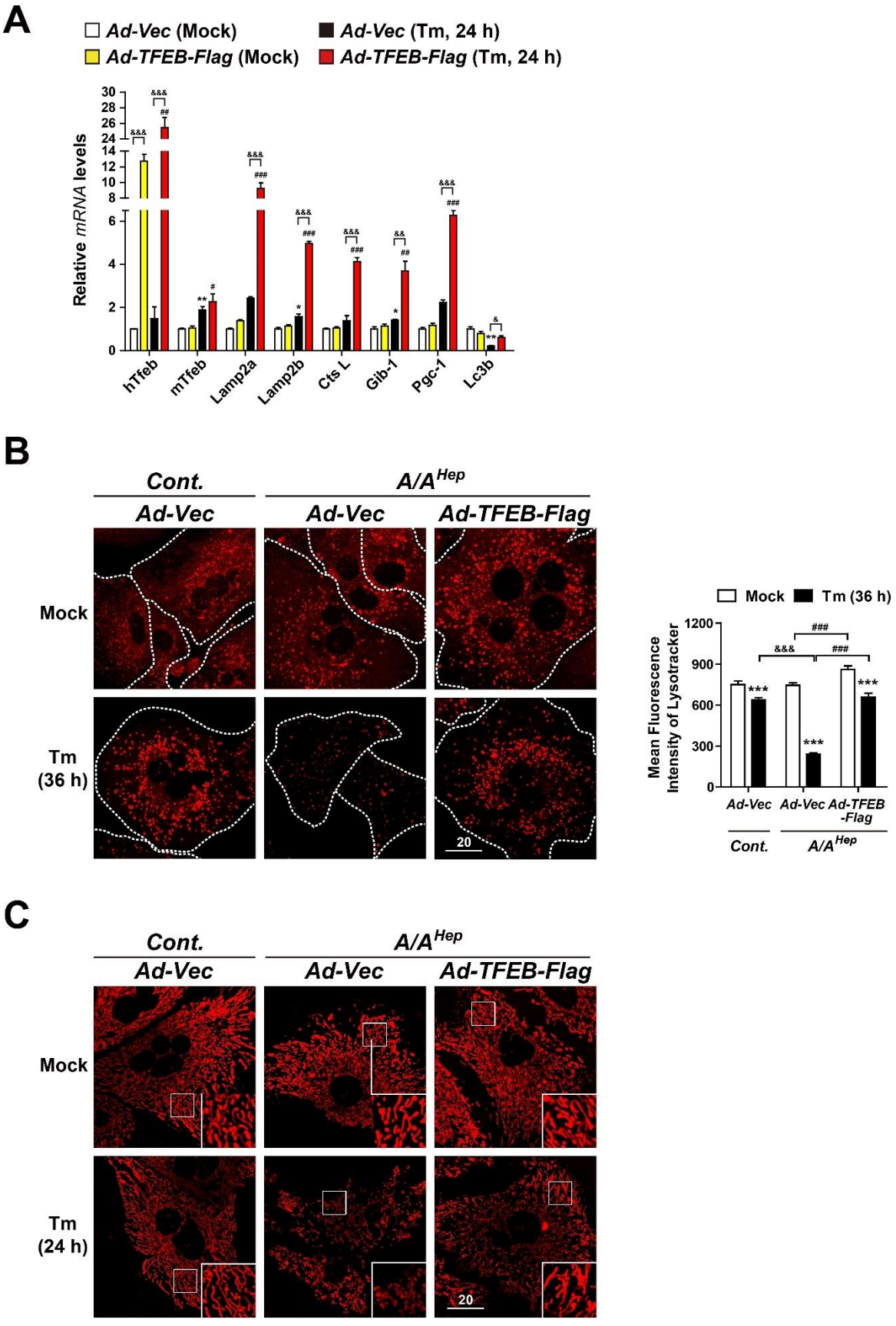
A
Ad-Vec (Mock)
Ad-Vec (Tm, 24 h)
Ad-TFEB-Flag (Mock)
Ad-TFEB-Flag (Tm, 24 h)
Relative mRNA levels
hTfeb
mTfeb
Lamp2a
Lamp2b
Cts L
Gib-1
Pgc-1
Lc3b
B
Cont.
A/A Hep
Ad-Vec
Ad-Vec
Ad-TFEB-Flag
Mock
Tm (36 h)
20
Mock
Tm (36 h)
Mean Fluorescence Intensity of Lysotracker
Ad-Vec
Ad-Vec
Ad-TFEB -Flag
Cont.
A/A Hep
C
Cont.
A/A Hep
Ad-Vec
Ad-Vec
Ad-TFEB-Flag
Mock
Tm (24 h)
20

Figure 14. TFEB overexpression restores lysosome functionality and mitochondrial dynamics in eIF2α phosphorylation-deficient primary hepatocytes upon ER stress.

(A) Expression profiles of TFEB dependent genes. Quantitative real-time PCR was performed by using total RNAs of *Ad-TFEB-Flag* or *Ad-Vec* infected *A/A^{Hep}* primary hepatocytes treated with tunicamycin (1 μg/ml) for 24 h (n=3 independent experiments at each time point per group).

(B) *Control* (*Cont.*) primary hepatocytes were infected with *Vector* adenovirus (*Ad-Vec*) for 24 h and then treated with tunicamycin (Tm,1 μg/ml) for 36 h. *A/A^{Hep}* primary hepatocytes were infected with TFEB-Flag expressing (*Ad-TFEB-Flag*) or *Vector* (*Ad-Vec*) adenovirus for 24 h and then treated with tunicamycin (Tm,1 μg/ml) for 36 h. Next, the cells were labeled with lysotracker (400 nM) to observe active lysosomes for 30 min. Mean fluorescence intensities (MFI) of lysotracker staining were measured with image analysis software (n=50 at each time point per group). All data are mean ± SEM (n=3 mice per group); ***p < 0.001; Mock vs 36 h in each group, $^{###}$p < 0.001; *A/A^{Hep}* vs *Ad-TFEB-Flag*-infected *A/A^{Hep}* cells, $^{\&\&\&}$p < 0.001; *Control* (*Cont.*) vs *A/A^{Hep}* cells. Scale bars: 20 μm.

(C) *Control* (*Cont.*) primary hepatocytes were infected with *Vector* adenovirus (*Ad-Vec*) for 24 h and then treated with tunicamycin (Tm,1 μg/ml) for 24 h. *A/A^{Hep}* primary hepatocytes were infected with TFEB-Flag expressing (*Ad-TFEB-Flag*) or *Vector* (*Ad-Vec*) adenovirus for 24 h and then treated with tunicamycin (Tm,1 μg/ml) for 24 h. Next, the cells were labeled with 50 nM Mitotracker-Red CMXRos and 4 μg/ml Hoechst 33258 to observe change of mitochondrial morphology for 30 min. Insets show magnified views of the area outlined in the white boxes. Scale bars: 20 μm.

Figure 15.

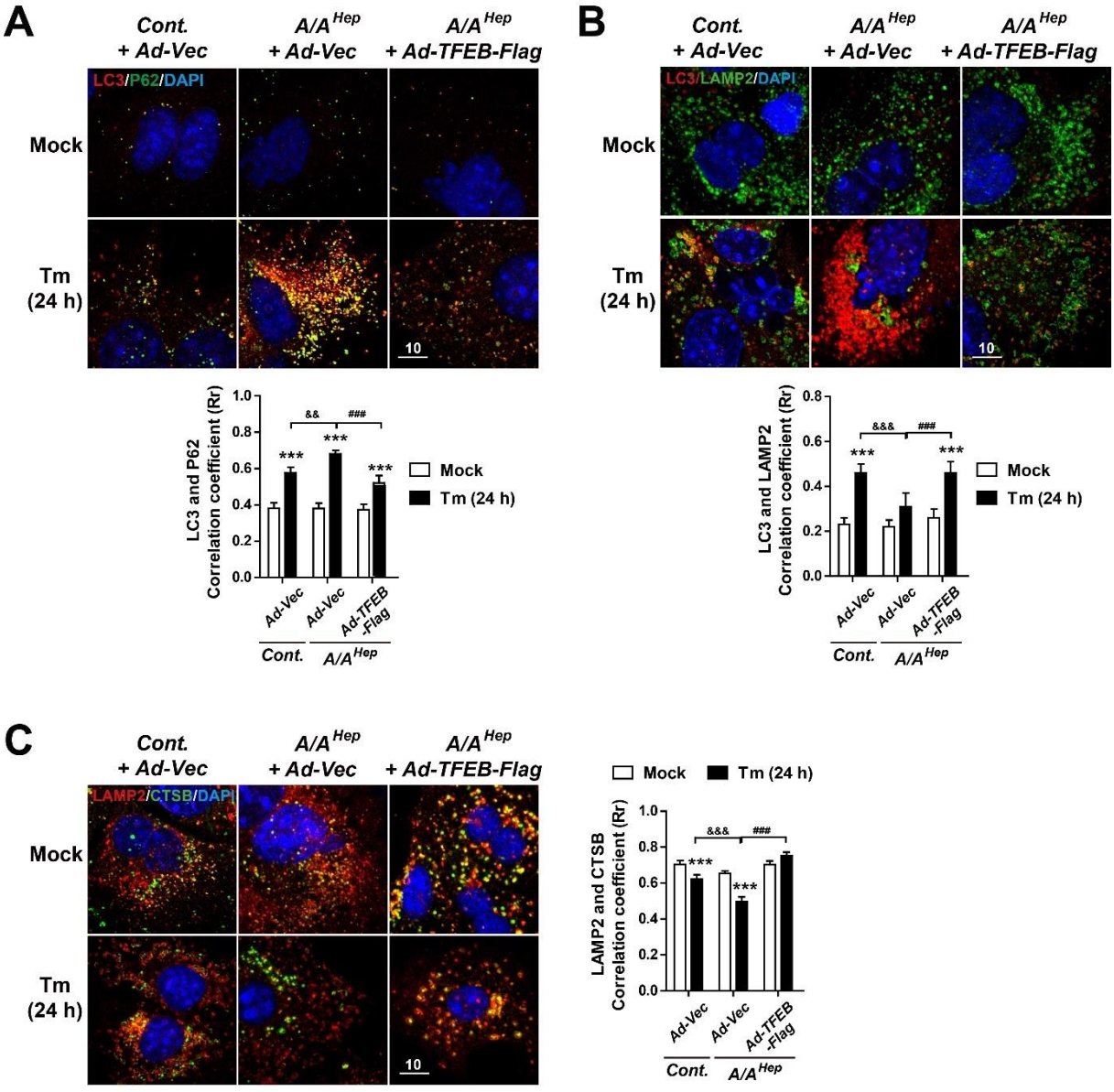
A
Cont. + Ad-Vec
A/A Hep + Ad-Vec
A/A Hep + Ad-TFEB-Flag
LC3/P62/DAPI
Mock
Tm (24 h)
10
LC3 and P62 Correlation coefficient (Rr)
Mock
Tm (24 h)
Ad-Vec
Ad-Vec
Ad-TFEB -Flag
Cont.
A/A Hep
B
Cont. + Ad-Vec
A/A Hep + Ad-Vec
A/A Hep + Ad-TFEB-Flag
LC3/LAMP2/DAPI
Mock
Tm (24 h)
10
LC3 and LAMP2 Correlation coefficient (Rr)
Mock
Tm (24 h)
Ad-Vec
Ad-Vec
Ad-TFEB -Flag
Cont.
A/A Hep
C
Cont. + Ad-Vec
A/A Hep + Ad-Vec
A/A Hep + Ad-TFEB-Flag
LAMP2/CTSB/DAPI
Mock
Tm (24 h)
10
Mock
Tm (24 h)
LAMP2 and CTSB Correlation coefficient (Rr)
Ad-Vec
Ad-Vec
Ad-TFEB -Flag
Cont.
A/A Hep

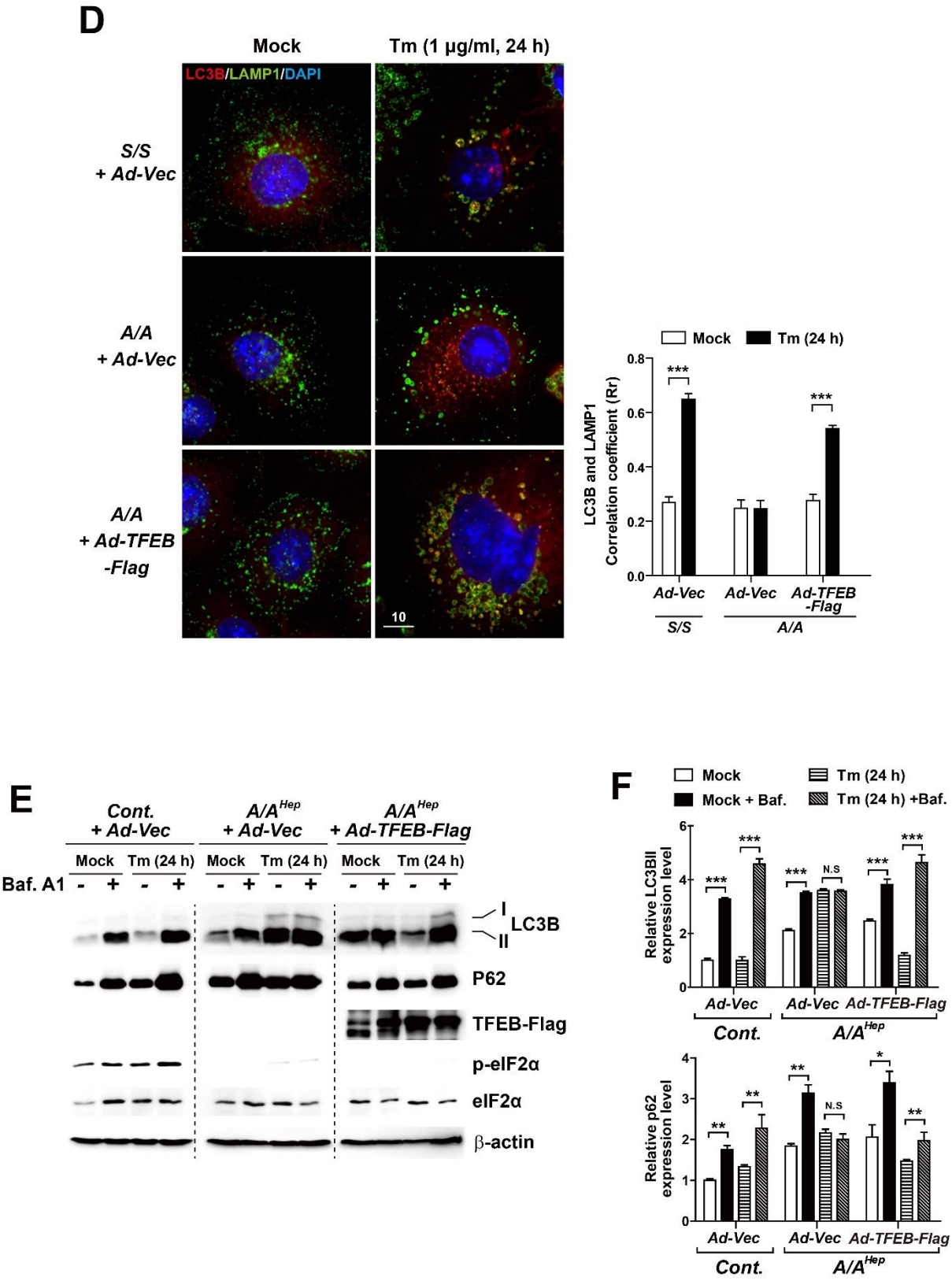
D
Mock
Tm (1 μg/ml, 24 h)
LC3B/LAMP1/DAPI
S/S
+ Ad-Vec
A/A
+ Ad-Vec
A/A
+ Ad-TFEB
-Flag
10
Mock
Tm (24 h)
LC3B and LAMP1
Correlation coefficient (Rr)
0.8
0.6
0.4
0.2
0.0
***
***
Ad-Vec
Ad-Vec
Ad-TFEB
-Flag
S/S
A/A
E
Cont.
+ Ad-Vec
A/A^Hep
+ Ad-Vec
A/A^Hep
+ Ad-TFEB-Flag
Mock
Tm (24 h)
Mock
Tm (24 h)
Mock
Tm (24 h)
Baf. A1
- + - + - + - + - + - +
I
II
LC3B
P62
TFEB-Flag
p-eIF2α
eIF2α
β-actin
F
Mock
Tm (24 h)
Mock + Baf.
Tm (24 h) +Baf.
Relative LC3BII
expression level
6
4
2
0
***
***
***
***
N.S
***
***
Ad-Vec
Ad-Vec
Ad-TFEB-Flag
Cont.
A/A^Hep
Relative p62
expression level
4
3
2
1
0
**
**
**
N.S
*
**
Ad-Vec
Ad-Vec
Ad-TFEB-Flag
Cont.
A/A^Hep

Figure 15. TFEB overexpression ameliorates the impairment of the autophagy-related pathway in eIF2α phosphorylation-deficient primary hepatocytes upon ER stress

(A-C) Immunofluorescence analyses of (A) LC3B and P62, (B) LC3 and LAMP2, (C) LAMP2 and Cathepsin B(CTSB) were performed in the *Ad-Vec* or *Ad-TFEB-Flag*-infected *Control* (*Cont.*) and *A/A*^{Hep} primary hepatocytes treated with tunicamycin (Tm, 1 μg/ml) for 24 h. To measure co-localization of (A) LC3 and P62, (B) LC3 and LAMP2, or (C) LAMP2 and Cathepsin B(CTSB) proteins, Pearson correlation coefficients (Rr) were calculated by FV10-ASW software (Olympus). Scale bars: 10 μm. All data are mean ± SEM (n=3 mice per group); ***p < 0.001; Mock vs 24 h in each group, $^{###}$p < 0.001; *Ad-Vec* vs *Ad-TFEB-Flag* in *A/A*^{Hep} cells, $^{\&\&}$p < 0.01 and $^{\&\&\&}$p < 0.001; *Cont.* vs *A/A*^{Hep} cells.

(D) Immunofluorescence analysis of LC3B and LAMP1 in the *Ad-Vec* or *Ad-TFEB-Flag*-infected *S/S*(*Control)* and *A/A* hepatocyte cell lines treated with tunicamycin (Tm, 1 μg/ml) for 24 h. To measure co-localization of LC3B and LAMP1 proteins, Pearson correlation coefficients (Rr) were calculated by FV10-ASW software (Olympus). Scale bars: 10 μm. All data are mean ± SEM (n=3 mice per group); ***p < 0.001; Mock vs 24 h in each group.

(E, F) Primary hepatocytes isolated from *Control* and *A/A*^{Hep} mice were infected with recombinant adenovirus expressing TFEB-Flag (*Ad-TFEB-Flag*) or empty (*Ad-Vec*) for 24 h.

(E) Western blot analyses of LC3B and P62 were performed in the liver lysates of the *Control* and *A/A*^{Hep} mice treated with tunicamycin (Tm,1 mg/kg) for indicated times. Bafilomycin A1 (Baf.A1, 200 nM) was treated for 3 h prior to harvest. (F) Band intensities of LC3B and P62 were quantified and analyzed with ImageJ software after normalizing the expression levels of protein to β-actin. All data are mean ± SEM (n=3 mice per group); **p < 0.01 and ***p < 0.001; Mock vs 24 h in each group.

Discussion

In this study, I investigated novel mechanistic links between eIF2α phosphorylation, which is essential for the activation of all three UPR pathways, and autophagy in the ER stress condition. The current observations demonstrate that eIF2α phosphorylation is a critical contributor to maintaining functional and degradative autophagy flux in response to ER stress.

This study was conducted with a mouse model of hepatocyte-specific eIF2α phosphorylation deficiency to determine the physiological role played by eIF2α phosphorylation in ER stress. As recent studies reported previously [13,14, 15, 65, 85], I showed that eIF2α phosphorylation deficiency impaired three UPR signaling pathways in response to ER stress. Thus, eIF2α phosphorylation controls not only translation but also transcription to regulate gene expression during ER stress [65, 86].

It is believed that the ER membrane expands to increase the ER capacity to fold proteins during ER stress. Such cellular adaptation is conducted by the UPR signaling pathway [27, 87]. Notably, XBP1s leads to the biosynthesis of ER membrane by upregulating membrane precursor lipids and phospholipid [59, 88]. Activated ATF6α also promotes the biosynthesis of phosphatidylcholine for the new synthesis of ER membrane [58, 89]. TEM analyses revealed that eIF2α phosphorylation deficient mice displayed abnormal ER morphology, with condensed ER cisternae with electron-dense materials, whereas the ER cisternae were enlarged or distended in the hepatocytes of *Cont.* mice under ER stress (Fig. 2B). These results suggest that eIF2α phosphorylation deficiency interferes with ER expansion and membrane biogenesis, possibly through the inactivation of UPR signaling pathways.

The interplay between the ER and mitochondria plays a crucial role in several cellular pathways, including autophagy, mitochondrial dynamics, calcium homeostasis and lipid transfer as well as providing energy production for protein folding under stressful cellular conditions [90-95]. Furthermore, mitochondria are dynamic organelles engaged in the

mitochondrial dynamics of fission and fusion, as well as the mitochondrial quality control pathway that manages mitophagy and mitochondrial biogenesis [96]. Several UPR transcription factors, including ATF4, XBP1s, and activated ATF6α, are important for mitochondrial function [28]. In the present study, I observed the role of eIF2α phosphorylation, which is responsible for the expression of ATF4, XBP1s and activated ATF6α, in mitochondrial homeostasis under ER stress. The ultrastructural and fluorescence analysis of mitochondria demonstrate that in hepatocytes lacking eIF2α phosphorylation, ER stress disrupts the integrity of mitochondria through abnormal swelling and enlargement, with disrupted cristae, as well as triggering an imbalance in mitochondrial dynamics that results in mitochondrial fragmentation and depolarization (Fig. 3).

Mitochondria try to maximize their energy conversion efficiency during autophagy and provide the membrane for autophagosome formation [97]. Mitochondrial elongation could be essential to increase their efficiency in ATP production. On that account, elongated mitochondria should be excluded from immediate autophagic elimination [98]. ER stress triggers mitochondrial fragmentation, but in the absence of eIF2α phosphorylation, the mitochondria might not be able to elongate; therefore, it is possible that mitochondrial dysfunction could contribute to defects in the autophagic process under ER stress conditions.

Autophagy is involved in the renewal of cellular organelles and in the maintenance of energy levels, protein synthesis and essential metabolic processes through the recycling of amino acids and nutrients [99]. During autophagy, amino acid limitation triggers the activation of the eIF2α kinase GCN2 through an increase in uncharged tRNA. The transcription factor ATF4 regulates the transcription of genes related to amino acid transportation and synthesis in response to amino acid starvation [12, 100]. In response to ER stress, eIF2α phosphorylation facilitates the selective translation of ATF4 mRNA which can transactivate the genes encoding ER chaperones and ER-Golgi trafficking machinery [101]. Furthermore, several reports have shown that ER stress elevates autophagy as a survival mechanism

through UPR-mediated transcriptional regulation of autophagy machinery components [102, 103]. In this study, I focused on the role of eIF2α phosphorylation in ER stress-mediated autophagy. Interestingly, I observed that the expression of autophagy-related genes was suppressed, whereas the proteins of the autophagosome formation markers LC3B and P62 accumulated in the livers of eIF2α phosphorylation-deficient mice upon ER stress (Fig. 4A, B). Furthermore, an ultrastructural analysis revealed that double-membraned autophagic vesicles, the *autophagosome*, clustered and accumulated excessively in the livers of eIF2α phosphorylation-deficient mice challenged with Tm (Fig. 5A, B). Therefore, eIF2α phosphorylation deficiency can cause dysregulation of the autophagic pathways.

Phosphorylation at the alpha subunit of the eIF2 complex is a key mechanism regulating translation initiation under cellular stress conditions [9]. EIF2α phosphorylation causes the attenuation of global protein synthesis by activating the eIF2α kinase PERK upon ER stress. However, in eIF2α phosphorylation-deficient conditions, PERK activation cannot lead to the phosphorylation of eIF2α upon prolonged ER stress. When eIF2α is sustained in a state of non-phosphorylation, unfolded proteins continuously accumulate through everlasting translation. Those unfolded proteins should be recognized as autophagic cargoes destined for degradation. In the absence of eIF2α phosphorylation, my observations show that the cytosolic form of LC3-I is converted to the LC3-II lipidated form, which is then bound to the autophagosomal membrane. In addition, I found that LC3B puncta (LC3-II) successfully co-localize with P62 puncta, but the number of LC3 and P62 positive autophagosome is abnormally increased and accumulated upon ER stress (Fig. 4D, 4F, 7A, 15A). Therefore, deficiency in eIF2α phosphorylation causes an accumulation of autophagosomes upon ER stress, which could be caused by the blockage of autophagy flux.

Autophagy flux describes the series of processes from autophagosome formation to the completion of cargo degradation by the autolysosome. Autophagosome maturation, also called autolysosome formation, describes the process of fusion between the nascent

autophagosome and the degradative lysosome [38]. By using functional autophagy assays, I found that eIF2α phosphorylation affects degradation activity and autophagosome maturation. In the absence of eIF2α phosphorylation, multiple results show that LC3- and P62-positive autophagic cargoes could not be delivered to the lysosome (Figs. 6A, 6B, 6D, 7B, 7C, 8C, 8D,15B, 15D), indicating that autophagosome-lysosome fusion was defective. In line with those observations, bafilomycin A1-mediated LC3 and P62 flux measurements indicate that eIF2α phosphorylation is essential for autophagy flux upon ER stress (Figs. 6D, 7E, 15E).

Because the autolysosome allows complete degradation of its contents through lysosomal hydrolytic enzymes, lysosomal function is important to the capacity of degradation in autophagy flux. In this study, a deficiency in eIF2α phosphorylation reduced the expression of autophagy-, lysosome-, and fusion-related genes (Figs. 4A, 9A-D, 10C-E) and produced lysosomal dysfunction (Figs. 11A-G, 14B), including attenuated lysosomal enzyme activity and a reduced number of active lysosomes. In addition, I showed that a deficiency in eIF2α phosphorylation prevented nuclear translocation of TFEB under ER stress (Fig. 13). However, the lysosomal dysfunction was recovered by TFEB overexpression in eIF2α phosphorylation deficient cells (Fig. 14 B).

Tail-anchored membrane proteins such as SNARE STX17 are inserted into the ER through a post-translational pathway and a transmembrane domain that requires cytosolic chaperones and recognition of an ER-localized receptor [104, 105]. Furthermore, STX17, as an ER resident SNARE protein, translocates to the outer membrane of the completed autophagosome. Recruitment of STX17 to the autophagosome is sufficient for SNARE-mediated membrane fusion. In addition, membrane-localized SNARE proteins, including STX17, SNAP29, and Vamp7, are essential for fusion between the autophagosome and the lysosome [106]. Notably, during autophagy, STX17 translocation to the autophagosome allows the assembly of SNARE complexes and the recruitment of the HOPS complex to the autophagosome, which enables it to couple with lysosome-localized VAMP7 [76, 106-108]. In

this study, I found that STX17 was not translocated to the LC3-positive autophagosome in eIF2α phosphorylation-deficient cells under ER stress (Fig. 12A). It then could not interact with the lysosomal SNARE VAMP7, suggesting that eIF2α phosphorylation is required for the assembly of SNARE complexes and autophagosome-lysosome fusion in response to ER stress (Fig. 12B). Therefore, recruitment of STX17 to the autophagosome might be affected by disruption of the ER tubular structure and the downregulated expression of ER chaperones caused by deficiency of eIF2α phosphorylation during prolonged ER stress. In addition, it is unclear whether eIF2α phosphorylation affects ER membrane targeting of cytosolic STX17 or whether eIF2α phosphorylation contributes to the recruitment of STX17 to the autophagosome. Further studies are needed to clarify those points in detail. Nevertheless, my observations suggest that eIF2α phosphorylation is required for autophagosome-lysosome fusion and autophagy flux upon ER stress.

The transcription factors TFEB and TFE3 play a crucial role in regulating lysosomal biogenesis and autophagy. Notably, TFEB coordinates transcriptional programs by binding the promoter regions of autophagy and lysosome-related genes. Several studies have reported that TFEB regulates the expression of a broad number of target genes involved in lysosomal biogenesis, lysosomal exocytosis, autophagosome biogenesis, and autophagosome-lysosome fusion [45, 109]. Furthermore, TFEB and TFE3 are activated for cellular adaptation under prolonged ER stress. A recent study reported that TFE3 facilitates ER homeostasis by directly binding a CLEAR element present in the promoter region of ATF4, a crucial regulator of the integrated stress response [52]. Interestingly, recent research has also found that TFEB induces lysosomal exocytosis, by which lysosomes fuse to the plasma membrane [110]. In this study, I found that TFEB overexpression was sufficient to upregulate the transcripts of several lysosomal genes (Fig. 14A) and improve lysosomal biogenesis and positioning in response to ER stress (Fig. 14B). Furthermore, TFEB overexpression increased the transcript level of PGC-1α, which controls energy metabolism by modulating mitochondrial biogenesis

and function [109]. Therefore, it is possible that increased PGC-1α levels might improve the balance of mitochondrial dynamics and mitochondrial biogenesis under ER stress.

In this study, I speculate that TFEB overexpression could enhance lysosomal catabolic activity and the autophagic fusion event because eIF2α phosphorylation deficiency prevents the activation of TFEB by limiting its nuclear translocation, which limits the degradative capacity of autophagy under ER stress. As expected, I found that overexpressing TFEB improved the autophagosome-lysosome fusion event and facilitated autophagic degradation (Figs. 14B, 15A-E). However, it remains unclear how eIF2α phosphorylation affects the TFEB nuclear translocation required to regulate lysosomal and fusion-related genes. Further studies are needed to clarify those points in detail.

In conclusion, this study reports that eIF2α phosphorylation plays a critical role in regulating UPR signaling and the autophagy-lysosome pathway to adapt to ER stress. These observations suggest that eIF2α phosphorylation contributes to the nuclear translocation of TFEB for functional autophagy flux. Furthermore, chronic and strong ER stress can impair autophagy, which results in the failure to eliminate pathogenic accumulation and aggravates the progression of metabolic liver injury. The current study highlights that TFEB is a potential therapeutic target that could enhance autophagic flux and maintain the homeostasis of intracellular organelles, including the ER and mitochondria, through the ER stress-mediated autophagy mechanism.

Reference

1. Sano R, Reed JC: **ER stress-induced cell death mechanisms**. *Biochim Biophys Acta* 2013, **1833**(12):3460-3470.
2. Iurlaro R, Munoz-Pinedo C: **Cell death induced by endoplasmic reticulum stress**. *FEBS J* 2016, **283**(14):2640-2652.
3. Rashid HO, Yadav RK, Kim HR, Chae HJ: **ER stress: Autophagy induction, inhibition and selection**. *Autophagy* 2015, **11**(11):1956-1977.
4. Johnson AE, Haigh NG: **The ER translocon and retrotranslocation: is the shift into reverse manual or automatic?** *Cell* 2000, **102**(6):709-712.
5. Yalcin A, Hotamisligil GS: **Impact of ER protein homeostasis on metabolism**. *Diabetes* 2013, **62**(3):691-693.
6. Schroder M, Kaufman RJ: **The mammalian unfolded protein response**. *Annu Rev Biochem* 2005, **74**:739-789.
7. Song S, Tan J, Miao Y, Li M, Zhang Q: **Crosstalk of autophagy and apoptosis: Involvement of the dual role of autophagy under ER stress**. *J Cell Physiol* 2017, **232**(11):2977-2984.
8. Song S, Tan J, Miao Y, Zhang Q: **Crosstalk of ER stress-mediated autophagy and ER-phagy: Involvement of UPR and the core autophagy machinery**. *J Cell Physiol* 2018, **233**(5):3867-3874.
9. Sonenberg N, Hinnebusch AG: **Regulation of translation initiation in eukaryotes: mechanisms and biological targets**. *Cell* 2009, **136**(4):731-745.
10. Proud CG: **eIF2 and the control of cell physiology**. *Semin Cell Dev Biol* 2005, **16**(1):3-12.
11. Wek RC, Jiang HY, Anthony TG: **Coping with stress: eIF2 kinases and translational control**. *Biochem Soc Trans* 2006, **34**(Pt 1):7-11.
12. B'Chir W, Maurin AC, Carraro V, Averous J, Jousse C, Muranishi Y, Parry L, Stepien G, Fafournoux P, Bruhat A: **The eIF2alpha/ATF4 pathway is essential for stress-induced autophagy gene expression**. *Nucleic Acids Res* 2013, **41**(16):7683-7699.
13. Teske BF, Wek SA, Bunpo P, Cundiff JK, McClintick JN, Anthony TG, Wek RC: **The eIF2 kinase PERK and the integrated stress response facilitate activation of ATF6 during endoplasmic reticulum stress**. *Mol Biol Cell* 2011, **22**(22):4390-4405.
14. Adachi Y, Yamamoto K, Okada T, Yoshida H, Harada A, Mori K: **ATF6 is a transcription factor specializing in the regulation of quality control proteins in the endoplasmic reticulum**. *Cell Struct Funct* 2008, **33**(1):75-89.
15. Majumder M, Huang C, Snider MD, Komar AA, Tanaka J, Kaufman RJ, Krokowski D,

Hatzoglou M: **A novel feedback loop regulates the response to endoplasmic reticulum stress via the cooperation of cytoplasmic splicing and mRNA translation**. *Mol Cell Biol* 2012, **32**(5):992-1003.

16. Ron D, Walter P: **Signal integration in the endoplasmic reticulum unfolded protein response**. *Nat Rev Mol Cell Biol* 2007, **8**(7):519-529.
17. Deegan S, Saveljeva S, Gorman AM, Samali A: **Stress-induced self-cannibalism: on the regulation of autophagy by endoplasmic reticulum stress**. *Cell Mol Life Sci* 2013, **70**(14):2425-2441.
18. Kroemer G, Marino G, Levine B: **Autophagy and the integrated stress response**. *Mol Cell* 2010, **40**(2):280-293.
19. Hetz C, Thielen P, Matus S, Nassif M, Court F, Kiffin R, Martinez G, Cuervo AM, Brown RH, Glimcher LH: **XBP-1 deficiency in the nervous system protects against amyotrophic lateral sclerosis by increasing autophagy**. *Genes Dev* 2009, **23**(19):2294-2306.
20. Margariti A, Li H, Chen T, Martin D, Vizcay-Barrena G, Alam S, Karamariti E, Xiao Q, Zampetaki A, Zhang Z *et al*: **XBP1 mRNA splicing triggers an autophagic response in endothelial cells through BECLIN-1 transcriptional activation**. *J Biol Chem* 2013, **288**(2):859-872.
21. Haze K, Yoshida H, Yanagi H, Yura T, Mori K: **Mammalian transcription factor ATF6 is synthesized as a transmembrane protein and activated by proteolysis in response to endoplasmic reticulum stress**. *Mol Biol Cell* 1999, **10**(11):3787-3799.
22. Shen J, Chen X, Hendershot L, Prywes R: **ER stress regulation of ATF6 localization by dissociation of BiP/GRP78 binding and unmasking of Golgi localization signals**. *Dev Cell* 2002, **3**(1):99-111.
23. Chen X, Shen J, Prywes R: **The luminal domain of ATF6 senses endoplasmic reticulum (ER) stress and causes translocation of ATF6 from the ER to the Golgi**. *J Biol Chem* 2002, **277**(15):13045-13052.
24. Ye J, Rawson RB, Komuro R, Chen X, Dave UP, Prywes R, Brown MS, Goldstein JL: **ER stress induces cleavage of membrane-bound ATF6 by the same proteases that process SREBPs**. *Mol Cell* 2000, **6**(6):1355-1364.
25. Hotamisligil GS: **Endoplasmic reticulum stress and the inflammatory basis of metabolic disease**. *Cell* 2010, **140**(6):900-917.
26. Marciniak SJ, Ron D: **Endoplasmic reticulum stress signaling in disease**. *Physiol Rev* 2006, **86**(4):1133-1149.
27. Bernales S, McDonald KL, Walter P: **Autophagy counterbalances endoplasmic reticulum expansion during the unfolded protein response**. *PLoS Biol* 2006,

4(12):e423.

28. Senft D, Ronai ZA: **UPR, autophagy, and mitochondria crosstalk underlies the ER stress response**. *Trends Biochem Sci* 2015, **40**(3):141-148.
29. Acevo-Rodriguez PS, Maldonado G, Castro-Obregon S, Hernandez G: **Autophagy Regulation by the Translation Machinery and Its Implications in Cancer**. *Front Oncol* 2020, **10**:322.
30. Hurley JH, Young LN: **Mechanisms of Autophagy Initiation**. *Annu Rev Biochem* 2017, **86**:225-244.
31. Mizushima N: **Autophagy: process and function**. *Genes Dev* 2007, **21**(22):2861-2873.
32. Bampton ET, Goemans CG, Niranjan D, Mizushima N, Tolkovsky AM: **The dynamics of autophagy visualized in live cells: from autophagosome formation to fusion with endo/lysosomes**. *Autophagy* 2005, **1**(1):23-36.
33. Mizushima N: **The ATG conjugation systems in autophagy**. *Curr Opin Cell Biol* 2020, **63**:1-10.
34. Li F, Guo H, Yang Y, Feng M, Liu B, Ren X, Zhou H: **Autophagy modulation in bladder cancer development and treatment (Review)**. *Oncol Rep* 2019, **42**(5):1647-1655.
35. Bestebroer J, V'Kovski P, Mauthe M, Reggiori F: **Hidden behind autophagy: the unconventional roles of ATG proteins**. *Traffic* 2013, **14**(10):1029-1041.
36. Doring T, Zeyen L, Bartusch C, Prange R: **Hepatitis B Virus Subverts the Autophagy Elongation Complex Atg5-12/16L1 and Does Not Require Atg8/LC3 Lipidation for Viral Maturation**. *J Virol* 2018, **92**(7).
37. Allaire M, Rautou PE, Codogno P, Lotersztajn S: **Autophagy in liver diseases: Time for translation?** *J Hepatol* 2019, **70**(5):985-998.
38. Zhao YG, Zhang H: **Autophagosome maturation: An epic journey from the ER to lysosomes**. *J Cell Biol* 2019, **218**(3):757-770.
39. McEwan DG, Popovic D, Gubas A, Terawaki S, Suzuki H, Stadel D, Coxon FP, Miranda de Stegmann D, Bhogaraju S, Maddi K *et al*: **PLEKHM1 regulates autophagosome-lysosome fusion through HOPS complex and LC3/GABARAP proteins**. *Mol Cell* 2015, **57**(1):39-54.
40. Lou X, Shin YK: **SNARE zippering**. *Biosci Rep* 2016, **36**(3).
41. Muppirala M, Gupta V, Swarup G: **Syntaxin 17 cycles between the ER and ERGIC and is required to maintain the architecture of ERGIC and Golgi**. *Biol Cell* 2011, **103**(7):333-350.
42. Itakura E, Kishi-Itakura C, Mizushima N: **The hairpin-type tail-anchored SNARE**

syntaxin 17 targets to autophagosomes for fusion with endosomes/lysosomes. *Cell* 2012, **151**(6):1256-1269.

43. Bonifacino JS, Neefjes J: **Moving and positioning the endolysosomal system**. *Curr Opin Cell Biol* 2017, **47**:1-8.
44. Kimura S, Noda T, Yoshimori T: **Dynein-dependent movement of autophagosomes mediates efficient encounters with lysosomes**. *Cell Struct Funct* 2008, **33**(1):109-122.
45. Settembre C, Di Malta C, Polito VA, Garcia Arencibia M, Vetrini F, Erdin S, Erdin SU, Huynh T, Medina D, Colella P *et al*: **TFEB links autophagy to lysosomal biogenesis**. *Science* 2011, **332**(6036):1429-1433.
46. Raben N, Puertollano R: **TFEB and TFE3: Linking Lysosomes to Cellular Adaptation to Stress**. *Annu Rev Cell Dev Biol* 2016, **32**:255-278.
47. Hu YB, Dammer EB, Ren RJ, Wang G: **The endosomal-lysosomal system: from acidification and cargo sorting to neurodegeneration**. *Transl Neurodegener* 2015, **4**:18.
48. Vega-Rubin-de-Celis S, Pena-Llopis S, Konda M, Brugarolas J: **Multistep regulation of TFEB by MTORC1**. *Autophagy* 2017, **13**(3):464-472.
49. Medina DL, Di Paola S, Peluso I, Armani A, De Stefani D, Venditti R, Montefusco S, Scotto-Rosato A, Prezioso C, Forrester A *et al*: **Lysosomal calcium signalling regulates autophagy through calcineurin and TFEB**. *Nat Cell Biol* 2015, **17**(3):288-299.
50. Tsunemi T, La Spada AR: **PGC-1alpha at the intersection of bioenergetics regulation and neuron function: from Huntington's disease to Parkinson's disease and beyond**. *Prog Neurobiol* 2012, **97**(2):142-151.
51. Dabrowska A, Venero JL, Iwasawa R, Hankir MK, Rahman S, Boobis A, Hajji N: **PGC-1alpha controls mitochondrial biogenesis and dynamics in lead-induced neurotoxicity**. *Aging (Albany NY)* 2015, **7**(9):629-647.
52. Martina JA, Diab HI, Brady OA, Puertollano R: **TFEB and TFE3 are novel components of the integrated stress response**. *EMBO J* 2016, **35**(5):479-495.
53. Zhao E, Ding J, Xia Y, Liu M, Ye B, Choi JH, Yan C, Dong Z, Huang S, Zha Y *et al*: **KDM4C and ATF4 Cooperate in Transcriptional Control of Amino Acid Metabolism**. *Cell Rep* 2016, **14**(3):506-519.
54. Timosenko E, Ghadbane H, Silk JD, Shepherd D, Gileadi U, Howson LJ, Laynes R, Zhao Q, Strausberg RL, Olsen LR *et al*: **Nutritional Stress Induced by Tryptophan-Degrading Enzymes Results in ATF4-Dependent Reprogramming of the Amino Acid Transporter Profile in Tumor Cells**. *Cancer Res* 2016, **76**(21):6193-6204.

55. Rutkowski DT, Wu J, Back SH, Callaghan MU, Ferris SP, Iqbal J, Clark R, Miao H, Hassler JR, Fornek J *et al*: **UPR pathways combine to prevent hepatic steatosis caused by ER stress-mediated suppression of transcriptional master regulators**. *Dev Cell* 2008, **15**(6):829-840.
56. Niccolai V, Wascher E, Stoerig P: **Distinct neural processes in grapheme-colour synaesthetes and semantic controls**. *Eur J Neurosci* 2012, **36**(11):3593-3601.
57. Schuck S, Prinz WA, Thorn KS, Voss C, Walter P: **Membrane expansion alleviates endoplasmic reticulum stress independently of the unfolded protein response**. *J Cell Biol* 2009, **187**(4):525-536.
58. Bommiasamy H, Back SH, Fagone P, Lee K, Meshinchi S, Vink E, Sriburi R, Frank M, Jackowski S, Kaufman RJ *et al*: **ATF6alpha induces XBP1-independent expansion of the endoplasmic reticulum**. *J Cell Sci* 2009, **122**(Pt 10):1626-1636.
59. Sriburi R, Jackowski S, Mori K, Brewer JW: **XBP1: a link between the unfolded protein response, lipid biosynthesis, and biogenesis of the endoplasmic reticulum**. *J Cell Biol* 2004, **167**(1):35-41.
60. Sriburi R, Bommiasamy H, Buldak GL, Robbins GR, Frank M, Jackowski S, Brewer JW: **Coordinate regulation of phospholipid biosynthesis and secretory pathway gene expression in XBP-1(S)-induced endoplasmic reticulum biogenesis**. *J Biol Chem* 2007, **282**(10):7024-7034.
61. Promlek T, Ishiwata-Kimata Y, Shido M, Sakuramoto M, Kohno K, Kimata Y: **Membrane aberrancy and unfolded proteins activate the endoplasmic reticulum stress sensor Ire1 in different ways**. *Mol Biol Cell* 2011, **22**(18):3520-3532.
62. Volmer R, van der Ploeg K, Ron D: **Membrane lipid saturation activates endoplasmic reticulum unfolded protein response transducers through their transmembrane domains**. *Proc Natl Acad Sci U S A* 2013, **110**(12):4628-4633.
63. Eisner V, Picard M, Hajnoczky G: **Mitochondrial dynamics in adaptive and maladaptive cellular stress responses**. *Nat Cell Biol* 2018, **20**(7):755-765.
64. Youle RJ, van der Bliek AM: **Mitochondrial fission, fusion, and stress**. *Science* 2012, **337**(6098):1062-1065.
65. Back SH: **Roles of the Translation Initiation Factor eIF2alpha Phosphorylation in Cell Structure and Function**. *Cell Struct Funct* 2020, **45**(1):65-76.
66. Lebeau J, Saunders JM, Moraes VWR, Madhavan A, Madrazo N, Anthony MC, Wiseman RL: **The PERK Arm of the Unfolded Protein Response Regulates Mitochondrial Morphology during Acute Endoplasmic Reticulum Stress**. *Cell Rep* 2018, **22**(11):2827-2836.
67. Karbowski M, Arnoult D, Chen H, Chan DC, Smith CL, Youle RJ: **Quantitation of**

mitochondrial dynamics by photolabeling of individual organelles shows that mitochondrial fusion is blocked during the Bax activation phase of apoptosis. *J Cell Biol* 2004, **164**(4):493-499.

68. Lee WS, Yoo WH, Chae HJ: **ER Stress and Autophagy**. *Curr Mol Med* 2015, **15**(8):735-745.
69. Li L, Tong M, Fu Y, Chen F, Zhang S, Chen H, Ma X, Li D, Liu X, Zhong Q: **Lipids and membrane-associated proteins in autophagy**. *Protein Cell* 2020.
70. Schutter M, Giavalisco P, Brodesser S, Graef M: **Local Fatty Acid Channeling into Phospholipid Synthesis Drives Phagophore Expansion during Autophagy**. *Cell* 2020, **180**(1):135-149 e114.
71. Rambold AS, Lippincott-Schwartz J: **Mechanisms of mitochondria and autophagy crosstalk**. *Cell Cycle* 2011, **10**(23):4032-4038.
72. Cohen-Kaplan V, Livneh I, Avni N, Fabre B, Ziv T, Kwon YT, Ciechanover A: **p62- and ubiquitin-dependent stress-induced autophagy of the mammalian 26S proteasome**. *Proc Natl Acad Sci U S A* 2016, **113**(47):E7490-E7499.
73. Haspel J, Shaik RS, Ifedigbo E, Nakahira K, Dolinay T, Englert JA, Choi AM: **Characterization of macroautophagic flux in vivo using a leupeptin-based assay**. *Autophagy* 2011, **7**(6):629-642.
74. Massey AC, Kaushik S, Sovak G, Kiffin R, Cuervo AM: **Consequences of the selective blockage of chaperone-mediated autophagy**. *Proc Natl Acad Sci U S A* 2006, **103**(15):5805-5810.
75. Vitner EB, Dekel H, Zigdon H, Shachar T, Farfel-Becker T, Eilam R, Karlsson S, Futerman AH: **Altered expression and distribution of cathepsins in neuronopathic forms of Gaucher disease and in other sphingolipidoses**. *Hum Mol Genet* 2010, **19**(18):3583-3590.
76. Jiang P, Nishimura T, Sakamaki Y, Itakura E, Hatta T, Natsume T, Mizushima N: **The HOPS complex mediates autophagosome-lysosome fusion through interaction with syntaxin 17**. *Mol Biol Cell* 2014, **25**(8):1327-1337.
77. Palmieri M, Impey S, Kang H, di Ronza A, Pelz C, Sardiello M, Ballabio A: **Characterization of the CLEAR network reveals an integrated control of cellular clearance pathways**. *Hum Mol Genet* 2011, **20**(19):3852-3866.
78. Sardiello M, Palmieri M, di Ronza A, Medina DL, Valenza M, Gennarino VA, Di Malta C, Donaudy F, Embrione V, Polishchuk RS *et al*: **A gene network regulating lysosomal biogenesis and function**. *Science* 2009, **325**(5939):473-477.
79. Cabukusta B, Neefjes J: **Mechanisms of lysosomal positioning and movement**. *Traffic* 2018, **19**(10):761-769.

80. Kumar S, Jain A, Farzam F, Jia J, Gu Y, Choi SW, Mudd MH, Claude-Taupin A, Wester MJ, Lidke KA *et al*: **Mechanism of Stx17 recruitment to autophagosomes via IRGM and mammalian Atg8 proteins**. *J Cell Biol* 2018, **217**(3):997-1013.
81. Nakamura S, Yoshimori T: **New insights into autophagosome-lysosome fusion**. *J Cell Sci* 2017, **130**(7):1209-1216.
82. Feeney EJ, Spampanato C, Puertollano R, Ballabio A, Parenti G, Raben N: **What else is in store for autophagy? Exocytosis of autolysosomes as a mechanism of TFEB-mediated cellular clearance in Pompe disease**. *Autophagy* 2013, **9**(7):1117-1118.
83. Puertollano R, Ferguson SM, Brugarolas J, Ballabio A: **The complex relationship between TFEB transcription factor phosphorylation and subcellular localization**. *EMBO J* 2018, **37**(11).
84. Zhang Z, Yan J, Bowman AB, Bryan MR, Singh R, Aschner M: **Dysregulation of TFEB contributes to manganese-induced autophagic failure and mitochondrial dysfunction in astrocytes**. *Autophagy* 2020, **16**(8):1506-1523.
85. Han J, Back SH, Hur J, Lin YH, Gildersleeve R, Shan J, Yuan CL, Krokowski D, Wang S, Hatzoglou M *et al*: **ER-stress-induced transcriptional regulation increases protein synthesis leading to cell death**. *Nat Cell Biol* 2013, **15**(5):481-490.
86. Scheuner D, Song B, McEwen E, Liu C, Laybutt R, Gillespie P, Saunders T, Bonner-Weir S, Kaufman RJ: **Translational control is required for the unfolded protein response and in vivo glucose homeostasis**. *Mol Cell* 2001, **7**(6):1165-1176.
87. Ron D, Hampton RY: **Membrane biogenesis and the unfolded protein response**. *J Cell Biol* 2004, **167**(1):23-25.
88. Shaffer AL, Shapiro-Shelef M, Iwakoshi NN, Lee AH, Qian SB, Zhao H, Yu X, Yang L, Tan BK, Rosenwald A *et al*: **XBP1, downstream of Blimp-1, expands the secretory apparatus and other organelles, and increases protein synthesis in plasma cell differentiation**. *Immunity* 2004, **21**(1):81-93.
89. Lykidis A, Jackowski S: **Regulation of mammalian cell membrane biosynthesis**. *Prog Nucleic Acid Res Mol Biol* 2001, **65**:361-393.
90. Yang Z, Zhao X, Xu J, Shang W, Tong C: **A novel fluorescent reporter detects plastic remodeling of mitochondria-ER contact sites**. *J Cell Sci* 2018, **131**(1).
91. Hoppins S, Nunnari J: **Cell Biology. Mitochondrial dynamics and apoptosis--the ER connection**. *Science* 2012, **337**(6098):1052-1054.
92. Rizzuto R, Pinton P, Carrington W, Fay FS, Fogarty KE, Lifshitz LM, Tuft RA, Pozzan T: **Close contacts with the endoplasmic reticulum as determinants of mitochondrial Ca2+ responses**. *Science* 1998, **280**(5370):1763-1766.

93. Lev S: **Nonvesicular lipid transfer from the endoplasmic reticulum**. *Cold Spring Harb Perspect Biol* 2012, **4**(10).
94. Wu H, Carvalho P, Voeltz GK: **Here, there, and everywhere: The importance of ER membrane contact sites**. *Science* 2018, **361**(6401).
95. Chu Q, Martinez TF, Novak SW, Donaldson CJ, Tan D, Vaughan JM, Chang T, Diedrich JK, Andrade L, Kim A *et al*: **Regulation of the ER stress response by a mitochondrial microprotein**. *Nat Commun* 2019, **10**(1):4883.
96. Stotland A, Gottlieb RA: **Mitochondrial quality control: Easy come, easy go**. *Biochim Biophys Acta* 2015, **1853**(10 Pt B):2802-2811.
97. Hailey DW, Rambold AS, Satpute-Krishnan P, Mitra K, Sougrat R, Kim PK, Lippincott-Schwartz J: **Mitochondria supply membranes for autophagosome biogenesis during starvation**. *Cell* 2010, **141**(4):656-667.
98. Gomes LC, Di Benedetto G, Scorrano L: **During autophagy mitochondria elongate, are spared from degradation and sustain cell viability**. *Nat Cell Biol* 2011, **13**(5):589-598.
99. Mizushima N, Komatsu M: **Autophagy: renovation of cells and tissues**. *Cell* 2011, **147**(4):728-741.
100. Zhang P, McGrath BC, Reinert J, Olsen DS, Lei L, Gill S, Wek SA, Vattem KM, Wek RC, Kimball SR *et al*: **The GCN2 eIF2alpha kinase is required for adaptation to amino acid deprivation in mice**. *Mol Cell Biol* 2002, **22**(19):6681-6688.
101. Cao SS, Wang M, Harrington JC, Chuang BM, Eckmann L, Kaufman RJ: **Phosphorylation of eIF2alpha is dispensable for differentiation but required at a posttranscriptional level for paneth cell function and intestinal homeostasis in mice**. *Inflamm Bowel Dis* 2014, **20**(4):712-722.
102. Luhr M, Torgersen ML, Szalai P, Hashim A, Brech A, Staerk J, Engedal N: **The kinase PERK and the transcription factor ATF4 play distinct and essential roles in autophagy resulting from tunicamycin-induced ER stress**. *J Biol Chem* 2019, **294**(20):8197-8217.
103. Ogata M, Hino S, Saito A, Morikawa K, Kondo S, Kanemoto S, Murakami T, Taniguchi M, Tanii I, Yoshinaga K *et al*: **Autophagy is activated for cell survival after endoplasmic reticulum stress**. *Mol Cell Biol* 2006, **26**(24):9220-9231.
104. Hegde RS, Keenan RJ: **Tail-anchored membrane protein insertion into the endoplasmic reticulum**. *Nat Rev Mol Cell Biol* 2011, **12**(12):787-798.
105. Borgese N, Fasana E: **Targeting pathways of C-tail-anchored proteins**. *Biochim Biophys Acta* 2011, **1808**(3):937-946.
106. Wang Y, Li L, Hou C, Lai Y, Long J, Liu J, Zhong Q, Diao J: **SNARE-mediated**

membrane fusion in autophagy. *Semin Cell Dev Biol* 2016, **60**:97-104.

107. Tian X, Teng J, Chen J: **New insights regarding SNARE proteins in autophagosome-lysosome fusion**. *Autophagy* 2020:1-9.
108. Lorincz P, Juhasz G: **Autophagosome-Lysosome Fusion**. *J Mol Biol* 2020, **432**(8):2462-2482.
109. Napolitano G, Ballabio A: **TFEB at a glance**. *J Cell Sci* 2016, **129**(13):2475-2481.
110. Medina DL, Fraldi A, Bouche V, Annunziata F, Mansueto G, Spampanato C, Puri C, Pignata A, Martina JA, Sardiello M *et al*: **Transcriptional activation of lysosomal exocytosis promotes cellular clearance**. *Dev Cell* 2011, **21**(3):421-430.
111. Nam SA, Kim WY, Kim JW, Park SH, Kim HL, Lee MS, Komatsu M, Ha H, Lim JH, Park CW, Yang CW, Kim J, Kim YK *et al:* **Autophagy attenuates tubulointerstital fibrosis through regulating transforming growth factor-β and NLRP3 inflammasome signaling pathway** *Cell Death Dis*. 2019, **10**(2): 78

국문 요약

항산화 스트레스와 자가 포식 작용에서 eIF2α 인산화의 역할 연구

단백질의 합성은 세포내 대사 과정의 가장 기본적인 부분이며 여러 유전자의 발현을 조절하는 중요한 과정이다. mRNA 로부터 단백질이 생성되는 번역 과정 중 시작 과정이 단백질의 합성을 조절하는 중요한 단계이다. 단백질 번역은 번역 개시 인자인 eIF2α은 번역 개시를 촉진할 뿐만 아니라, eIF2α 인산화를 통해 번역을 제한하여 단백질의 합성을 조절하고 스트레스를 개선에 기여한다.

먼저, 산화 스트레스에 의해 유도되는 EGFR 신호 전달 체계에서 eIF2α 인산화 역할을 연구하였다. 활성산소는 생체 내 신호전달 및 생명 현상에 중요한 역할을 하지만, 지속적인 과다 생성시 산화 스트레스로 작용하여 여러 병증의 주요 원인이 된다. 활성산소에 의해 세포에 산화 스트레스가 가해지면 DNA 변형이나 지질의 산화뿐만 아니라, 단백질 변성을 유도함으로써 세포 손상 및 세포 사멸을 야기한다. eIF2α 인산화는 산화 스트레스나 과당섭취로 인한 간 섬유화로부터 간세포를 보호하는 데에 기여하는 중요한 인자이다. 간세포에서 eIF2α 인산화는 항산화 관련 단백질을 적절한 수준으로 유지시킨다. 산화 스트레스는 세포 증식과 생존에 관여하는 신호전달 경로들을 활성화시킨다. EGFR 신호 전달 체계는 세포 증식 및 분화, 생존에 중요한 역할을 한다. 또한 EGFR 신호 전달에 의한 산화-환원 조절은 세포를 산화 스트레스로부터 보호하는데 기여한다. 산화 스트레스를 통해 활성화된 EGFR 신호 전달 체계는 PI3K/ATK, MAPK, JAK/STAT 신호전달을 포함하는 생존 및 성장 신호 전달 경로들을 활성화시키는 타이로신 인산화 수용체이다. 하지만 eIF2α 인산화 결핍 간세포는 EGFR 의 발현이 감소되고, EGFR 신호 전달 체계 이상을 나타낸다. 활성산소인 과산화 수소 (Hydrogen peroxide) 와 메나디온 (Menadione)으로 산화적 스트레스를 유도하여 활성산소를 증가시켜 EGFR 신호 전달 체계를 활성시키고, eIF2α 인산화를 유도한다.

EGFR knock-down 세포주에서 EGFR 발현 감소는 활성산소 제거 능력을 감소시키고 활성산소 매개 세포 사멸에 감수성을 띄게 한다. eIF2α 인산화 결핍 간세포에서 EGFR 과발현은 활성산소 제거능이 향상되어 세포 사멸을 약화시킨다. eIF2α 인산화 결핍 간세포에서 나타나는 EGFR 발현 감소는 산화 스트레스에 대한 감수성을 항진하는 중요한 인자로 의미가 있다.

둘째, 소포체 스트레스에 의해 유도되는 자가 포식 작용에서 eIF2α 인산화 역할을 연구하였다. 생리적 혹은 병리적 환경에 의해 소포체가 처리할 수 있는 능력 이상의 미성숙 단백질이 소포체 내에 축적되면 세포는 이를 소포체 스트레스로 인식하고, 이러한 스트레스를 회복하기 위한 방어기전으로 잘못 접힌 단백질 반응 (Unfolded protein response)이 유도된다. UPR 반응으로 소포체 기능을 회복할 수 없을 때, 소포체 스트레스에 대한 적응 반응으로 생존을 증진시키기 위한 기작으로 자가 포식 작용 (autophagy)가 유도된다. eIF2α 인산화가 결핍된 간 세포와 간 조직 특이적으로 eIF2α 인산화가 제거된 동물모델을 이용하였다. 소포체 스트레스에 노출된 eIF2α 인산 화 결핍 간조직과 간세포에서 autophagosome 마커 단백질인 LC3B 와 오토 파지 기질이며 기질 유도단백질인 P62/SQSTM1 의 비정상적인 축적이 관찰되었다. 또한 소포체 스트레스에 노출된 eIF2α 인산화 결핍 세포에는 다수의 autophagosome 이 축적되어 있는 것과 이와 반대로 autolysosome 숫자는 상대적으로 대조군에 비해 적음이 간세포 투과전자현미경 관찰을 통하여 확인되었다. 따라서 소포체 스트레스에서 eIF2α 인산화는 Autophagosome 형성보다 Autolysosome 형성에 중요한 역할을 함을 알 수 있었다. Autophagosome-lysosome 융합 그리고 autolysosome 산성화는 오토 파지 flux 를 유지하는 오토 파지 과정의 중요한 마지막 step 이다. 그런데 소포체 스트레스에 노출된 eIF2α 인산화 결핍 세포에서 autophagosome 마커 단백질인 LC3B 와 lysosome 단백질 (Lamp1/2 그리고 Cathepsin B/D/L)들의 colocalization 이 감소되어 있는 것이 관찰되었다. 더 나아가 lysosome 단백질 분해효소 억제제 leupeptin 을 활용한 오토 파지 flux 조사법들로 부터 소포체 스트레스에 노출된 eIF2a 인산화 결핍 간 조직 또는 간세포에선 leupeptin 에 의한 LC3B 단백질 축적이 나타나지 않으며 낮은 pH 를 가진 autolysosome 의 숫자가 대조군에 비하여 월등이 적음이 관찰되었다. 이런 사실들은 소포체 스트레스에 노출된 eIF2α 인산화 결핍 간 조직 또는 간세포는 정상적인 오토 파지 flux 유지에 필요한 autophagosome-lysosome 융합 과 autolysosome 산성화 능력에 문제가 있음을 의미한다. 소포체 스트레스에 노출된 eIF2a 인산화 결핍 간조직에서 대부분의 lysosome 단백질 분해효소 유전자들과 다수의 Rabs, soluble N-ethylmaleimide–sensitive factor attachment protein receptors (SNAREs) 그리 고 tethers 포함한 autophagosome-lysosome fusion machinery 관련 유전자들의 mRNA 발현이 줄어든 것과 상통되게 eIF2α 인산화 결핍 간세포에선 오토 파지 마스터 조절자로 알려진 TFEB 와 TFE3 전사인자의 소포체 스트레스 유도 핵 전이 현상이 일어나지 않는 것이 관찰되었다. 그러나 TFEB 를 과발현 시킬 경우 eIF2α 인산화 결핍 세포에서 소포체

스트레스에 의한 세포사멸이 감소되었다. 더 나아가 이러한 TFEB 과발현은 소포체 스트레스에 노출된 eIF2α 인산화 결핍 간조직에서 관찰되었던 autophagosome-lysosome 융합 문제와 autolysosome 산성화 능력 문제를 포함한 오토 파지 flux 이상 현상을 개선시켰다. 따라서 본 연구는 오토 파지 마스터 조절자 TFEB 와 TFE3 전사인자의 소포체 스트레스 유도 핵 전이를 조절하는 eIF2α 인산화는 잘못 접힌 단백질의 축적으로 촉발된 소포체 스트레스를 억제하는 오토 파지의 flux 유지에 꼭 필요한 현상임을 입증한다.

따라서, 본 연구는 산화 스트레스에 의한 EGFR 신호 전달 체계와 소포체 스트레스에 의한 자가 포식 작용에서 eIF2α 인산화의 역할을 규명한다.

Appendix

Butyrate Prevents TGF-β1-Induced Alveolar Myofibroblast Differentiation and Modulates Energy Metabolism

Metabolites 2021 Apr 22;11(5):258.